

University of Vermont

UVM ScholarWorks

Graduate College Dissertations and Theses

Dissertations and Theses

2022

Three Branch Diversity Systems for Multi-Hop IoT Networks

Sakil Ahmed Chowdhury
University of Vermont

Follow this and additional works at: <https://scholarworks.uvm.edu/graddis>



Part of the [Electrical and Electronics Commons](#)

Recommended Citation

Chowdhury, Sakil Ahmed, "Three Branch Diversity Systems for Multi-Hop IoT Networks" (2022). *Graduate College Dissertations and Theses*. 1574.

<https://scholarworks.uvm.edu/graddis/1574>

This Dissertation is brought to you for free and open access by the Dissertations and Theses at UVM ScholarWorks. It has been accepted for inclusion in Graduate College Dissertations and Theses by an authorized administrator of UVM ScholarWorks. For more information, please contact scholarworks@uvm.edu.

THREE BRANCH DIVERSITY SYSTEMS FOR MULTI-HOP IoT NETWORKS

A Dissertation Presented

by

Sakil Ahmed Chowdhury

to

The Faculty of the Graduate College

of

The University of Vermont

In Partial Fulfillment of the Requirements
for the Degree of Doctor of Philosophy
Specializing in Electrical Engineering

August, 2022

Defense Date: May 4, 2022

Dissertation Examination Committee:

Jeff Frolik, Ph.D., Advisor

Abderrahim Benslimane, Ph.D., Co-advisor

Laurent Hébert-Dufresne, Ph.D., Chairperson

Safwan Wshah, Ph.D.

Tian Xia, Ph.D.

Cynthia J. Forehand, Ph.D., Dean of the Graduate College

Abstract

Internet of Things (IoT) is an emerging technological paradigm connecting numerous smart objects for advanced applications ranging from home automation to industrial control to healthcare. The rapid development of wireless technologies and miniature embedded devices has enabled IoT systems for such applications, which have been deployed in a variety of environments. One of the factors limiting the performance of IoT devices is the multipath fading caused by reflectors and attenuators present in the environment where these devices are deployed. Leveraging polarization diversity is a well-known technique to mitigate the deep signal fades and depolarization effects caused by multipath. However, neither experimental validation of the performance of polarization diversity antenna with more than two branches nor the potency of existing antenna selection techniques on such antennas in practical scenarios has received much attention.

The objectives of this dissertation are threefold. First, to demonstrate the efficacy of a tripolar antenna, which is specifically designed for IoT devices, in harsh environments through simulations and experimental data. Second, to develop antenna selection strategies to utilize polarized signals received at the antenna, considering the restrictions imposed due to resource limitations of the IoT devices. Finally, to conduct comparative analyses on the existing standard diversity techniques and proposed approaches, in conjunction with experimental data.

Accordingly, this dissertation presents the testing results of tripolar antenna integrated with Arduino based IoT devices deployed in environments likely to be experienced by IoT devices in real life applications. Both simulation and experimental results from single point-to-point wireless links demonstrate the advantage of utilizing tripolar antennas in harsh propagation conditions over single branch antenna. Motivated by these empirical results, we deploy a small-scale IoT network with tripolar antenna based nodes to analyze the impact of tripolar antenna on neighbor nodes performance as well as to investigate end-to-end network performance. This work illustrates that the selection of antenna branches, while considering network architecture and the level of congestion on the repeater nodes, minimizes excessive antenna switching and energy consumption. Similar results are shown for IoT networks with predetermined and dynamic routing protocols, where the proposed techniques yielded lower energy consumption than the conventional diversity schemes. Furthermore, a probabilistic, low complexity antenna selection approach based on Hidden Markov model is proposed and implemented on wireless sensor nodes aiming to reduce energy consumption and improve diversity gain. Finally, we develop a dual-hop based technique where a node selects the antenna element for optimal performance based on its immediate network neighbors antenna configuration status during selection. The performance of the proposed technique, which is verified through simulation and measured data, illustrates the importance of considering network-wide evaluations of antenna selection techniques.

Citations

Material from this dissertation has been published in the following forms:

Chowdhury S. A., Frolik J., and Benslimane A.. “Switching-based Selection Techniques for Tripolar Antennas in Multi-hop IoT Networks.” in *IEEE Internet of Things Journal*, doi: 10.1109/JIOT.2022.3151638. **Early Access. February 7, 2022.**

Chowdhury S. A., Frolik J., and Benslimane A.. “Coordinating Three-Branch Diversity Switching Using a Hidden Markov Model.” in *IEEE Internet of Things Journal*, vol. 7, no. 1, pp. 258-268, 2019.

Chowdhury S. A., Hébert-Dufresne L., and Frolik J.. “Effective Implementation of Energy Aware Polarization Diversity for IoT Networks Using Eigenvector Centrality,” in *International Conference on Network Science*. Springer, pp. 245-257, 2020.

Chowdhury S. A., Golmohamadi M., and Frolik J.. “Improving reliability in hybrid mesh networks with tripolar antennas,” *2018 IEEE International Symposium on Antennas and Propagation & USNC/URSI National Radio Science Meeting*, pp. 189–190, 2018.

Chowdhury S. A., Frolik J., and Benslimane A.. “Polarization matching for networks utilizing tripolar antenna systems,” in *2018 IEEE Global Communications Conference (GLOBECOM)*. IEEE, pp. 206–212, 2018.

Chowdhury S. A., Jamison J., and Frolik J.. “Leveraging tripolar antenna diversity to improve link reliability in severe multipath environments,” in *2018 IEEE 19th Wireless and Microwave Technology Conference (WAMICON)*. IEEE, 2018.

Acknowledgements

Firstly, it is my utmost pleasure to dedicate this work to my dear parents and my family, who have *always* been supportive of my academic pursuits and actively encouraging of them.

My mother, Amina Begum, has been my de facto therapist for all these years to manage my constant stress. My father, Shahid Ullah, was just the absolute example of a hard-working, family loving dad, whose passing encouraged me to begin this journey.

Thank you to my dear wife Farzana who has stood by me as I worked late nights and weekends on this, and to my dear kids Afnan and Aaraf who are the light of my life. This work would not have been possible without the support and taunting of Shahana and Shetu who are my best friends in life.

I wish to express my appreciation and thanks to those who provided their time, effort and support for this project. To the members of my dissertation committee, thank you for your support, insightful comments and encouragement. I owe a big thank you to Dr. Benslimane, who has helped me continually in my academic research. I would also like to thank my labmates: Marcia, Blake and Jimmy, who helped me tremendously along the way.

Finally, a special thanks to Dr. Jeff Frolik for his continuous support, encouragement and guidance. Thank you for always backing me and being patient throughout my unusually rewarding PhD journey. I have learned more than I could have ever imagined during my time at the UVM and I owe most of that to him.

Table of Contents

Citations	ii
Acknowledgements	iii
List of Figures	x
List of Tables	xi
1 Introduction	1
1.1 Motivation	1
1.2 Background	2
1.2.1 Internet of Things definition and applications	2
1.2.2 IoT network topologies	3
1.2.3 Routing protocols for IoT networks	4
1.2.4 Multipath Fading	6
1.2.5 Rayleigh fading model	7
1.2.6 Polarization and depolarization	8
1.2.7 Forms of antenna diversity	10
1.2.8 Diversity combining techniques	13
1.2.9 Tripolar antenna	17
1.3 Research Objectives and Organization	18
2 Improving Network Reliability Using Tripolar Antenna	20
2.1 Improving Reliability in Hybrid Mesh Networks with Tripolar Antennas	20
2.1.1 Abstract	20
2.1.2 Introduction	21
2.1.3 Methodology	22
2.1.4 Simulation results	23
2.1.5 Conclusion	24
2.2 Leveraging Tripolar Antenna Diversity to Improve Link Reliability in Severe Multi-path Environments	26
2.2.1 Abstract	26

2.2.2	Introduction	26
2.2.3	Methodology	28
2.2.4	Empirical results	30
2.2.5	Conclusion	31
3	Polarization Matching for Networks Utilizing Tripolar Antenna Systems	33
3.1	Abstract	33
3.2	Introduction	34
3.3	System Model	36
3.4	Neighbor Matching Technique	37
3.5	Opportunistic Polarization Matching	39
3.6	Simulation Results	42
3.7	Conclusion	45
4	Effective Implementation of Energy Aware Polarization Diversity for IoT Networks Using Eigenvector Centrality	47
4.1	Abstract	47
4.2	Introduction	48
4.3	Related Works	50
4.4	System Model	51
4.5	Distributed Eigenvector Centrality	53
4.5.1	Centrality based diversity scheme	55
4.6	Performance Evaluation	56
4.6.1	Simulation model	56
4.6.2	Simulation results	58
4.7	Conclusion	59
5	Coordinating Three-Branch Diversity Switching Using a Hidden Markov Model	61
5.1	Abstract	61
5.2	Introduction	62
5.3	Background	64
5.4	HMM Coordinated Switching	66
5.4.1	An overview of HMM	68
5.4.2	Proposed HMM approach	68

5.5	Defining State Transition Probability	71
5.6	Implementation and Performance Evaluation	75
5.6.1	Data collection	75
5.6.2	Learning HMM parameters:	77
5.6.3	Results	79
5.7	Conclusion	83
5.8	Appendix	84
6	Switching-based Selection Techniques for Tripolar Antennas in Multi-hop IoT Networks	86
6.1	Abstract	86
6.2	Introduction	87
6.3	Related Works	88
6.4	Proposed Multi-hop Based Switched Diversity for Tripolar Antennas	90
6.4.1	Joint SNR maximization (Max-Sum)	92
6.4.2	Maximization of the minimum SNR (Max-Min)	96
6.5	Experimental Setup	100
6.6	Performance Analysis	102
6.6.1	Simulation model	102
6.6.2	Performance of two-hop network	104
6.6.3	Performance of four-hop network	106
6.6.4	Diversity performance	106
6.6.5	End-to-end reliability	107
6.6.6	Switching frequency	108
6.6.7	Energy efficiency	108
6.6.8	Impact of network size	109
6.6.9	Algorithmic complexity	110
6.7	Conclusion	111
7	Conclusion and Future Work	113
7.1	Summary	113
7.2	Future Work	116
7.2.1	Real life implementation	116
7.2.2	Testing scalability and robustness	117

7.2.3	Leveraging machine learning techniques	118
7.2.4	Different fading environments	118
7.2.5	Hybrid approaches combining routing and antenna diversity	119
7.3	Final Comments	120
References		121

List of Figures

1.1	Typical example of an IoT network. End nodes forward data to nearest router to route the data to the base station.	3
1.2	Example of various topologies used in IoT networks: (a) point-to-point, (b) star, (c) mesh and (d) hybrid mesh topology.	3
1.3	Categories of routing protocols based on IoT network organization.	5
1.4	Reflected, scattered multipath components received at the antenna.	6
1.5	<i>Left:</i> Sample sensor data collected over time in an harsh multipath environment using single branch antenna where y-axis is showing the received signal power, <i>Right:</i> Histogram plot of the received signal level along with a fitted Rayleigh curve.	8
1.6	Different types of polarization of an electromagnetic wave	9
1.7	Block diagram of selection diversity with three antenna branches	14
1.8	Block diagram of a receiver using switched diversity technique with three diversity branches	15
1.9	An Arduino based sensor node with humidity sensor and a thermistor.	17
2.1	<i>Left:</i> Fabricated prototype 3D tripolar antenna on top of a wireless sensor node. <i>Right:</i> Example channel loss (i.e., S_{21}) for each of the three elements of the tripolar antenna [1].	21
2.2	Hybrid mesh network topology	23
2.3	Link loss for 50 transmissions with single element and with tripolar antenna systems. Threshold (τ) = <i>Mean</i> - 3 dB.	24
2.4	Dropped packet rates for single antenna element and tripolar antenna networks. Threshold (τ) = <i>Mean</i> - 3 dB.	24
2.5	A tripolar antenna connected to an XBee wireless module and controlled by an Arduino embedded system.	27
2.6	A simple network with end devices and coordinator.	28
2.7	RSSI data for three elements of the tripolar node taken at 50 different positions in the track	30
2.8	RSSI data for 50 transmissions for monopole antenna and tripolar antenna systems. Threshold (τ) = <i>Mean</i> - 3 dB.	30
3.1	<i>Left:</i> Fabricated prototype of single-piece additive manufactured 3D tripolar antenna. <i>Right:</i> Example channel loss (i.e., S_{21}) for each of the three elements of the tripolar antenna [2].	35
3.2	Fig. showing different polarization patterns selected by nodes and routers. Here H and V are the traditional horizontal and vertical in 2D and P is orthogonal to both.	36
3.3	Typical example of data forwarding from source to coordinator for tree-based ZigBee network.	38
3.4	Different phases of polarization selection in a tree-based ZigBee network	39
3.5	Example of available routes for nodes in a ZigBee network in presence of mobile routers.	40
3.6	Different phases of polarization selection for a node in ZigBee network where mobile routers are present.	41
3.7	Tripolar antenna placed inside of a reverberation chamber for channel measurement.	41
3.8	<i>Left:</i> Comparison between dropped packet rates for NM scheme and simple diversity technique, <i>Right:</i> Comparison between dropped packet rates for OPM scheme and simple diversity technique	43
3.9	<i>Left:</i> Power loss comparison between NM and simple diversity technique, <i>Right:</i> Power loss comparison between OPM and simple diversity technique,	43
3.10	<i>Left:</i> Comparison of polarization mismatches between NM and simple diversity technique, <i>Right:</i> Comparison of polarization mismatches between OPM and simple diversity technique.	44
4.1	Block diagram of transmission and reception using tripolar antenna.	52
4.2	Sample network of two routers and five sensor nodes with routers depicted in green and sensors depicted in light blue color.	53

4.3	An illustration of data transmission by sensors and router. Solid circles indicate usage of selection diversity before transmission while empty circles indicate no antenna switching occurred and colors represent different polarizations. <i>Top</i> : Router $R1$ uses conventional selection diversity <i>Bottom</i> : $R1$ uses centrality based selection diversity.	55
4.4	(a): Basic architecture of an IoT network consisting of 50 sensors and 10 routers. Colors represents different polarizations, sizes represents different type of IoT devices. (b): Representation of the network presented in Fig. (a) using DEC. Color coding and size indicates centrality of sensor and router nodes. Less central nodes have smaller size and lighter color compared to more central nodes which have larger size and darker colors.	56
4.5	(a): The number of packets received by routers, plotted against their normalized centrality. We observe that routers which receive more data packets have higher centrality. (b): Comparison between selection diversity and the proposed technique in terms of switching frequency. Routers are plotted in ascending order based on the number of switching. Note that the number of switching is decreased for high scoring routers.	58
4.6	Comparison between selection diversity and the proposed technique for different values of α in terms of (a) packet drop rate and (b) energy consumption rate, for a network consisting of 50 sensor nodes and 10 routers. As can be seen in the figure, for $\alpha = 3$, our proposed scheme has approximately 99% successful packet delivery rate and reduces energy consumption by 13% compared to the selection diversity technique.	59
5.1	<i>Left</i> : A 3D tripolar antenna on top of a commercial sensor node. <i>Right</i> : Channel loss data (i.e., S_{21}) for each of the three mutually orthogonal elements of the tripolar antenna (i.e., V , H , and W) [3].	62
5.2	Block diagram of an HMM-based diversity system. H , V , and W correspond to the three mutually orthogonal antenna elements as well as the three hidden states in the HMM. O_t is the observable state (RSSI) at time t .	66
5.3	Block diagram of HMM states. Observations, O_t , i.e., RSSI values, which are explicit and antenna polarizations (H , V , W), which are hidden.	68
5.4	An example of partitioning RSSI values in three groups Z_1 , Z_2 and Z_3 , where τ is the predetermined threshold. The likelihood that the antenna selects one of the polarizations at each time step under a given observed state is provided in emission probability matrix B .	69
5.5	(a) Utilizing a compact reverberation chamber along with the end node (i.e., IoT sensor) on top of a linear track to create harsh propagation environment (b) Block diagram of the experimental setup used to collect signal strength data from embedded devices enabled with tripolar antenna system.	76
5.6	Empirical CDF of measurement data obtained from horizontal (H), vertical (V), and the third element (W) of the tripolar antenna, where mean values of the RSSI values obtained from three branches are $\alpha = -63$ dBm, $\beta = -61$ dBm and $\gamma = -64$ dBm, respectively	78
5.7	Flowchart of basic operation of the Arduino temperature sensor utilizing the proposed HMM approach	79
5.8	Comparison of empirical CDF among selection diversity, switched diversity, HMM approach and non-diversity techniques when tripolar antenna is used	80
5.9	Comparison between selection diversity, switched diversity, HMM approach and non-diversity schemes in terms of data packet delivery	81
5.10	Current consumption vs time during packet transmission for different diversity techniques	82
5.11	Comparison between selection diversity, switched diversity and the proposed HMM approach in terms of battery energy consumption	82
6.1	Correlation between RSSI values obtained at upper-level node and lower-level node when the intermediate node used vertical (V) polarization.	90

6.2	A block diagram of IoT network with end nodes and routers illustrating upper hop and lower hop node from router R_2 's perspective.	91
6.3	Illustration of an IoT network where router R_2 utilizes channel information from two hops for antenna selection. H , V and W represent the three branches of tripolar antenna and the highlighted elements represent the currently used branch of nodes R_1 and R_3 . Received signal strengths for the hop branches are represented by L_H, L_V, L_W, U_H, U_V , and U_W , where L and U depicts the lower and upper hops, respectively.	92
6.4	Outage probability of Max-Sum (Eq. (30)) and Max-Min (Eq. (44)) scheme for three independent but non-identical Rayleigh branches with mean values (in dBm) as follows: (a) Max-Sum with $\mathbf{E}[l_h] = -61$, $\mathbf{E}[l_v] = -63$, $\mathbf{E}[l_w] = -64$, $\mathbf{E}[u_h] = -62$, $\mathbf{E}[u_v] = -64$ and $\mathbf{E}[u_w] = -65$. (b) Max-Sum with mean - 3 dB (c) Max-Sum with mean + 3 dB, (d) Max-Min (e) Max-Min with mean - 3 dB (f) Max-Min with mean + 3 dB.	99
6.5	Block diagram of testbed setup that utilizes a reverberation chamber to create a severe multipath environment. The fabricated prototype tripolar antenna acts as a transmitter and receiver for the XBee module.	100
6.6	Cumulative distribution function (CDF) plots of RSSI data for three individual antenna elements of the end node (Fig. 6.5) when the router node is vertically polarized, where the mean RSSI values of H , V and W antenna branch are -63 dBm, -61 dBm and -64 dBm, respectively	101
6.7	Diversity gain comparison of Max-Sum and Max-Min with selection diversity (simulated) for different switching thresholds with $\mathbf{E}[l_h] = -61$, $\mathbf{E}[l_v] = -63$, $\mathbf{E}[l_w] = -64$, $\mathbf{E}[u_h] = -62$, $\mathbf{E}[u_v] = -64$ and $\mathbf{E}[u_w] = -65$	104
6.8	Comparison of CDF of signal strength values, which a router receives from the upper-hop router in a forty (40) node four-hop IoT network, for various antenna selection strategies in multipath environment with channel characteristics akin to those from our empirical data set (Fig. 6.6).	105
6.9	Average number of dropped packets for selection diversity, Max-Sum, Max-Min, switched diversity and single element antenna system.	107
6.10	Comparison of antenna branch switching between selection diversity, Max-Sum, Max-Min and switched diversity scheme. Note: switching is not applicable to the single element approach.	108
6.11	Energy consumption comparison of single element antenna and tripolar antenna system while using various diversity schemes.	109

List of Tables

2.1	Percentage of failed packet transmissions	24
2.2	Comparison between empirical and simulated data	31
2.3	Packet delivery statistics for tripolar node	31
3.1	Loss of power due to polarization mismatch	42
3.2	Comparative analysis of NM scheme	44
3.3	Comparative analysis of OPM scheme	45
4.1	Simulation parameters	57
5.1	List of Notations	67
5.2	Calculated HMM Parameters	78
5.3	Gain Comparison Among Various Schemes	80
6.1	Comparison of simulated performance between diversity schemes for various network sizes	110

1 Introduction

1.1 Motivation

The Internet of Things (IoT) will be enabled by the integration of everyday objects and sensors allowing them to collect and exchange information gathered from the environment without necessarily human intervention. Networks consisting of interconnected low-powered autonomous sensors and embedded devices have already shown great potential in home automation, smart grid, environmental and industrial monitoring [4, 5]. However, a major challenge for IoT systems is the need to mitigate multipath fading effects. A transmitted radio signal may be scattered, reflected and attenuated by different objects during propagation resulting multiple copies of the same signal at the receiver end [6]. The phase shifting and interference caused by these waves are known as multipath effect. Multipath fading also depolarizes electromagnetic waves which alters the orientation of the transmitted wave and transforms energy to other orthogonal planes from the original plane [7]. It has been shown that approximately one in every five transmitted message can be lost or received incorrectly due to signal strength fluctuations resulting from severe multipath fading [8]. Retransmitting data packets would prompt the IoT device to remain active longer, require more transmit power, and increase latency (delay) of the overall network. Since most IoT devices are battery powered and more than two-thirds of their energy is spent for sensing, transmission and reception purposes [9], mitigating packet loss and lowering energy consumption is crucial for IoT networks.

Polarization diversity antenna with two or more branches have been researched extensively due to their ability to mitigate multipath fading and depolarization effects [10, 11]. In harsh propagation environments, the wireless link for each branch of the antenna becomes sufficiently decorrelated and the probability that all branches will experience deep fading simultaneously becomes very low making polarization diversity an effective mechanism to combat the fading. Additionally, the compact size of the polarization diversity antenna due to the colocated antenna branches provides added advantage in seamlessly integrating the antenna with miniature embedded devices. Although closed form analytical solutions such as deriving bit error rate, outage probability, etc., showing the efficiency of the multi-branch antennas are available in literature [12, 13], performance evaluation of such antennas, particularly through experimental setup has received less attention. In a harsh propagation environment, which changes randomly, the fading response are statistically independent and consequently, the signal power at different branches varies over time thereby motivating a means to choose the antenna element that satisfies the application requirement during transmission and

reception. Using optimal selection strategy for multi-element antenna leads to better diversity gain, which improves the signal-to-noise ratio at the receiver and increases wireless link resilience. Additionally, improvement in diversity gain also reduces packet retransmission rate and improves energy efficiency and lifetime of the IoT network.

Most of the existing antenna diversity techniques require complex calculations, large memory [14], and sometimes external hardware [15] to exploit antenna diversity, which is not suitable for existing or envisioned IoT devices due to resource limitation and low energy. Developing adaptive algorithms to utilize polarized signals received at the antenna while taking into account of the restrictions imposed due to low resource of the IoT devices can improve overall performance of the IoT networks significantly.

1.2 Background

In this section, the overview of some fundamental concepts and background material that have been largely used throughout this dissertation is provided.

1.2.1 Internet of Things definition and applications

Internet of Things (IoT) can be described as a network of interconnected things or devices that enables seamless machine-to-machine and human-to-machine communication in a continuous basis [16–18]. IoT consists of spatially distributed sensors, actuators with routers, which can communicate with each other using wireless links, to monitor and produce sensory data based on real-time events. The low cost sensor nodes, with or without data forwarding capabilities, act as end-nodes and connects to router to facilitate information gathering and decision making. The sensory data is forwarded to a remote base station or to remote server in cloud for data collection, data analysis, and controlling these devices in real time. Fig. 1.1 depicts a typical IoT architecture with multiple routers and end nodes.

IoT aims to integrate human beings with their surroundings through numerous context aware and responsive IoT devices, which opens door for diverse applications in different domains. IoT applications range widely from automation such as industrial [19] and automotive control systems [20] to energy efficiency such as, smart grids [21] and residential energy control systems [22]. Besides, in recent years interest has grown on IoT based healthcare application for personal health monitoring, patient support and fitness programs [23, 24]. Advances in sensor technology have made it convenient to use IoT for environmental and agricultural purposes [25, 26]. Among some of the existing

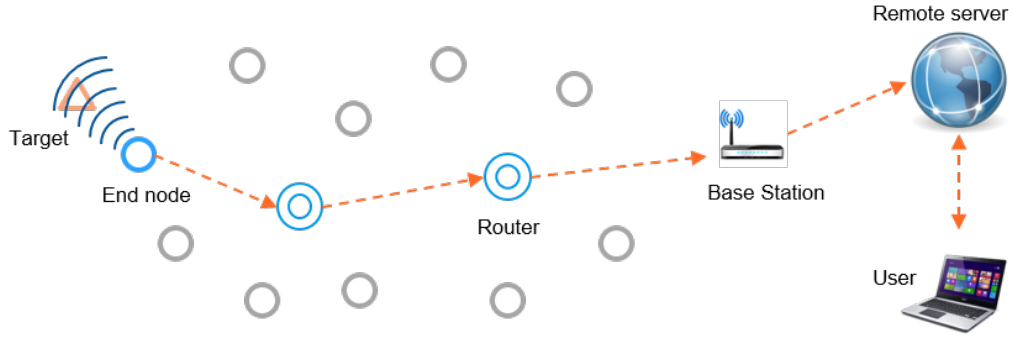


Figure 1.1: Typical example of an IoT network. End nodes forward data to nearest router to route the data to the base station.

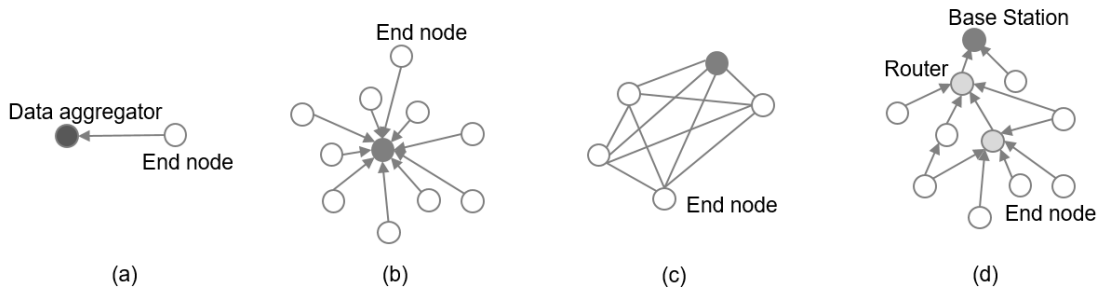


Figure 1.2: Example of various topologies used in IoT networks: (a) point-to-point, (b) star, (c) mesh and (d) hybrid mesh topology.

environmental applications of IoT are pollution monitoring [27], wildfire surveillance [28], and water quality monitoring [29]. More recently, researchers have been developing IoT based solutions for traffic monitoring [30], underground mining [31] and structural health monitoring [32]. The growing interest on miniature sensor devices and their expanding capabilities will inspire many other useful applications in the years to come.

1.2.2 IoT network topologies

While IoT devices can be used in isolation depending on the application type, integration of multiple devices in higher-level topologies are used to deliver real-world applications. For wireless communication, network topology refers to the layout of the network which defines how a network communicates with different devices [33]. IoT devices can be deployed using either random or a predetermined strategy. In a predetermined topology, the routes are determined before they are needed and individual nodes are aware of the relative locations of the neighbors [34]. While in random deployment, nodes are unaware of the topology and discover their neighbours during routing [35]. IoT networks are built using point-to-point or multi-level based configurations:

- Point-to-point topology: This is the simplest topology which connects two end devices, for

example, a single sensor node and a smartphone, as shown in Fig.1.2(a).

- **Star topology:** In small IoT networks, where devices and the base station are in close proximity, the end nodes can communicate directly with the base directly without any repeater node [33]. Fig. 1.2(b) demonstrates how all data traffic flows through the base, which acts as a central node. A personal area network where a smartphone gathers data from indoor IoT devices, is an example of such topology.
- **Mesh topology:** Most IoT applications require substantial number of devices to be deployed to cover large area, where base is outside of the communication range of the end nodes. In such cases, nodes establish communication path from source to base through multiple router nodes which acts as a repeater node in multi-hop fashion [36]. As shown in Fig. 1.2(c), in a fully connected mesh network, each device is connected with every other device, which is redundant and difficult to realize in large IoT networks. While hybrid mesh networks (Fig. 1.2(d)), utilizes sparse connections to reduce redundancy and easier to install.

For large-scale IoT networks, such as industrial IoT and smart grids, hybrid mesh networks enables increased coverage and seamless connectivity by allowing autonomous nodes to act routers and hosts simultaneously in a self-organizing manner [37]. The energy efficiency, reduced routing overhead, and better adaptability to frequent topology changes offered by hybrid mesh networks encouraged us to adopt such topology for our research [38,39].

1.2.3 Routing protocols for IoT networks

Routing protocol decides data transmission path from source to destination. Since IoT consists of devices with limited power supply, limited memory and little computation capability, routing protocols are mostly designed to be energy efficient and non-redundant. Although the topology of the IoT networks are mostly static, some applications consider mobile routers or sink nodes which affects the network structure and subsequently the routing paths need to updated dynamically. There are many ways to classify network architecture and routing [40,41]. Depending on network structure, routing protocols can be classified in four sub-categories, as shown in Fig. 1.3, which we describe here briefly [42].

- **Location based:** In this category, the location of each nodes, which is determined either by Global Positioning System (GPS) or localization techniques, is used during routing of the

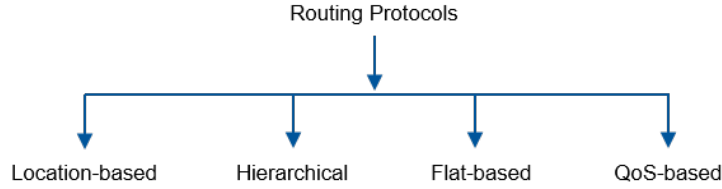


Figure 1.3: Categories of routing protocols based on IoT network organization.

sensory data. Examples of such techniques are discussed in [43] and [44], where geographic information about neighboring regions are used to deliver data.

- **Hierarchical:** In a hierarchical network, nodes play different roles according to their classification. The nodes with high energy level and high capability can be assigned as router to receive and forward data packets from other nodes, while the nodes with a lower energy level can be specified as end nodes with no data forwarding capability. Commonly used protocols for hierarchical network architecture, as presented in [45] and [46], uses cluster-based approach to reduce power consumption of IoT devices.
- **Flat-based:** In flat-based network topology, every node is considered to have same functionality and uses flooding or broadcasting to deliver data. A node simply broadcasts data to all the nearest neighbor nodes, who then repeat the same process until the data is received at the destination. To address the data redundancy and energy consumption, other enhanced version of flat-based network architecture such as directed diffusion protocol [47] and negotiation based protocol [48] have been proposed which reduces redundant data.
- **QoS-based:** While many routing protocols for IoT networks prioritizes to minimize energy consumption, for some applications, for example, smart distribution grids [49], real-time video streaming applications [50], performance metrics such as end-to-end delay and throughput is also important. QoS based protocols use multi-path approach to establish routes between nodes considering remaining energy of a node, cost of the routing path (related to energy and/or delay) and then select a routing path based on QoS and packet priority.

To realize cost-effective IoT applications, large scale hybrid IoT networks are considered with a reduced number of routers which will be beyond the wireless transmission range for most of the power constrained IoT devices [51]. Hierarchical multihop routing allows IoT users to serve as a potential intermediate relaying node for their nearest neighboring devices and reduces routing overhead by eliminating the requirement of maintaining a fixed routing table [37]. Furthermore, hierarchical routing protocol achieves higher network bandwidth by transmitting data through multiple short

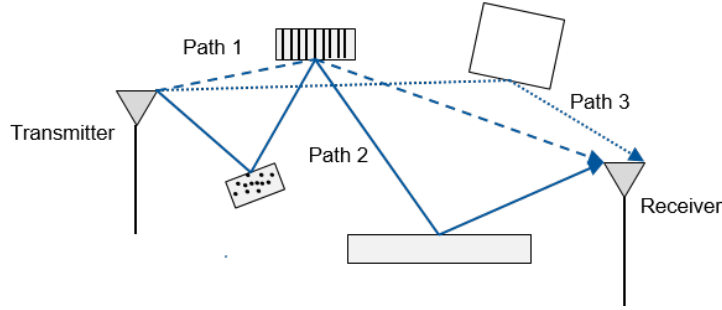


Figure 1.4: Reflected, scattered multipath components received at the antenna.

hops to the final destination, and hence is perfectly suitable for hybrid IoT network architecture that we considered here for our work [38].

1.2.4 Multipath Fading

In wireless communication, fading refers to the attenuation of the transmitted signal power due to changes in transmission medium or paths [38]. The loss of signal power due to fading results in reduced signal-to-noise ratio (SNR) and affects the quality of wireless links. During propagation, a radio signal can reach the receiver antenna from the transmitter antenna via two or more different paths, which is known as multipath propagation [52]. When a signal propagates through the transmission medium or radio channel, it can be reflected, refracted or diffracted by different interfering objects such as buildings, cars and wall, etc. As shown in Fig. 1.4, the resulting multipath signal components have distinct attenuation in power, delay, and angle of arrival, which lead to shifting in phase with respect to the line of sight path at the receiver. At the receiver, which sums the transmitted and multipath signals together, interference between the multipath components can be constructive or destructive, and often causes degradation of the quality of communications. The distortion of the radio signal and drop in signal-to-noise ratio seen at the receiver, is referred to as multipath induced fading. Different transmitted signals may experience distinct fading effects depending on the relation between signal properties (such as amplitude, phases etc.) and channel characteristics during multipath propagation.

Another concept related to fading is the coherence time which is a measure of time duration over which impulse response of the channel becomes decorrelated from the previous value. Typically, IoT devices are expected to send sensory data periodically, and hence, two different transmissions from same node arriving at the receiver with a time separation greater than the coherence time are affected differently by the channel. The receiver may take advantage of the varying channel conditions using antenna diversity to mitigate the multipath induced fading. The most common

type of fading used in the literature for IoT networks is flat fading, where the spectral features of the transmitted signal are conserved at the receiver but the received signal strength fluctuates with time because of the variations in gain of the channel caused by multipath [53]. Rayleigh distribution is frequently used to represent the statistical time varying properties of the received envelope of a signal that undergoes flat fading. For our work, we considered that IoT devices are deployed in an environment where channels exhibit Rayleigh fading, which we describe next.

1.2.5 Rayleigh fading model

Rayleigh distribution is a standard statistical model that is used to describe multipath fading effects where no direct line of sight content is present. Rayleigh channel model is widely used in wireless communication due to mathematical convenience and its excellent conjecture of many practical scenarios. The distribution depends only on mean received power, which can be derived either from measured data or various prediction methods. In Rayleigh fading, the magnitude of the received complex envelope $\alpha(t)$ has the Rayleigh distribution [53]

$$p_{\alpha}(r) = \frac{r}{\sigma^2} \exp\left(-\frac{r^2}{2\sigma^2}\right) \quad 0 \leq r \leq \infty \quad (1)$$

where, r , σ and σ^2 are the received signal amplitude, the rms value of the received signal strength and time-averaged power of the received signal before envelope detection, respectively. The corresponding cumulative distribution function is

$$P(R) = Pr(r \leq R) = 1 - \exp\left(-\frac{R^2}{2\sigma^2}\right) \quad (2)$$

The corresponding squared of the received complex envelope is exponentially distributed at any time t with density [54]

$$p_{\alpha^2}(r) = \frac{1}{\gamma} \exp\left(-\frac{r}{\gamma}\right), \quad \gamma \geq 0 \quad (3)$$

where $\bar{\gamma}$ is the mean power. At any time, the squared-envelope is proportional to the instantaneously received signal power at time t . Fig. 1.5 demonstrates received signal level power seen at the receiver which follows a Rayleigh distribution. In wireless communication, the Rayleigh distribution represents the worst case scenario with no line of sight signal component present, which helps designing robust systems. When planning for IoT networks, Rayleigh fading model are preferable as it provides a great approximation for large number of practical scenarios [6]. Additionally, it is mathematically convenient to derive probabilities and other parameters with Rayleigh distribution

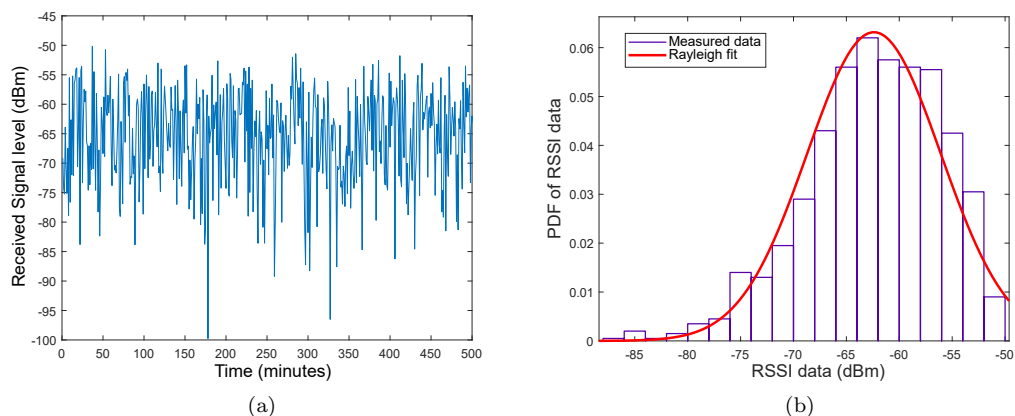


Figure 1.5: *Left*: Sample sensor data collected over time in an harsh multipath environment using single branch antenna where y-axis is showing the received signal power, *Right*: Histogram plot of the received signal level along with a fitted Rayleigh curve.

since it depends only a single parameter, which is the mean received power.

1.2.6 Polarization and depolarization

When incorporating an antenna into small wireless sensor devices, it is important to consider the desired application of the device, specially, the environment where the device will be deployed. An antenna with a particular polarization will obtain improved signal strength and performance gain when receiving signals aligned in orientation and polarization of that antenna and hence, will not be effective while receiving signals with different polarization. Here we discuss how polarization is determined and depolarization of the radio signal.

1.2.6.1 What is polarization? An electromagnetic wave's electric and magnetic field, which are perpendicular to each other, travel in single direction of the wave with no field variation between them. An electromagnetic wave's polarization refers to the direction of the electric field component or the plane in which the electric wave vibrates. There are several types of polarizations in antenna systems which we discuss briefly below [55]:

- **Linear polarization:** In a linear polarization, the oscillation of the electromagnetic wave's electric field is in one plane. Depending on the electric field vector, linear polarization can be vertical or horizontal. For example, a horizontally polarized wave has oscillating electric field parallel to the earth's surface while traveling along a direction. Conversely, when the electric field vector is transverse to the direction of the wave propagation, it is said to be vertically polarized. Fig. 1.6 illustrates different kinds of polarization.

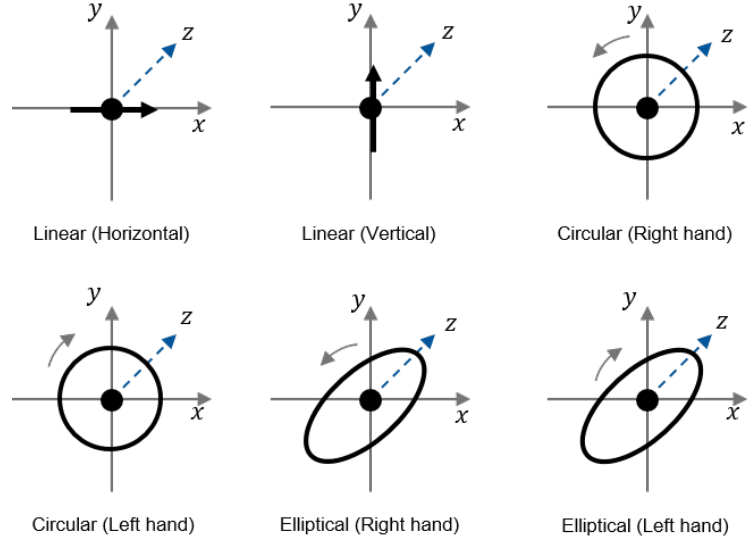


Figure 1.6: Different types of polarization of an electromagnetic wave

- Circular polarization: In circular polarization, the electric field vector will have both x and y components and the tip of the vector will form a circle (i.e., rotating electric field) as the signal propagates. If the rotation is clockwise then it is called Right Hand Circular Polarization (RHCP) and if the wave rotates counterclockwise then its is Left Hand Circularly Polarization (LHCP).
- Elliptical polarization: When the electromagnetic wave consists of two electric field components that are perpendicular to each other and different in magnitude, then the curve traced at a given position as a function of time will be an ellipse.

In our work, we considered IoT devices equipped with either single branch or multiple branch antenna systems. The single branch antenna has only one linearly polarized antenna branch with either vertical or horizontal polarization. On the other hand, a tripolar antenna system consists of three, mutually orthogonal and linearly-polarized elements with vertical polarization, horizontal polarization and a third polarization which is perpendicular to the other two.

1.2.6.2 Depolarization The partial scattering of an electromagnetic wave during its propagation over an environment consist of reflectors and retarders is known as depolarization. In this process, the polarization of a wave changes as the original plane of polarization losses electromagnetic energy which appears in opposite plane. For example, a horizontally polarized radio signal may have both vertical and horizontal components during propagation due to depolarization effect. The ratio of the consequential horizontal to vertical components is used to measure depolarization, which

is referred to as cross-polar discrimination, or XPD. Moreover, in a highly cluttered environment, depolarization causes a three-dimensional effect where a signal of a given polarization is transformed into all three planes [56].

1.2.7 Forms of antenna diversity

The idea of diversity is to use multiple channels to increase the signal to noise ratio where the propagation environment is affected by random fading losses. The use of multiple replicas of the signal reduces the probability that all of the replicas will see deep fading simultaneously and thus, effectively mitigates performance degradation due to multipath fading. Diversity can be achieved in several ways and each has its advantages and disadvantages. Next we discuss the most common antenna diversity methods [6].

1.2.7.1 Time diversity Time diversity technique leverages the time variance property of wireless propagation channel and transmits a symbol at different times to achieve decorrelation [57]. For sufficient decorrelation, the temporal distance must be at least half of the maximum Doppler frequency [58]. The simplest form of time diversity can be achieved by repetition coding, where the signal is repeated several times with intervals long enough to make the signal uncorrelated [59]. While repetition achieves diversity, it causes redundancy and loss of spectral efficiency. Another approach is using automatic repeat request where receiver sends acknowledgement message to the transmitter indicating whether the received signal is acceptable or not [60]. If the received signal does not have sufficient quality, the transmitter will resend the message after a certain wait period to achieve decorrelation. While this technique is more efficient than repetition coding, a feedback channel is required between the receiver and transmitter to send acknowledgement messages. An advanced and popular version of time diversity is combination of interleaving and forward error correction (FEC) coding where a transmitter transmits different symbols of a codeword at different times to ensure that at least some of them are received with sufficient quality [61]. When FEC is applied, a loss of one data packet is dispersed over multiple blocks of data interleaved into packets that could be recovered and reconstructed by the receiver. However, the available rate for sources decreases due to the increase of data transmission rate due to FEC approach.

1.2.7.2 Frequency diversity Frequency diversity uses multiple replicas of information signal over several frequency bands [62]. Frequencies that are further apart than the coherence bandwidth will experience uncorrelated frequency response and thus at least one will have strong signal. Instead

of repeating the same information at two different frequencies, it is spread over a large bandwidth to ensure that the small parts of the transmitted information are carried by different frequency components. The diversity is then achieved at the receiver, which resolves the multipaths caused by the inherent diversity in frequency-selective channels [63]. Since only one symbol can be transmitted in every delay spread, the diversity gain achieved by frequency diversity is nullified by consumption of extra bandwidth. Frequency diversity also suffers from inter-symbol interference (ISI), where delayed replicas of previously transmitted symbols interfere with the current symbols. Several approaches exist that address the mitigation of ISI while exploiting frequency diversity in a wideband channel. One such approach leverages linear and non-linear processing at the receiver to mitigate ISI, which enables the receiver to detect the current symbol with very low interference from the other symbol and have lower complexity [64]. Another technique, known as direct sequence spread spectrum, modulates the information symbols by a pseudonoise sequence and transmit them at very low rate over a bandwidth that is much larger than the data rate [65]. Although this technique simplifies the receiver structure, it also reduces the total degrees of freedom of the system. Orthogonal Frequency Division Multiplexing (OFDM) is the most common frequency diversity technique where ISI channel is converted to non-interfering orthogonal sub-carriers by using transmit precoding across the symbols [66]. While all the different techniques can increase the bit error rate and decrease the effects of fading, the use of frequency diversity requires the channel to be frequency selective.

1.2.7.3 Space diversity Since multipath fading changes rapidly over space, the received signal at antennas across space can have a low correlation coefficient. Space diversity is achieved by placing multiple antennas far apart such that the channel gains between different antenna pairs become independent [67]. The required separation between antenna elements not only depends on the local scattering environment but also on the carrier frequency. Mobile devices in a cellular system are generally near the ground with many scattering objects around which decorrelates the channel over shorter spatial distances. Additionally, the waves are assumed to be received by the mobile receiver from all directions, where multipath components (either constructive or destructive interference) are apart approximately by $\lambda/4$ [68]. Thus, for standard cellular systems at the 1800 MHz band the distance between antenna elements is about 4 cm, which can be achieved readily [69]. However, for base stations in cellular systems, all the incident waves are from one direction and the arrival of incident waves are not uniform. Therefore, the correlation coefficient will be much higher for the base stations resulting in further increase of antenna spacing to obtain sufficient decorrelation. Numerical evaluations of the correlation coefficient as a function of antenna spacing (Figure 13.1, [6]) illustrate

that antenna spacing has to be on the order of 2–20 wavelengths for angular spreads between 1° and 5° in order to achieve decorrelation. The results also implied that the required antenna spacing is determined by the rms angular spread and the impact of the shape of the angular power spectrum is insignificant. While space diversity is widely used for cellular systems, it can not be applied to compact IoT devices where space is very limited.

1.2.7.4 Polarization diversity Most channel models that analyze propagation of transmitted and received waveform consider vertical polarization. Transmitted signal from a vertically polarized antenna gets scattered and diffracted resulting in energy being transferred into the horizontal polarization component before reaching at the receiver antenna [70]. Since the amplitude and phase of the depolarized signals with opposite polarizations will be dissimilar due to different reflection coefficient, they can be considered to be nearly uncorrelated. These signals can be processed separately using a dual-polarized receiver antenna with vertically (co-polarized) and horizontally (cross-polarized) polarized element, which is known as polarization diversity [71]. Depending on the deployed environment, the horizontally polarized signal can be some 3–20 dB weaker than the vertical signal and vice versa. Various antenna arrangements have been proposed in order to achieve polarization diversity. The antenna elements can be horizontal/vertical or $\pm 45^\circ$ slanted ensuring that the antenna elements are orthogonal to achieve uncorrelated signals [72]. Polarization antenna can also be reconfigured in a way such that it can switch between linear and circular polarization [73]. Experiments with dual-polarized base station antenna with various configurations showed that the diversity gain received from polarization diversity is approximately 1 dB less than the gain received from space diversity [74]. The study also revealed that the performance of polarization diversity is strongly dependent on the environment where the receiver is deployed and the inclination angle of the transmitting antenna. For example, when the terminals were deployed in sub-urban areas, which are less densely populated than cities, results were identical for both space and polarization diversity technique. While historically polarization diversity antennas have been favoured for mobile radio base stations, the collocated positions of the antenna branches allows the antenna to be compact and makes it suitable to integrate with embedded devices used in IoT networks.

1.2.7.5 Antenna diversity used in this work Performance of wireless communication systems can be enhanced by utilizing diversity techniques [75]. Spatial diversity and polarization diversity are the most commonly used techniques among all other diversity techniques, due to the simplicity of their implementation. Although spatial diversity is capable of realizing great range improvements,

it comes at the cost of substantial separation between the antennas, making it impractical to use for miniature low-cost IoT devices. On the other hand, polarization diversity offers diversity by leveraging multiple antenna elements with separate vertically and horizontally polarized receivers and provides a simple and effective way to reduce the fading effects in harsh wireless propagation environment. Furthermore, polarization diversity can achieve up to three or more additional degrees of diversity by exploiting three possible components of the electric field and magnetic field [6], which can be utilized to combat multipath fading efficiently. Considering the benefits of compact size and performance superiority, we focused on polarization diversity antenna systems at the transmitter and receiver end for our work.

1.2.8 Diversity combining techniques

To take advantage of antenna diversity, we need to combine two or more independent and uncorrelated faded signals available at the diversity branches of the antenna. Diversity combining, which increases SNR or the received power of the signal, can be applied for both transmission and reception to choose the optimum signal. The signals from diversity branches can be combined coherently before detection (i.e., pre-detection) or after detection (i.e., post-detection). We now describe four diversity techniques that are most used in wireless communication.

1.2.8.1 Selection Combining Under selection combining, the receiver monitors all the diversity branches and selects the antenna branch with the highest SNR, i.e., the diversity branch with the strongest instantaneous signal-to-noise ratio (SNR), for signal reception [76]. Thus, selection combining ensures the best possible performance among the other diversity schemes that uses only one receiver chain but requires monitoring the SNR on each branch simultaneously. Additionally, selection combining can be used with either coherent or differential modulation since it uses a single branch output and does not require co-phasing of multiple branches [77]. Fig. 1.7 illustrates the technique through a block diagram. In the literature, several approaches have been considered to analyze the performance of selection combining under various fading conditions. For example, [78], [79] studied the performance of selection combining for independent Rayleigh, Rician, and Nakagami- m fading channels. However, the fading among the channels can be correlated, which will degrade the diversity gain of the system. Various selection diversity based models have been proposed corresponding to correlated channels with specific fading conditions [80–82]. In [80], the authors studied the effect of correlation and fading parameter on an N-order conventional selection diversity system under the assumption that diversity branches experience Nakagami- m fading conditions. The

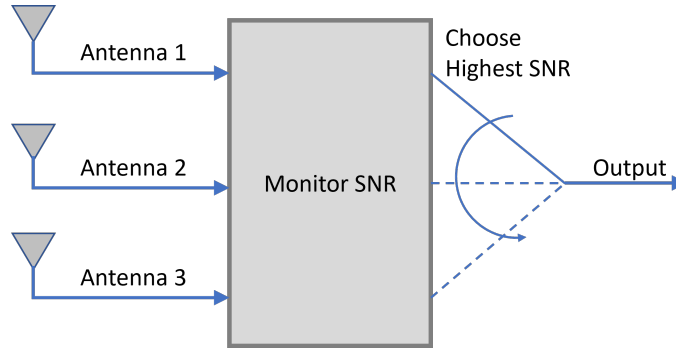


Figure 1.7: Block diagram of selection diversity with three antenna branches

authors derived the joint distribution of the output of a dual-diversity selection combining receiver and obtained the average probability of error by averaging the conditional probability of error over the distribution of the output of the combiner. Later, the authors in [81] derived an analytical expression of the switching rate for correlated dual selection diversity combining by considering balanced and unbalanced correlated Rayleigh channels that are identical but nonindependent. An approach to the performance analysis of a selection-diversity system over correlated Rician fading channels is presented in [82], which derived the closed-form expressions of converged sums for both outage and average error probabilities. However, most of these approaches are limited to the case of dual diversity and do not consider the space or energy constraint of low-cost embedded IoT devices.

1.2.8.2 Switched Combining Monitoring all diversity branches is infeasible for most of the applications due to implementation complexity and energy consumption. Switched diversity monitors the currently used branch only and switches to other branches when signal quality falls below a certain threshold [83]. Since antenna branches of a diversity antenna experience independent fading, the switching to a better branch lead to certain amount of diversity gain. Many variants of switched diversity have been proposed depending on how an antenna branch during switching and also depending on how the threshold is determined over the past four decades. For example, Blanco and Zdunek proposed switch-and-stay combining where switching depends on two consecutive channel quality estimates, and switching between diversity branches occurs only when a downward crossing of the predetermined threshold is identified [84]. Later, Abu-Dayya and Beaulieu [85,86] introduced threshold based switched diversity technique, where an antenna switches branch only when the current signal level or SNR is below the predetermined threshold. In this case, the receiver uses only the current channel estimate and uses a single receiver chain only, which is simpler to implement. The structure of typical threshold based switched diversity receivers is shown in Fig. 1.8. In [87] and [88], the authors analyzed the performance of switched diversity based approach in conjunction

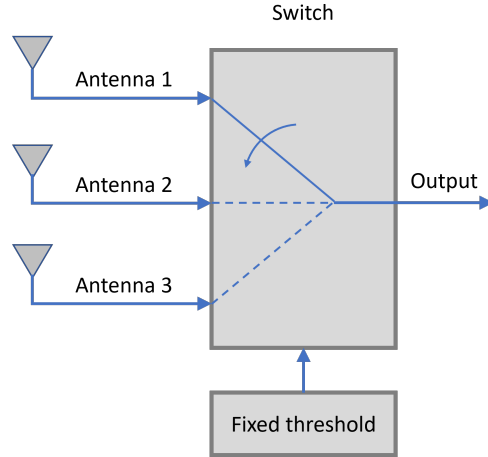


Figure 1.8: Block diagram of a receiver using switched diversity technique with three diversity branches

with binary non-coherent frequency shift-keying (BFSK) for correlated diversity branches over the Rician and Nakagami- m fading environments. The outage probability and average error-rate performance of the switched diversity technique for predetermined and adaptive switching threshold have been analyzed in [89] and [90], where the authors considered general fading/branch scenarios along with various modulation schemes. Selecting an optimal switching threshold is crucial for switched diversity. Two different approaches exist for selecting switching threshold in the literature, one based on analytical derivation [91], and another based on the minimum receivable power by the actual antenna [92]. While switched diversity offers simpler implementation and reduction of complexity, the diversity gain achieved by selection diversity is better than switched diversity. Also, the existing works on switched diversity mostly considered dual-branch antenna scenarios and have not addressed a network-wide analysis of such techniques.

1.2.8.3 Maximal Ratio Combining (MRC) In this technique, signals received at different antenna branches are co-phased and summed using optimal weighting by using summing circuits. The weight factor, which is proportional to the SNR of the received signal, amplifies the strong signal and attenuates the weak signal to maximize the combiner output SNR [93]. For an efficient communication system that uses MRC, it is required to estimate complex channel gains as well as to quantify the effect of noisy channel estimates on the error probability performance. Several studies have addressed the performance of MRC with noisy channel estimates. The performance of MRC on independent Rayleigh-fading channels was analyzed through a pilot signal, which is decorrelated from the data signal, in [94]. In [95], the authors derived the pdf of the SNR at the output of MRC for Rayleigh-fading channels. Additionally, the outage probability of MRC and the density function

of the MRC combiner has been extensively analyzed for other fading channels models such as Rician and Nakagami- m fading [96,97]. Recently, the authors in [98] obtained the bit error performance of MRC for dual-branch diversity system under the assumption of one dominant cochannel interference in a Rayleigh fading environment. While MRC achieves best performance, most of the studies are constrained to dual branch antenna systems only. Furthermore, the requirement of phase correction and multiple receiver chain makes MRC unsuitable for low-complexity, low-powered IoT devices.

1.2.8.4 Equal Gain Combining (EGC) Similar to the MRC, the EGC technique co-phases the received signals and then adds them together. Unlike, MRC there is no weighting of the signals. By adjusting the phase for each received signal and adding the in-phase vectors, EGC achieves better performance than selection diversity [99]. Various analytical techniques have been proposed to analyze the performance of EGC for different fading channel conditions (e.g., [100–104]). In [100], a frequency-domain EGC scheme was proposed with an aim to improve the receive performance of a single tap receiver or a minimum mean square error (MMSE) receiver with distributed antenna systems (DAS). Fucheng *et al.* investigated a synchronous fast-frequency-hopping M -ary frequency shift keying system with non-coherent envelop detection over Rayleigh fading channels. The proposed algorithm selects multiple most likely estimations based on the EGC outcome and then uses maximum likelihood detector to make final decision [101]. Recently, the authors in [102] derived error-rate formulas based on EGC with BPSK/QPSK signalling over Rayleigh fading channels with independent diversity branches using Gauss hyper-geometric functions. Additionally, hybrid schemes that combines EGC with other existing diversity scheme such as selection or switch diversity have also been studied for different channel conditions [103] and [104]. However, most of the works in the literature considered EGC for cellular systems as it requires additional circuitry and complex algorithms for detection, which is incompatible for IoT devices.

1.2.8.5 Diversity technique used in this work In the context of low complexity diversity reception, conventional selection diversity as well as switched diversity are promising enabling technique for low powered IoT devices due to low cost implementation. While selection diversity continuously selects the branch with the largest signal-to-noise ratio (SNR) among the available branches, the hardware requirement of multiple RF-chains and energy consumption with continuously monitoring each branch is not suitable for energy constrained IoT devices, especially as the number of branches grows [6]. An alternative approach for IoT devices is switched diversity which offers a cost-effective technique by using single RF chain to monitor a particular branch and switches to an-

other branch when the signal strength drops below a predetermined threshold. However, the power gain achieved by the conventional switched diversity technique is less than selection diversity and the complexity of switched diversity increases when the number of antenna elements extends more than two due to the time required to sense all the available diversity branches. Motivated by these findings, we focused on developing specific implementations of switched diversity technique which will provide increased link reliability and energy efficiency compared to the conventional switched diversity.

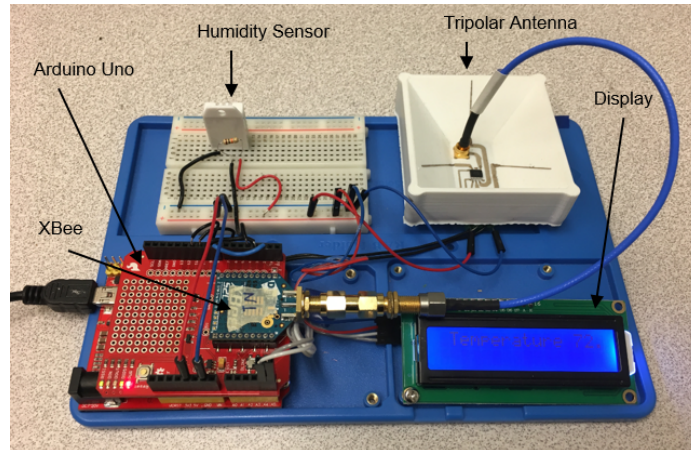


Figure 1.9: An Arduino based sensor node with humidity sensor and a thermistor.

1.2.9 Tripolar antenna

When an IoT device equipped with a multi-element antenna is deployed in a harsh environment, for example, inside of a factory, it will experience distinct fading conditions at different antenna branches [105]. A tripolar antenna, with three orthogonal antenna elements has been presented in [106], where through simulated and empirical data the authors showed how tripolar antenna can mitigate the multipath fading effects using antenna diversity. The proposed antenna, which can be readily integrated with sensor devices, has three $\lambda/4$ monopoles tuned at 2.4 GHz. Using 3D printing and additive manufacturing techniques the antenna branches are at an angle of 45° relative to a vertical antenna to achieve orthogonality which enables them to receive signals with any polarization (X , Y , or Z). Fig. 1.9 demonstrates an Arduino based sensor node with XBee wireless module and tripolar antenna.

1.3 Research Objectives and Organization

The main research question addressed in this thesis was: given the harsh wireless propagation environment experienced by resource-constrained IoT devices, how can multi-branch diversity antenna selection techniques provide high link reliability and increase energy efficiency in such diversity-rich environment.

The specific objectives of this research were to: (1) conduct comparative analysis of tripolar antenna and single element antenna based on single point-to-point link using simulations and experimental data; (2) conduct end-to-end network assessments for existing diversity techniques using prototype tripolar antennas, including developing three-branch antenna diversity techniques that takes into account the network structure and routing protocols; (3) conduct a probabilistic antenna selection approach and determine its suitability by varying threshold and leveraging over-the-air testing data; and (4) develop and assess the performance of dual-hop based antenna selection techniques compared to single hop based techniques. The dissertation is organized as seven chapters. Chapters 2-6 are presented as published or submitted for publication. Chapter 7 presents the conclusions and avenues for future work. Each Chapter's goal is summarized as follows.

- The efficacy of using polarization diversity with multi-branch antenna has received much attention due to the high diversity gain and compact size of the antenna elements. However, demonstrating the performance in real-life scenarios through experiments has not been studied in detail so far in the context of IoT. In Chapter 2, the performance of a 3D printed tripolar antenna system is analyzed based on single point-to-point link performance by leveraging an Arduino platform with a XBee wireless module and highlights the impact of tripolar antenna in mitigating multipath effects.
- In Chapter 3, we conduct experiment on the impact of tripolar antennas from a network-wide perspective. While existing works focus on point-to-point links only, we demonstrate that a network-wide consideration is necessary as selection of antenna branch effects the signal power of its neighbor nodes that exchange data packets with the node. Through simulation and empirical results, it was illustrated that polarization aware antenna selection techniques can improve link reliability and increase network lifetime.
- The results obtained in Chapters 2 and 3 motivated development of diversity technique that exploits the IoT network architecture. Chapter 4 focuses on determining crucial routers of a network using 'centrality' measures by leveraging Complex Network theory. The representation

of an IoT network using graph objects and subsequent identification of highly congested routers, enables implementing adaptive antenna selection where antenna switching varies according to the load of the router and thus reduces excessive antenna switching.

- In Chapter 5, a switched diversity technique based on Hidden Markov model (HMM) is developed in consideration of the limited capabilities of the IoT devices. The proposed HMM coordinated approach utilizes empirical data and determines the best antenna branch for switching when the current antenna branch's signal quality drops below a certain threshold under uncorrelated, independent and non-identical Rayleigh fading conditions. Both analytical and simulation results show that the proposed approach can reduce unnecessary switching and improve diversity gain of IoT devices deployed in harsh wireless environments.
- The diversity gain provided by multi-branch antennas has motivated the exploration of various diversity schemes analytically by means of deriving expression for bit error rate and outage probability. There is, however, little knowledge about end-to-end network performance of these diversity schemes. Chapter 6 discusses a switched based diversity technique that considers neighbor nodes antenna configuration status and adapts antenna selection accordingly. The study explores the impact of the multi-branch polarization antenna from network-wide perspective and demonstrate that using local antenna configuration knowledge leads to better antenna selection for the IoT devices.
- Conclusions and avenues for future work are summarized in Chapter 7.

2 Improving Network Reliability Using Tripolar Antenna

Foreword

This chapter studies the performance of a tripolar antenna in harsh wireless propagation environment likely to be seen by practical IoT devices. Section 2.1 is the work as presented at the *2018 Antennas and Propagation & USNC/URSI National Radio Science Meeting*. In this work, we introduce a hybrid mesh wireless network simulator, explicitly designed for IoT applications operating at 2.4 GHz and then discuss how it realizes multitude of links for single element and multi-branch antenna in different instances. Thereafter, performance comparison between single element and the tripolar antenna is provided based on simulation results which leveraged empirical channel data measured in slowly-varying, severe multipath environment. However, relying on simulation heavily can be a problem as modeling precision worsens in a complex network with multiple interconnected users or devices including many variables not associated with the output. Therefore, to verify the simulation results, we extend the work by building a testbed with two prototype sensor devices equipped with tripolar antennas inside of a reverberation chamber. Section 2.2 presents the paper published at the *2018 IEEE Wireless and Microwave Technology Conference*, which compares the empirical data obtained from 3D printed tripolar antennas with the simulation results. Experimental results show that the tripolar antenna is capable of maintaining the same packet delivery ratio (i.e., three times better than monopole antenna) both under static and dynamic conditions with various antenna switching rates.

2.1 Improving Reliability in Hybrid Mesh Networks with Tripolar Antennas

2.1.1 Abstract

The work herein demonstrates how hybrid mesh network reliability can be improved by leveraging the channel diversity enabled by a compact, tripolar antenna. Specifically, through simulation, we show that a tripolar antenna can reduce packet drops to a third of that of when a single element antenna is used. These results were achieved assuming a slowly-varying, but highly-multipath, propagation environment such as those that may be expected in industrial IoT settings [2].

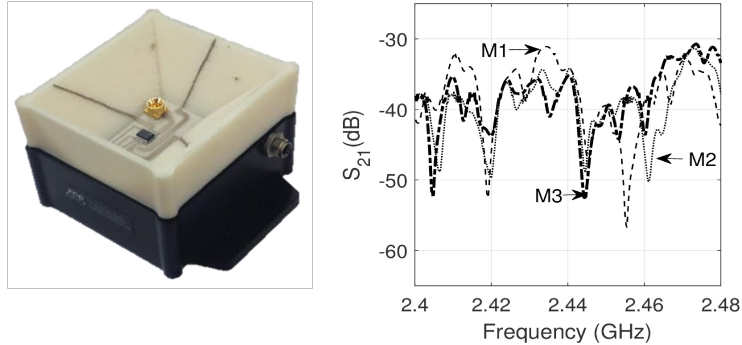


Figure 2.1: *Left*: Fabricated prototype 3D tripolar antenna on top of a wireless sensor node. *Right*: Example channel loss (i.e., S_{21}) for each of the three elements of the tripolar antenna [1].

2.1.2 Introduction

The Internet of Things (IoT) will be built from networks of connected embedded devices and will couple physical infrastructure with information and communication technologies [107]. These devices will be wireless and will smartly monitor, manage and transmit sensory data to a central system. A multi-hop, expandable and hybrid mesh network, which does not rely on dedicated central infrastructure, will be necessary to enable the devices to perform such activities [108].

Depending on the IoT application, devices (i.e., network nodes) may be deployed in less than ideal propagation environments, such as inside of a vehicle or a factory. In these highly cluttered environments, critical information might be lost due to fading and multipath effect and therefore will affect the performance and robustness of a hybrid mesh network.

Diversity techniques such as two dimensional multi-polarization, maximum ratio combining, and equal-gain combining have been long considered to mitigate multipath effects in wireless communications [109]. Our recent work [1] has shown that a compact 2.4 GHz tripolar antenna (65 mm \times 60 mm \times 21 mm) can leverage polarization diversity to mitigate fading in a single point-to-point communication link. This 3D antenna system was realized using single-piece additive manufacturing and can be integrated with a commercially available wireless sensor hardware.

In this paper, we compare, via simulation, the reliability of a hybrid mesh network consisting of a multitude of links, where in one instance devices use a single element antenna and in the second instance, a tripolar antenna system. Channel data utilized in this this work was that measured in a slowly-varying, high-multipath environment. Simulation results showed that networks leveraging nodes with tripolar antennas performed approximately three times better in terms of packet delivery than those with nodes using a single element antenna.

2.1.3 Methodology

2.1.3.1 Channel measurements For this work, we leveraged the channel data measured for and presented in [1]. To emulate a slowly-varying, high-multipath propagation environment, S_{21} measurements were made between transmit and receive antennas placed in a compact reverberation chamber. This chamber is capable of creating conditions ranging from benign (i.e., Rician, high- K) to severe (i.e., hyper-Rayleigh). With the transmit antenna fixed, the receive antenna systems were placed on a track and moved to 50 repeatable positions in 1 cm increments. At each location, S_{21} measurements were made for each antenna element at 551 frequencies in the 2.40 to 2.48 GHz band.

2.1.3.2 Hybrid mesh network simulator We developed a Python-based simulator to implement a hybrid mesh topology network. The network allows communication from end nodes to a base station through a router node as illustrated in Fig. 2.2. The network uses IEEE 802.15.4 standard for transmission, which is ideal for IoT applications operating at 2.4 GHz. Each simulation starts with user defined field size, number of end nodes, number of routers and total number of transmissions per end node. The randomly deployed end nodes, which do not relay data from other nodes, send their own data to a router. End nodes maintain their own routing table and if a router stops functioning, end nodes can use an alternate router. Routers form a mesh network among themselves and find an optimized route to relay the information until it reaches the base station.

The simulator implements a simple communication protocol which allocates communication channels between network entities without collisions. Each end node is assigned S_{21} (i.e., channel loss) data described in the previous section. For the case where the network's end nodes implement a single element antenna, this data is a single list of 551 values. For the tripolar case, each end node has three lists of channel loss data. When a node with a tripolar antenna prepares to transmit a message, the simulator randomly assigns S_{21} values to each element of the antenna from the node's three lists. The lowest link loss is then associated with the message. For linearly polarized antenna, the simulator picks only one S_{21} value. When entity sends a message, the message contains the sender and receiver address and channel loss value. The receiver sends an acknowledgement message if the channel loss is above a certain S_{21} threshold (τ). Otherwise it discards the message (i.e., the simulated packet is "dropped"). τ is calculated separately for each node based on its own lists of S_{21} values. The simulation stops after simulating specified number of transmissions per node (e.g., 1000).

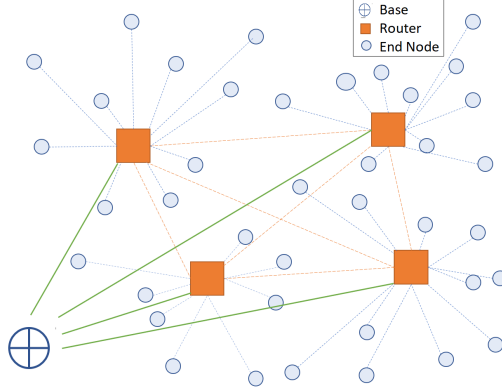


Figure 2.2: Hybrid mesh network topology

2.1.4 Simulation results

For the presented results, we set the field size to 1000 m^2 , total number of end nodes to fifty (50) with four (4) routers and one base station. Fig. 2.3 illustrates the channel loss associated with a single end node for both antenna configurations. The number of times the S_{21} value went below the threshold value for an end node with tripolar antenna was much lower than for the node with the single element antenna. Fig. 2.4 compares the performance of 50 sensor nodes with and without tripolar antenna systems in terms of successful data transmission from one node to another when $\tau = \text{Mean} - 3 \text{ dB}$.

Mesh networks employing tripolar systems had considerably higher packet transmission success rate (82-95%) than nodes using single element antennas (55-78%). Table 2.1 compares the performance for various threshold values in terms of packet throughput. Consistently, the percentage of average number of failed transmissions for single element antenna nodes was approximately three times higher than for when nodes used the tripolar antenna system.

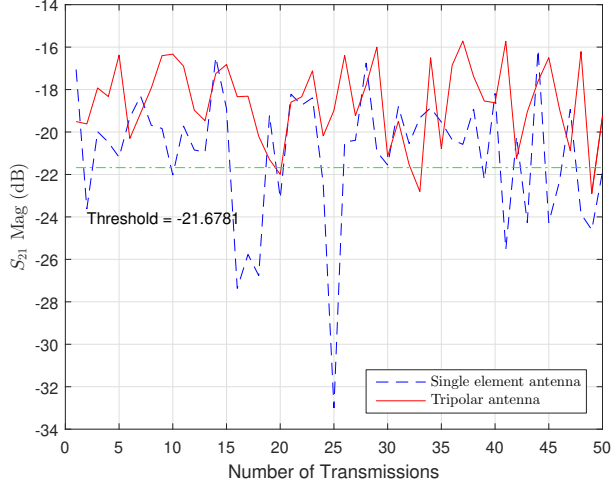


Figure 2.3: Link loss for 50 transmissions with single element and with tripolar antenna systems. Threshold (τ) = $Mean - 3$ dB.

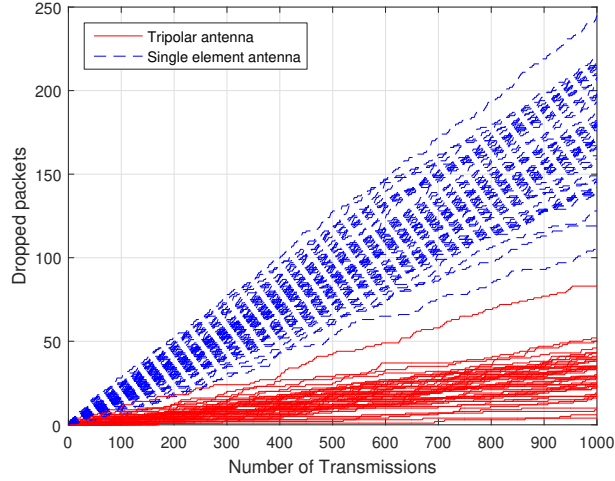


Figure 2.4: Dropped packet rates for single antenna element and tripolar antenna networks. Threshold (τ) = $Mean - 3$ dB.

Table 2.1: Percentage of failed packet transmissions

Threshold (τ)	Tripolar Antenna	Single Element Antenna
<i>Mean</i>	31%	53%
<i>Mean - 1 dB</i>	9%	30%
<i>Mean - 3 dB</i>	4%	15%
<i>Mean - 10 dB</i>	2%	9%

2.1.5 Conclusion

In this work, we compared the link reliability for two hybrid mesh networks, one network utilized wireless nodes with a single element antenna, in the second, nodes leveraged diversity enabled by

a tripolar antenna system. Results, using measured channel loss data sets, show that the tripolar antenna can significantly improve the communication reliability in such networks. Subsequent work will implement these approaches in hardware to demonstrate the benefits in practice.

2.2 Leveraging Tripolar Antenna Diversity to Improve Link Reliability in Severe Multipath Environments

2.2.1 Abstract

In this work, empirical results demonstrate the efficacy of tripolar antenna diversity to improve data packet delivery in environments prone to severe multipath, i.e., those that may be seen for industrial IoT applications. The work leveraged an Arduino platform with a XBee wireless module and compared performance (i.e., link reliability) when a baseline monopole antenna was used versus a prototype, 3D printed tripolar antenna system. The testing was conducted by placing both antennas inside of a compact reverberation chamber. We also compared empirical data with simulated data and showed that for both cases, the tripolar antenna system performed approximately three times better than the monopole antenna. Finally, we conducted tests under dynamic conditions where the wireless node switched, at various rates, between the three antenna elements, choosing the best option to send data packets and results showed that the tripolar antenna can mitigate the high multipath effect with 95% successful packet delivery [110].

2.2.2 Introduction

The Internet of Things (IoT) will be enabled by the integration of billions of sensory devices with physical objects and through collecting and exchanging information without direct human intervention. Networks consisting of interconnected low-powered autonomous sensors and embedded devices have already shown great potential in home automation, smart grid, environmental and industrial monitoring [4], [5]. However, a major challenge for industrial IoT systems is the need to mitigate multipath fading effects caused by the highly reflective and dynamic environments in which these wireless embedded devices may be deployed. Such fading can impact network performance in terms of link reliability and data throughput.

Various diversity techniques such as frequency diversity [111], spatial diversity [112], and polarization diversity have been used to improve the link reliability and overcome fading loss. Consider the following as recent examples. A dual mode multi-band antenna, which used unit cell radiators in the horizontal and vertical plane to achieve polarization diversity, was introduced in [113]. The antenna was designed for vehicular networks and can operate at 2.4, 3.5 and 5.8 GHz. Another dual-polarized antenna used a single-layer frequency selective surface and can operate for ultra-wideband (UWB) applications [114]. Finally, the design presented in [115] consists of three-element

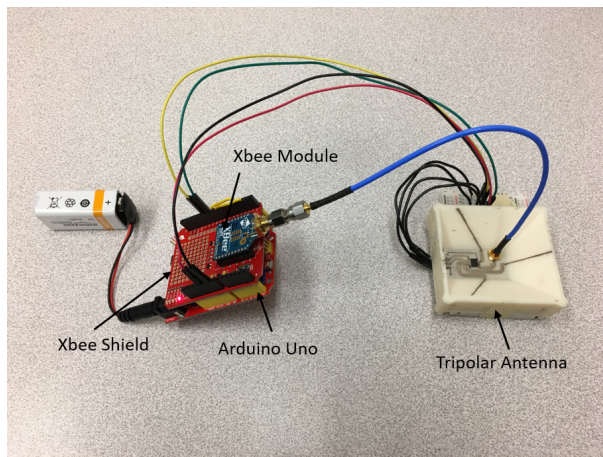


Figure 2.5: A tripolar antenna connected to an XBee wireless module and controlled by an Arduino embedded system.

multiple-input-multiple-output (MIMO) antenna. The technique used both pattern and polarization (linear/circular) diversity and was proposed for upper WLAN frequency band (5.6 GHz). Although these proposed techniques are promising, they are yet to be tested on a realistic scenario, for example with an IoT based smart device deployed in a high multipath environment.

Our recent work has shown that a compact ($65 \text{ mm} \times 60 \text{ mm} \times 21 \text{ mm}$) 2.4 GHz tripolar antenna, consisting of three mutually orthogonal elements, can improve channel induced losses such as depolarization and fading through polarization diversity [1]. This 3D antenna system was realized using single-piece additive manufacturing and is suitable for slowly-varying, high-multipath environment. We have also shown, using simulations, that the tripolar antenna performed approximately three times better than single element antenna in terms of data packet delivery for a single point-to-point communication link with harsh propagation conditions [2]. In the work herein, we validate these simulation results with experimental data.

The experiments were conducted by integrating a prototype tripolar antenna system with an Arduino-controlled XBee wireless module (Fig. 2.5). This antenna system, employing three-element selection diversity, was compared to a similar Arduino-controlled systems that leveraged a monopole antenna. The performance (i.e., success rate of data packet delivery) of the two designs are compared in static but highly-reflective environment and under dynamic conditions. Empirical evidence illustrated that the tripolar antenna system can achieve approximately 95% successful packet delivery versus 85% if a monopole antenna is used. At the same the tripolar antenna is capable of maintaining that success rate under dynamic conditions that require fast switching between antenna elements.

The remainder of this paper is organized as follows. In Section 2.2.3 we describe experimental

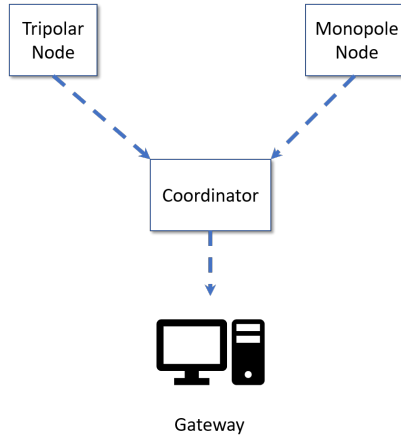


Figure 2.6: A simple network with end devices and coordinator.

setup and integration of the tripolar node with the XBee/Arduino platform. Empirical data showing the data delivery performance of the tripolar antenna in severe wireless propagation environment and in dynamic environment are presented in Section 2.2.4. We finish with concluding remarks in Section 2.2.5.

2.2.3 Methodology

The introduction of IoT based smart devices and processors for industrial automation has increased the possibilities of improved security, low-cost and high productivity. However, these devices are often deployed in heterogeneous environments, such as factories, complex and confined areas, which affects the wireless propagation environment. Therefore, any device intended for such dynamic environments should have the adaptability to mitigate the fading and multipath effects. In this section, we describe how we setup the experiment to create severe multipath environment to test the adaptability of the tripolar antenna.

2.2.3.1 Arduino-based nodes In an industrial IoT scenario, multiple embedded devices, i.e., sensor nodes or actuators, consists of microcontroller and sensors, acquires and forwards sensory data to a central location, known as IoT gateway. For our setup, we used XBee S2C modules, which work as a highly configurable wireless transceiver and an Arduino Uno as microcontroller to build a self-contained, battery-powered deployable node (Fig. 2.5). Nodes used the ZigBee communication protocol, which is based on an IEEE 802.15.4 standard and is suitable for low data-rate communication.

The tripolar and monopole antenna was connected to the XBee module through RPSMA connector and we refer to them as ‘tripolar node’ and ‘monopole node’ respectively. We used a coordinator

node, as illustrated in Fig. 2.6, to collect data from end devices and configure the network for point-to-point communication operating at 2.4 GHz. The coordinator node acts as a parent for the end devices by setting the Personal Area Network (PAN) ID of the network, handing out addresses and keeping the network secure.

XBee module can operate at AT/API mode. Using AT mode, also known as ‘Transparent’ mode, the XBee module can be configured by the user or a host microcontroller (Arduino) by first placing the module in command mode and then sending predefined AT commands. For large networks, where each XBee module communicates with multiple XBee modules, Application Programming Interface (API) mode is used. Using built-in library called ‘*xbee-arduino*’, an Arduino can build, send and receive API frames [116]. To measure the RSSI, the host Arduino sends AT command: ‘*AT DB*’, which reads the signal level in decibels (dB) of the latest received packet, to the XBee module through the UART port. Thus the receiver XBee module measures the strength of the signal and determine the quality of the communication link.

2.2.3.2 Test environment To emulate a slowly-varying, highly reflective and multipath propagation environment, RSSI measurements were made by putting an end device (tripolar or monopole node) inside of a compact reverberation chamber. This chamber is capable of creating conditions ranging from benign (i.e., Rician, high- K) to severe (i.e., hyper-Rayleigh). To make the setup realistic, only the end nodes were deployed inside the chamber and the coordinator node was on top of a table in normal propagation environment. With the coordinator node fixed, the end node was placed on a linear track and moved to 50 repeatable positions in 1 cm increments. At each location, the Arduino measures RSSI for each of the three elements of the tripolar antenna and then selects one antenna element with the best channel conditions for data transfer. Polarization switching of the tripolar antenna was achieved by the multiple analog and digital pins of the Arduino. The experiment was repeated for the monopole node.

The end devices send data message to the coordinator, i.e., receiver after certain time intervals, which contains the sender’s address and sensory data. The receiver checks the RSSI of the received packet and sends an acknowledgement message if the channel loss is above a certain RSSI threshold (τ). Otherwise it discards the message (i.e., the packet is lost). Fig. 2.7 shows sample RSSI measurement data from three antenna elements of the tripolar antenna deployed inside the chamber. To test the effectiveness of the tripolar antenna under high switching rate, we used various switching rate ranging from 100 ms to 1 second.

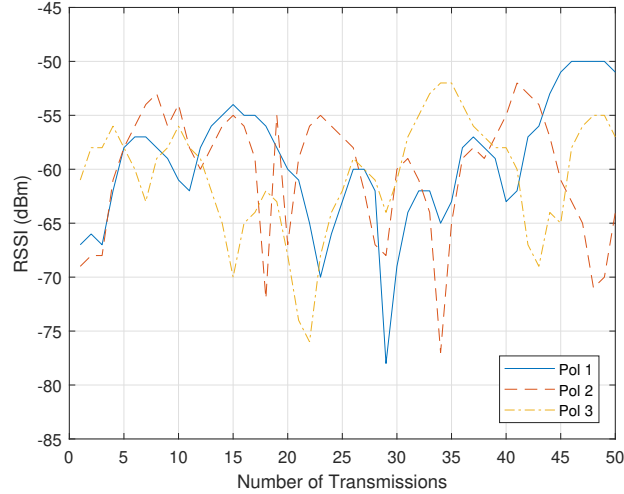


Figure 2.7: RSSI data for three elements of the tripolar node taken at 50 different positions in the track

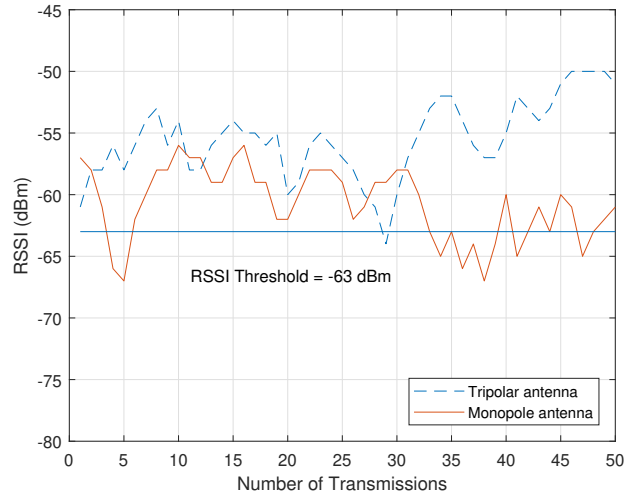


Figure 2.8: RSSI data for 50 transmissions for monopole antenna and tripolar antenna systems. Threshold (τ) = $Mean - 3$ dB.

2.2.4 Empirical results

For the presented results, the coordinator node was placed outside of the chamber and the distance between the nodes was 13 feet (approximately 4 meter). As illustrated in Fig. 2.7, signal strength varied when the node was moved along the linear track and it is unpredictable which antenna element will be dominant at a certain time. The Arduino chooses the best antenna element, which will provide highest RSSI before each transmission. An illustration of this technique can be seen in Fig. 2.8, where tripolar antenna uses polarization diversity to minimize channel loss. Fig. 2.8 also the signal strength values observed by the monopole node. We set the threshold value τ to $Mean - 3$ dB, where $Mean$ is calculated over all the RSSI values of both antenna systems. We can see that

Table 2.2: Comparison between empirical and simulated data

	Threshold (τ)	Packet Loss (%) Tripolar Node	Packet Loss (%) Monopole Node
Empirical	<i>Mean</i> - 3 dB	3	14
	<i>Mean</i> - 10 dB	1	7
Simulated	<i>Mean</i> - 3 dB	4	15
	<i>Mean</i> - 10 dB	2	9

Table 2.3: Packet delivery statistics for tripolar node

Polarization switching time (sec/pol.)	Avg. RSSI difference between highest and lowest element of the tripolar antenna (dBm)	Packet loss (%)
0.1	6.0300	4
0.2	4.1650	3
0.5	4.3600	1.5
1	5.2000	1

the number of times the RSSI value crossed the threshold value for the tripolar antenna was much lower than for the monopole node. Thus the tripolar node was able to avoid the deep fades caused by the severe multipath environments and reduces loss of data packets.

Table 2.2 provides an illustration of the link loss performance between the tripolar node and the monopole node and compares the empirical results with simulated data that were presented in [2]. When end devices were placed inside of the chamber, the packet loss was approximately three (3) times lower for the tripolar node. In [2], we used a simulator and chamber data to emulate severe wireless propagation environment. From the empirical evidence, the results were similar for both cases when τ was set to *Mean* - 3 dB and *Mean* - 10 dB, which not only validates the simulation results but also expands the possibility of reusing the simulator for future applications.

Table 2.3 compares the performance of the tripolar antenna for various polarization switching speed. To create fast fading propagation conditions, we measured the RSSI values when the track was moving. As can be seen from the Table 2.3, loss of data packets increased with the increase in switching rate. For example, packet loss was doubled when switching speed was changed to 200 ms from 500 ms. Still, we note that the tripolar antenna can reduce the packet loss and ensure better channel conditions for IoT based smart devices.

2.2.5 Conclusion

Herein, we compared the performance of two wireless systems, one that utilizes a tripolar antenna system and the other a monopole antenna, both deployed in a high multipath environment. Through

experimental data, we showed that a tripolar antenna can provide better link reliability and end-to-end network throughput in severe propagation environments, such as those expected for industrial IoT applications. For future work, we plan to use the empirical data to simulate a large-scale, mesh IoT network, where devices will use intelligent algorithm to find the optimal of the three polarizations considering both channel conditions and neighboring devices' polarization.

Summary

In this work, we illustrated the benefits of tripolar antenna systems over single branch antennas in point-to-point communication links. First, we developed a hybrid wireless IoT network simulator to analyze the performance of three-branch polarization diversity antenna systems and demonstrated that the multi-branch antenna systems can enhance the link reliability significantly in multipath environment compared to single branch antenna. Although simulation offers a low-cost solution, it is often difficult to emulate real life channel conditions due to complex interaction of many variables. Hence, we followed-up the work by using two Arduino based wireless modules with tripolar antennas deployed in a high multipath channel conditions. The real-life experimental work compliments the simulation model as empirical data collected from tripolar nodes exhibit similar performance to earlier results obtained through simulation. The observations prompted further investigation on the impact of using multi-branch polarization diversity antennas among the nodes of an IoT network in regards to antenna switching and energy performance, which we examine next.

3 Polarization Matching for Networks Utilizing Tripolar Antenna Systems

Foreword

The chapter is presented as published in *2018 IEEE Global Communications Conference* [117]. In this study, several experiments are conducted to investigate the impact of polarization mismatch between multi-branch transmitter and receiver antennas for different network architectures. First, a polarization matching technique is proposed for networks where nodes use predetermined routing paths to forward the data packets. In this router based approach, each router uses Binary Integer Linear Programming to reduce polarization mismatch with the active nodes under the router during data packet transmission. Next, a network with flexible routing is considered where nodes have multiple routers to forward the data packets and consider various factors such as router's distance and polarization, load on the router etc. to select antenna branch. The results show that implementing polarization-aware techniques can improve the packet delivery ratio by at least 6% compared to antenna systems that do not consider polarization matching.

3.1 Abstract

The recent proliferation of IoT based networks in diverse applications has seen various embedded devices deployed in harsh propagation environment. These conditions often induce polarization mismatch between transmitter and receiver antennas and degrade overall network performance. Our work proposes two techniques to prevent power loss due to polarization mismatch for IoT based sensor networks. We first propose the Neighbor Matching (NM) technique to find optimal polarization pattern by solving a Binary Integer Linear Programming optimization problem for routers in a network with fixed routes for data packets. Using empirical data and simulation results, we show that the NM technique has a successful data delivery ratio of approximately 88% compared to 71% for networks which do not consider polarization mismatch. Next, we propose Opportunistic Polarization Matching (OPM) technique for networks with flexible data packet forwarding routes to find polarizations for nodes and routers. Combined with load balancing approach, the proposed OPM technique improves polarization matching by 13% than simple diversity technique. We are also able to show that along with high link reliability both NM and OPM reduce power loss and extend lifetime of nodes [117].

3.2 Introduction

Internet of Things (IoT), which enable sensors, actuators or embedded devices to collect data, exchange information, and act on the environment without direct human intervention, has been considered in diverse applications, such as civil transportation, electric power grid, and medical treatment etc [118]. Unlike other wireless systems, sensors or actuators in an IoT are highly likely to be subject to harsh propagation environments, where multipath and fading may degrade the system performance significantly. Furthermore, these low cost, low powered tiny sensors often do not have any apriori knowledge about propagation conditions of the environment where they are deployed. Therefore, mitigating multipath effects and adapting to channel randomness in real time is crucial for end-to-end network throughput.

Performance of wireless systems can be improved by leveraging diversity techniques [75]. Among all the diversity techniques, spatial diversity and polarization diversity are most popular due to the simplicity of their implementation. While conventional spatial diversity can achieve significant range improvements, it requires large separation between antennas which is not practical for small sensors. On the other hand, polarization diversity, which replaces multiple antennas with separate vertically and horizontally polarized receiving antennas, offers simple and effective way to mitigate signal fading in a multipath environment. Considering these benefits, most studies have focused on dual polarized antennas at transmitter and receiver end [119]. In [73], authors proposed a polarization reconfigurable antenna for portable devices which can switch between linear and circular polarization. Both [120] and [121] proposed antennas with reconfigurable radiation pattern for biomedical applications with operating at 2.2 to 3.1 GHz and 2.45 GHz, respectively. Our recent work [106] has demonstrated that a tripolar antenna system (Fig. 3.1), which leverages three mutually orthogonal linear polarizations in 3D, is able to improve data delivery ratio of a ZigBee network by employing three-element selection diversity.

Nodes leveraging polarization diversity in an IoT network may select one of the available polarized antenna element to reduce frequency selective fading. However, due to distinct fading scenarios seen by different nodes, selection of the antenna element may vary, which causes polarization mismatch due between the transmitter and the receiver. As presented in [122], mismatch in polarization angle can result in loss of received power up to 12 dB approximately. Polarization-mismatch between linear-polarized antennas can be characterized using their misalignment angle; 0° and 90° represents completely aligned angle and completely mismatched angle, respectively. A polarization matching factor based on transmitting and receiving antenna pattern was introduced on [123]. In [124], the

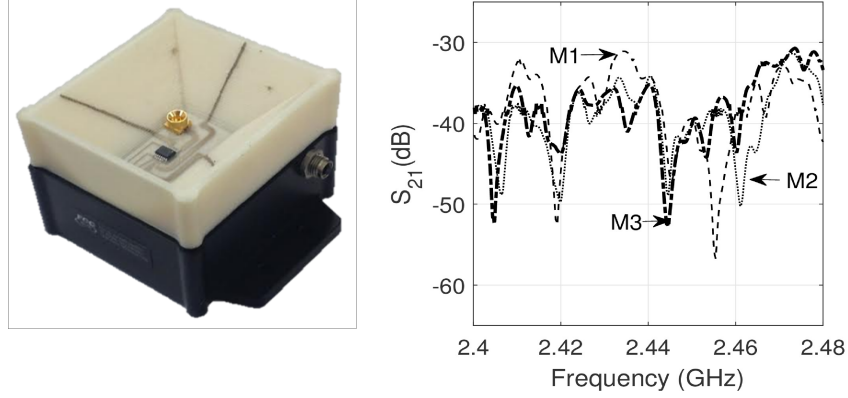


Figure 3.1: *Left*: Fabricated prototype of single-piece additive manufactured 3D tripolar antenna. *Right*: Example channel loss (i.e., S_{21}) for each of the three elements of the tripolar antenna [2].

authors proposed a polarization error matrix based on field circuit co-simulation model to analyze the impact of polarization basis mismatch. Both [125] and [75] showed that the performance of dual-polarized antenna can be improved by opportunistic polarization-matching through actual measurements and simulations. However, none of the works considered highly cluttered environment which can depolarize a transmitted signal across all three spatial dimensions [56].

We propose two polarization matching schemes between transmitting and receiving antennas to mitigate multipath effects for harsh propagation conditions, where IoT devices are likely to be deployed. The first one, Neighbor Matching (NM) technique, where routers' polarization selection are driven based on their child nodes' selected polarization, uses fixed routes for data forwarding. By solving a Binary Integer Programming problem, the proposed technique enables routers to reduce polarization mismatch when receiving packets from nodes and during forwarding packets to other routers. Our second technique, Opportunistic Polarization Matching (OPM), proposes a load aware packet forwarding scheme, where nodes' polarization selection are driven based on the polarization of their nearest static and mobile routers. For each node, the proposed scheme makes routing decision based on polarization, distance and their energy status to minimize power loss. Both NM and OPM scheme reduce polarization mismatch approximately by 40% and 13%, respectively compared to their baseline simple diversity technique and thus ensure extended network lifetime.

The work is organized as follows. Section 3.3 describes the system configuration of the IoT network that we consider for this work. We present polarization matching techniques for IoT based sensors in Section 3.4 and 3.5. Simulation methodologies and results are presented in Section 3.6 and Section 3.7 concludes the paper and gives future research directions.

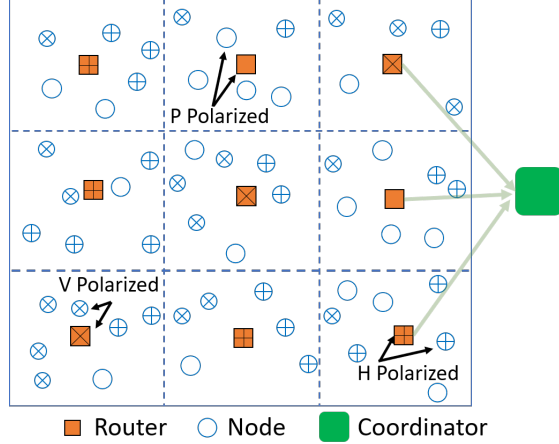


Figure 3.2: Fig. showing different polarization patterns selected by nodes and routers. Here H and V are the traditional horizontal and vertical in 2D and P is orthogonal to both.

3.3 System Model

In this section, we introduce the system architecture and assumptions underlying the network architecture. We consider a ZigBee tree-based network based on IEEE 802.15.4 standard which consists of a coordinator, multiple routers and end devices, i.e., nodes. Fig. 3.2 shows an illustration of different polarization patterns selected by nodes and routers of a network. The reliable, cost-effective and much lower power consumption of ZigBee network makes it suitable for applications such as smart home monitoring, inventory tracking, industrial control and monitoring. The coordinator, which receives data from nodes for further processing, are responsible for initialization, maintenance, and control functions for the network. Nodes autonomously gather physical sensing information and forward sensed data to the coordinator in a multi-hop manner through a sequence of routers. The sensing area is partitioned into equal sized square sub-areas and movement of routers are restricted along the grid lines only. Further, nodes are homogeneous, deployed randomly over the 2D sensing field and do not participate in routing packets. We assume that each node, which relies on batteries for power supply, has their location information and the routers may be static or mobile with reliable power supplies.

When a node joins the network, it first scans the network and chooses the nearest static router as parent device. Upon successful joining, the router assigns an address, which is unique within a particular network, to the node using a distributed address allocated mechanism. We consider that all the nodes and routers are equipped with tripolar antenna and they are deployed in highly cluttered propagation environment. Initially, nodes are in sleep mode. When any node intends to send data to the coordinator, it measures RSSI (received signal strength indicator) for each of the

three elements of the tripolar antenna and then selects one antenna element based on one of our proposed algorithm. For networks where mobile routers are present, each node maintains a routing table consisting of routers' address that are within its transmission range; otherwise it always sends data to the parent router. The receiver router checks RSSI of the received packet and sends an acknowledgement message if the channel loss is above a certain RSSI threshold (τ). Otherwise it discards the message which means the packet is lost.

3.4 Neighbor Matching Technique

In a tree-based ZigBee network, routing paths are pre-determined with focus on minimizing hop delay. Nodes forward data packets, which consists of sensed data, sender address and destination address, to the parent router. The router then forwards the data packet to the next router which is closer to the coordinator. Fig. 3.3 shows an illustration of such network where a data packet is forwarded from to the coordinator through intermediate routers. We can see that it is crucial for a router to match polarization with child nodes as well as with next router since it will forward all the received data packet to the next router. Considering this, we propose Neighbor Matching (NM) technique, which selects a polarization pattern for ZigBee routers, considering polarization pattern of both child nodes and next level router. When a child node joins the network, it exchanges messages with neighbor child nodes to discover nearest router. Based on the initial exchanges child nodes then determine best polarization to transmit sensed data. We assume that a parent router has knowledge of all child nodes' selected polarization. Sensor nodes are put into sleep modes to save energy and if they sense any event, they measure RSSI of all three polarizations to find best polarization first. After switching into best polarization, nodes send polarization information to the nearest router first to ensure that the router can switch its polarization based on child node's information and then send data packet to router. Routers' polarization is selected using top-down approach. The router that is closest to the coordinator selects best polarization and send information to the below routers. The bottom routers then use that information to find their polarization by solving an optimization problem which we describe next.

Lets assume $P = \{p_1, p_2, p_3\}$ is a set were p_1, p_2 and p_3 represents 3 different polarizations. Suppose a router has n child nodes and m neighbor routers. We denote, $N = [x_1, x_2, \dots, x_n]$ as polarization vector of child nodes, where x_i is the selected polarization pattern of the i th node and $x_i \in P$. If a router does not have information of a node or if a node's RSSI is below RSSI threshold, then router simply sets x_i to zero. We also define R^k to represent the polarization selected by next

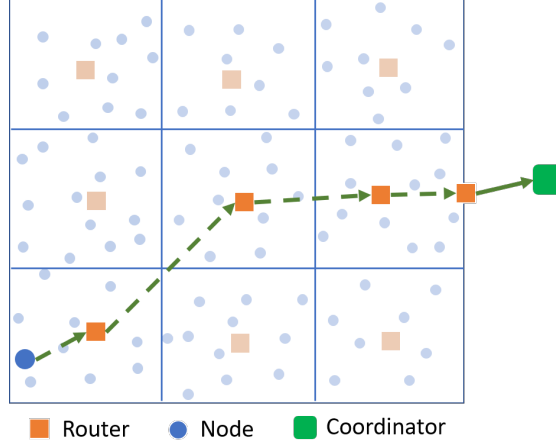


Figure 3.3: Typical example of data forwarding from source to coordinator for tree-based ZigBee network.

router, where $R^k \in P$. By leveraging child nodes' and next level router's polarization information, router tries to find a polarization that reduces polarization mismatches both during receiving packets from child nodes and forwarding packets to the next router. Routers update their polarization after certain time intervals and send messages to neighbor routers if they switch polarization. Fig. 3.4 shows different steps of polarization selection by routers and nodes in a flowchart. Let r , which represents polarization of the parent router, be the optimization variable and our goal is to find r that maximizes polarization matching.

Next, we formulate a Binary Integer Linear optimization problem where we let $r = p_1, p_2$ and p_3 , and compare total number of matches for each polarization selections. For example, when $r = p_1$, we compare r with each element of N . If $N_i = p_1$ then there is a match and we set $N_i r = 1$. However, if $N_i = p_2$ or p_3 , then there is no match and we set $N_i r = 0$. We do the same calculation for next router R^k and multiply the result, which is either 0 or 1, with n , since the parent router is expected to forward n data packets to the next router. Our optimization problems finds polarization that leads to highest number of matches between a parent router, child nodes and next router. Thus by solving equation (1), a parent router can find a suitable polarization in a distributed manner which

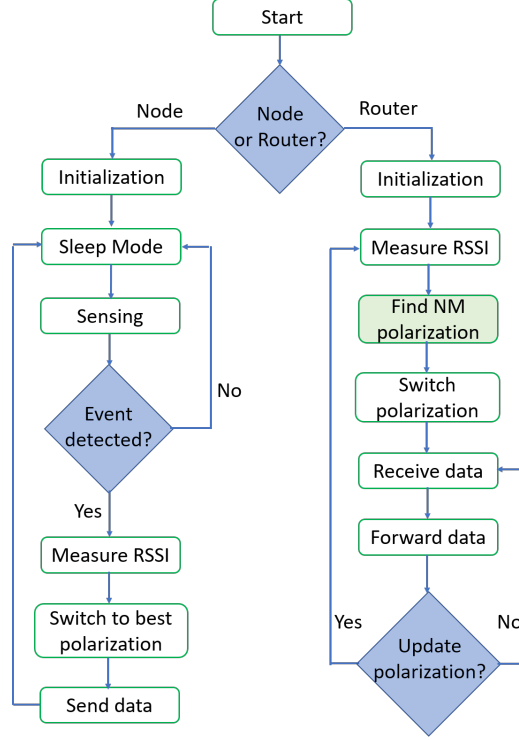


Figure 3.4: Different phases of polarization selection in a tree-based ZigBee network

reduces polarization mismatch.

$$\text{Maximize } \sum_{i=1}^n N_i r + n R^k r \quad (4)$$

$$\text{subject to: } N_i r = \begin{cases} 1, & \text{if } N_i = r. \\ 0, & \text{otherwise.} \end{cases} \quad (4a)$$

$$R^k r = \begin{cases} 1, & \text{if } R^k = r. \\ 0, & \text{otherwise.} \end{cases} \quad (4b)$$

$$r, R^k \in P \quad (4c)$$

$$r, R^k \geq \tau \quad (4d)$$

3.5 Opportunistic Polarization Matching

While tree-based network is simple, the downside is that with a rigid routing structure, if any router stops functioning, the performance of the network will be significantly affected. To fix this issue, mobile routers have been introduced, which collects sensory data from nodes and forwards to the

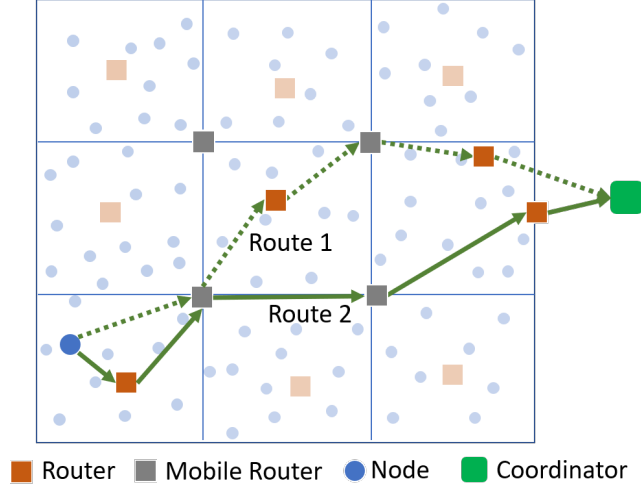


Figure 3.5: Example of available routes for nodes in a ZigBee network in presence of mobile routers.

next router which is closer to the coordinator [126]. Presence of mobile nodes also works as an alternative for nodes and routers to match their polarization (see Fig. 3.5). To route a packet to the coordinator, a device will check the polarization pattern of its neighbor routers and will try to reduce polarization mismatch by selecting the next level router which matches with the best polarization pattern of its own. Thus, the routing decision made by the device solely depends on polarization of neighbor routers and unlike tree-based network, nodes do not need to send their polarization information to their parent routers. However, since mobile nodes are not always available on the same area, nodes may forward data packets based on their routing table when mobile nodes are not present. If a node does not get any authentication message from mobile router after two attempts, it will forward the message to its parent router. Depending on the polarization pattern, nodes may forward data packets to a particular router only, which will slow down routers performance and eventually will affect the overall performance of the network. To prevent this, the proposed technique attempts to balance loads between routers through balance factor α . To identify which router is getting most flow of data packets, devices will keep track of the number of packets that they are sending to each neighbor routers. Assuming a node or router has m routers within its transmission range, we define α as:

$$\alpha_i = \frac{\text{Number of packets sent to } i\text{th router}}{\text{Total number of packets sent by the node}} \quad (5)$$

Devices compute α_i , where $i = 1, \dots, m$ and for any router when $\alpha_i > \alpha_L$, where α_L is the balancing threshold ($0 < \alpha_L < 1$), devices will select other router for data forwarding. Besides load balancing, these low-powered sensor nodes also need to be energy efficient. As the energy status of a device

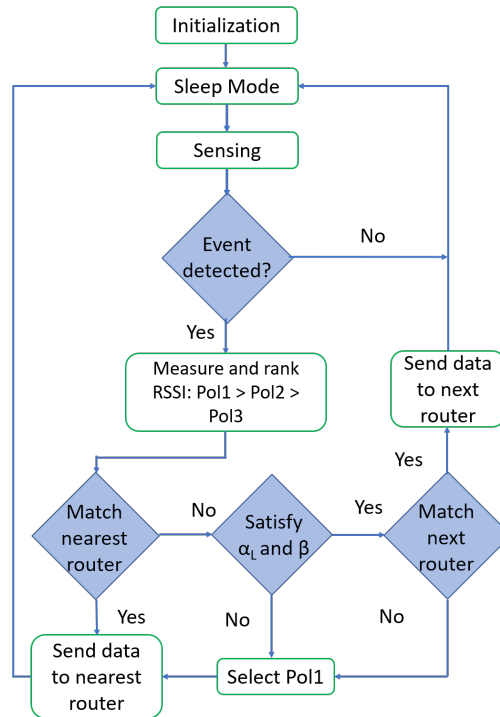


Figure 3.6: Different phases of polarization selection for a node in ZigBee network where mobile routers are present.

becomes low and gets below a threshold β , the device will prefer energy saving to load balancing and polarization matching, and will forward data packets to the nearest router instead of the router that is far away. By switching into this greedy forwarding mode, devices ensure to perform longer and maximize utilization of remaining energy. Fig. 3.6 shows steps of polarization selection for a device using Opportunistic Polarization Matching (OPM) technique. Routers will go through same phases except event detection and sleeping.

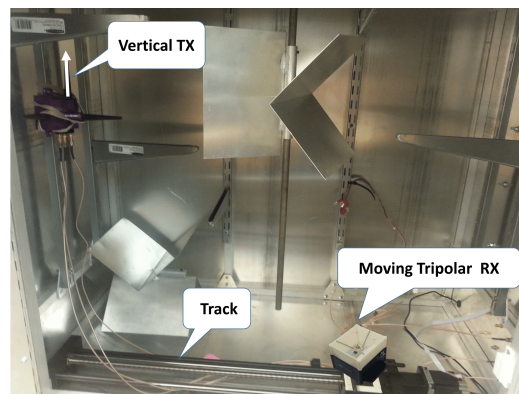


Figure 3.7: Tripolar antenna placed inside of a reverberation chamber for channel measurement.

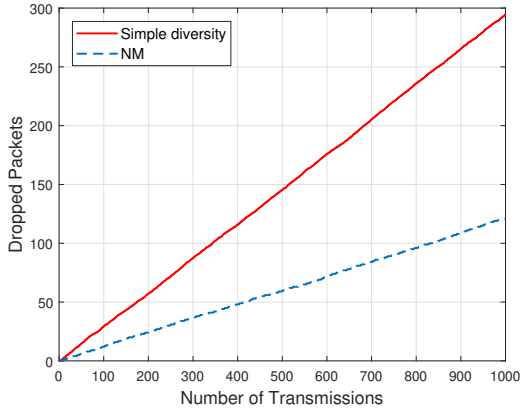
Table 3.1: Loss of power due to polarization mismatch

Alignment angle	Loss (dB)
± 0	0
± 15	0.301
± 30	1.249
± 45	3.010
± 60	6.020
± 75	11.740
± 90	∞

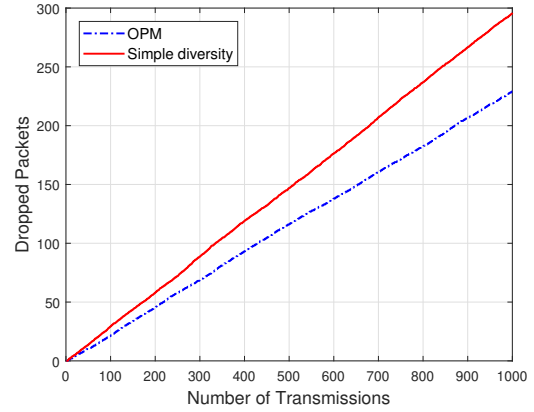
3.6 Simulation Results

For simulation, a 2D $100\text{m} \times 100\text{m}$ area is considered, where nodes are deployed randomly. After joining in a network, nodes add nearest router as their parent. Each node is initialized with same amount of energy and they do not route data packets. To emulate a slowly-varying, multipath propagation environment, we leveraged empirical data presented in [2]. For channel measurements, a tripolar antenna integrated with XBee and Arduino was placed on top of a linear track inside of a reverberation chamber (see Fig. 3.7) along with a linearly polarized antenna [56]. We moved the node to repeatable positions and at each position, measurements (in dBm) were taken for all three polarizations during transmissions and receptions. During simulations, we randomly assign these empirical data to nodes and routers and choose one of the three polarization based on the RSSI values or using polarization matching technique. When polarization mismatch occurs between a receiver and transmitter, the loss of power depends on the alignment angle of their respective antennas. For each transmission, our Python based simulator randomly assigns an alignment angle and uses data presented in Table 3.1 to calculate power loss due to polarization mismatch [122].

First, we present the performance of our proposed NM scheme. To analyze the performance of the proposed NM technique, we consider a network where data packet routing paths are fixed and all devices use tripolar antenna systems. We use simple diversity technique as the baseline, which allows each node and router to choose best polarization regardless of their next hop router's polarization. Fig. 3.8(a) illustrates the impact of NM scheme on reducing dropped packet rate. For the mentioned figures, we use fifty sensor nodes that are deployed randomly and we set RSSI threshold to -90 dBm. Fig. 3.8(a) illustrates that in a highly cluttered environment, the NM scheme, where routers' polarization selection decisions depends on neighbors' polarization, has approximately 88% successful data delivery rate compared to 71% data delivery rate achieved by simple diversity technique.

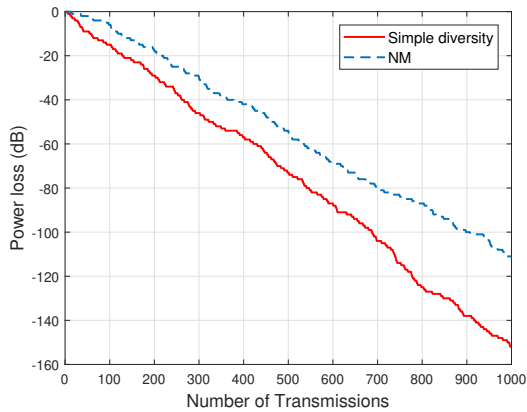


(a)

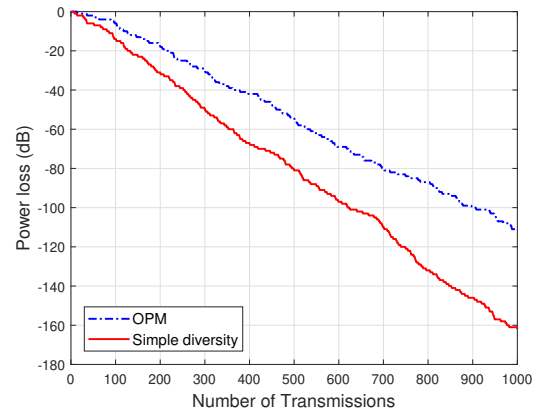


(b)

Figure 3.8: *Left:* Comparison between dropped packet rates for NM scheme and simple diversity technique, *Right:* Comparison between dropped packet rates for OPM scheme and simple diversity technique



(a)



(b)

Figure 3.9: *Left:* Power loss comparison between NM and simple diversity technique, *Right:* Power loss comparison between OPM and simple diversity technique, .

Table 3.2: Comparative analysis of NM scheme

Number of nodes	Packet drop (%)	Polarization mismatch (%)	Power loss (dB) per transmission (%)
50	12	26	1.57
100	12	27	1.62
150	13	28	1.67
200	13	28	1.65

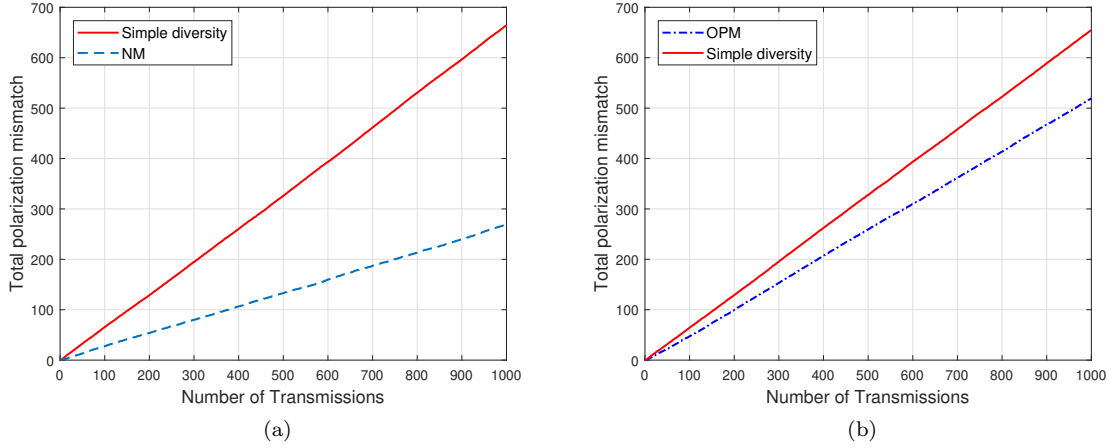


Figure 3.10: *Left:* Comparison of polarization mismatches between NM and simple diversity technique, *Right:* Comparison of polarization mismatches between OPM and simple diversity technique.

Fig. 3.9(a) and 3.10(a) compares performance of the NM technique with simple diversity technique in terms of power loss and polarization mismatch. Although average power consumed by simple diversity technique is less than the proposed NM scheme, simple diversity techniques are prone to more polarization mismatch. We can observe that the proposed NM scheme has approximately 28% polarization mismatches, compared to 66% of simple diversity technique. Minimizing polarization mismatch results in reduced power loss; as a result, the NM technique has an average -1.1 dB loss per transmission compared to -1.5 dB loss per transmission of simple diversity technique. By reducing power loss, the NM scheme successfully increases lifetime of nodes and routers and improves the performance of the network. Table 3.2 demonstrates scalability of the NM scheme where we varied number of nodes between 50 to 200 and the performance of the proposed scheme was consistent.

Next, we analyze the performance of the OPM scheme, which is employed in a network with mobile routers that provide alternate routes for nodes to transmit data packets. Simple diversity technique where nodes use tripolar antenna system to choose best polarization and forward data

Table 3.3: Comparative analysis of OPM scheme

Number of nodes	Packet drop (%)	Polarization mismatch (%)	Power loss (dB) per transmission
50	25	56	3.34
100	24	54	3.16
150	24	54	3.2
200	24	55	3.21

packet to the nearest router (either parent router or mobile router) regardless of the router’s polarization, is considered as a baseline for performance analysis. Fig. 3.8(b) and 3.9(b) and 3.10(b) illustrates the impact of the proposed OPM technique on data packet delivery rate, power loss, and polarization mismatch respectively. The OPM technique are able to reduce polarization mismatch by 13% comparing to simple diversity technique, where nodes use diversity but do not consider polarization matching. The OPM scheme, where devices aim to reduce power loss by matching polarization pattern with the next router, has 6% higher data delivery rate and less power loss than the simple diversity technique. Table 3.3 demonstrates that the performance of the OPM technique remains consistent when we varied the number of nodes up to 200.

3.7 Conclusion

Several polarization matching techniques that try to minimize the power loss due to polarization mismatch and improve data delivery ratio for an IoT based sensor network where nodes are equipped with tripolar antennas have been presented in this work. Our proposed Neighbor Matching and Opportunistic Polarization Matching techniques target networks that use fixed data packet routing and flexible data packet routing, respectively. Neighbor Matching scheme allows nodes to choose best polarization pattern and formulates a Binary Integer optimization problem to find suitable polarization pattern among three polarizations for each router. Opportunistic Polarization Matching scheme is designed to enable nodes and routers to choose next hop router in a manner that not only reduces polarization mismatch but also focuses on load balancing among routers. While both schemes require additional messages containing selected/desired polarization information between nodes and routers, the proposed schemes can still achieve high successful data delivery ratio than the baseline networks as manifested in our extensive simulations. For future works, we would like to implement the proposed schemes in real nodes and confirm the validity of simulation results presented in this paper.

Summary

In this chapter, we investigated the performance of multi-branch antenna diversity schemes for tripolar antenna systems by analyzing the power loss associated with selecting same or different antenna branch for transmitter and receiver, respectively. The proposed Neighbor Matching and Opportunistic Polarization Matching techniques utilized predetermined routing paths and dynamic routing paths, respectively with an aim to increase energy efficiency and link reliability. Results showed that better load balancing can be achieved among the nodes of an IoT network by leveraging the knowledge of the underlying network structure. These findings lead to several interesting research questions - whether implementation of diversity schemes should depend on the IoT network architecture, and how structure-dependant employment of antenna diversity technique will impact IoT network performance. In the next chapter we explore these issues by leveraging complex network theory.

4 Effective Implementation of Energy Aware Polarization Diversity for IoT Networks Using Eigenvector Centrality

Foreword

In this chapter, we focus on the implementation of an adaptive multi-polarized antenna selection approach that is aware of the IoT network structure. The work was presented in *2020 International Conference on Network Science* [127]. A criterion to evaluate the network-structure dependence of antenna branch selection is presented through the complex network representation of an IoT network. Analyzing a given network topology using complex network theory and eigenvector centrality measures helps to categorize highly congested nodes that see more data flow and have higher energy consumption rates than other nodes. The centrality metric, which is calculated autonomously by every nodes present in the network, is used to control the switching frequency of the tripolar antenna such that a node will alternate between selection diversity and switched diversity based on its centrality. The data shows that, in a propagation environment where each transmission sees independent fading, adaptive switching for multi-branch antenna reduces energy consumption by approximately 13% compared to standard diversity technique.

4.1 Abstract

The Internet of Things (IoT) is one the most promising area of applications for complex networks since we know that both the efficiency and fidelity of information transmission rely critically on our understanding of network structure. While antenna diversity schemes improve reliability and capacity for point-to-point links of an IoT network that employs multi-polarized antennas, it is currently unclear how implementation should depend on the network structure of the IoT and what impact structure-dependent implementations will have on the energy consumption of IoT devices. We propose an antenna diversity scheme that leverages local network structure and a distributed calculation of centrality to reduce power consumption by 13% when compared to standard selection diversity technique. The proposed approach exploits distributed eigenvector centrality to identify the most influential nodes based on data flow and then limits their antenna switching frequency proportionally to their centrality. Our results also demonstrate that by taking routers' centrality metric into account, a network can reduce antenna switching frequency by 17% while ensuring approximately 99% packet delivery rate. More broadly, this study highlights how network science

can contribute to the development of efficient IoT devices [127].

4.2 Introduction

The Internet of Things (IoT) interconnects heterogeneous entities like sensors, actuators, wearable items and phones to develop an integrated system where these multipurpose devices can monitor their surrounding environment, react to a certain event, collect sensory data and forward the data in multi-hop fashion to back-end systems for further processing [128]. The applications of IoT span from small scale implementation such as patient monitoring, smart homes, to large scale implementations of industrial monitoring, smart farming, smart cities, etc. [129,130]. In many of these potential applications, IoT devices are deployed in environments which are not ideal for wireless communication. Environments such as industrial facilities are particularly harsh where reflection, diffraction and scattering from metal structures cause distortion to the radio signal, known as multipath fading [131]. Signal attenuation, phase shifting and inter-symbol interference caused by multipath fading significantly degrade reliability and throughput of the network.

Multi-polarized antennas are an effective solution to overcome multipath effects as they allow the receiver to have multiple copies of the transmitted signal by using orthogonally polarized antenna elements [132]. However, the problem is then to choose which antenna polarization should be used given local conditions, including network structure. Selection diversity is the simplest diversity technique used in conjunction with multi-element antennas in which the antenna polarization having the highest signal strength is chosen for transmission or reception. Due to cost constraints and limited processing capabilities of IoT devices, selection diversity uses a single radio-frequency (RF) chain and switches between polarizations to determine the ‘best’ polarization using a RF switch. Existing works in the literature related to selection diversity schemes primarily focus on ensuring link reliability, minimizing low bit error rate (BER) and attaining high signal-to-noise (SNR) ratio. For example, the authors of Ref. [133] developed an algorithm with quartic complexity to select optimal subset of antennas that ensures maximum SNR for systems with many transmit antennas. In Ref. [134], a low-complexity generalized selection combining (GSC) scheme is introduced, which is able to match the performance of a full diversity system in terms of outage probability and symbol error rate while utilizing only a subset of the available antennas to transmit and receive. In Ref. [13], capacity maximizing suboptimal antenna selection algorithm for medium to high SNRs is proposed to determine the transmit antenna in a Rayleigh fading environment. However, all the mentioned works required either multiple RF chains to be active simultaneously or the device to solve complex

optimization problems, which is not suitable for low-cost, constrained IoT devices. Moreover, the network structures of IoT systems are often complex and hierarchical, suggesting that diversity technique might be an interesting avenue of research.

In multi-hop communication based routing, router nodes that are near the base station relay the data collected by the sensor nodes that are further away from the base. Thus, in this network, the closer a router is to the base, the higher its data traffic load will be, resulting in frequent use of selection diversity to select antenna polarization. This will cause faster depletion of energy of the routers with high data traffic compared to the routers with less traffic, i.e., far away routers. Intuitively, in an IoT network operating in multipath environment, the time between consecutive data transmission by a sensor node can be large compared to the coherence time (time over which the channel changes significantly) of the channel and thus, each transmission sees independent fading. On the contrary, as routers manage packets from multiple sensor nodes, the coherence time for routers is large relative to the time between consecutive transmission/reception which implies that the fading seen by packets are correlated. For example, IoT networks aimed at wildfire detection, forest environment and agriculture monitoring require geographically dispersed sensor nodes to transmit sensed information periodically at a low data rate. The base station can provide valuable forecast, improve safety and efficiency by integrating the sensed data that is relayed through routers [135,136]. The findings from above discussion motivates us to consider controlling the use selection diversity according to nodes' data traffic load as approximated by their position in the network structure. Indeed, an IoT network can be effectively represented as a complex network [137], a graph object whose vertices correspond to sensor or router nodes while edges stand for data transmission between nodes. More specifically, we consider the problem of finding routers with high data traffic in an IoT network as a problem of finding the crucial nodes in a complex network. Then, we can leverage centrality metrics [138], which rank the nodes of a network based on their importance in a network, to identify highly congested routers. Our focus in this paper is to apply ideas from complex network science in order to implement a device-specific diversity scheme that considers nonuniform depletion of energy of routers in an IoT network.

By combining complex network theory and the concept of antenna diversity, we propose a network-wide diversity technique, where devices will use selection diversity in a periodic manner instead of using it before every transmission or reception and the period will be proportional to their centrality. In summary, the main contributions of this paper are as follows.

1. We employ the concept of eigenvector centrality to determine crucial nodes in an IoT network

consisting of a large number of stationary nodes from the view point of data packet transmission and reception. The centrality is calculated by autonomous sensor and router nodes in a distributed manner which reduces computation complexity and ensures low-memory usage for low-resource, energy-constrained IoT devices compared to centralized computation.

2. In contrast to the conventional selection diversity technique that allows all devices to switch antenna element before every transmission or reception, our proposed energy-aware diversity scheme controls the switching of devices such that low-scoring routers are allowed to switch antenna more frequently compared to the high-scoring ones and hence, reduces excessive switching and is able to minimize antenna switching by at least 17%.
3. We demonstrate through simulation that the reduction of excessive antenna switching achieved by our Distributed Eigenvector Centrality (DEC) diversity approach decreases energy consumption of routers by at least 13% compared to simple network-wide selection diversity approach, without degrading network reliability.

The paper is organized as follows: Section 4.3 reviews related works. In Section 4.4, we give an overview of the type of target IoT networks and deployment environment considered. Section 4.5 introduces a distributed calculation of eigenvector centrality and proposes an implementation for IoT network in which an individual antenna switching rate is controlled based on its centrality in the network structure. Section 4.6 describes the comparison between our proposed centrality based diversity scheme and simple selection diversity scheme and Section 4.7 concludes the paper.

4.3 Related Works

A network consists of a set of nodes connected by edges which can be directed or undirected, weighted or unweighted. Centrality is often used in complex network systems to identify the relative influence of a node or edge with respect to the entire network. Various centrality measures such as betweenness, closeness and eigenvector centrality have been studied in the literature based on application context and different characteristics of a network. Betweenness centrality determines the amount of influence a node has over the information flow of a network. The algorithm first calculates the shortest path between every pair of nodes in a network and assigns a centrality to nodes based on how frequently they lie along shortest paths [139]. Closeness centrality is defined as the inverse of the average distance between a given node and all other nodes in the network [140] such that high closeness centrality indicates central nodes that have shorter distances to other nodes.

However, most centrality measures are calculated based on global topology information which is prohibitive for memory-constrained, low-cost devices of an IoT network with a large number of nodes. Another popular measure is eigenvector centrality, which calculates a node's importance in a network by summing the importance of its neighbors [138]. Eigenvector centrality is defined based on the eigenvector of the network adjacency matrix such that the centrality \vec{x} satisfies $A\vec{x} = \lambda\vec{x}$ where A is the $N \times N$ adjacency matrix, \vec{x} is the eigenvector associated to the greatest eigenvalue λ of A and N is the number of nodes.

Although a node which is central by one centrality measure may be central by other centrality measures, this is not necessarily always true. Compared to betweenness centrality (measures the number of paths that pass through each node) and closeness centrality (based on average distances), eigenvector centrality is based on the idea that a central node is connected to other central nodes, which is a natural definition for centrality in an IoT network. However, one of the major disadvantage of eigenvector centrality measure is that the calculation is quite complex and complexity grows as N increases which is challenging for battery-powered nodes with limited storage and processing capabilities. In this present work, we utilize the concept of eigenvector centrality and leverage the tree structure of our IoT networks for a distributed computation of centrality, where a node relies on its next hop neighbors only to compute its individual centrality. Restricting the topology means nodes do not have to obtain information about far-away nodes which reduces resource usage.

Recently, several studies have focused on exploiting eigenvector centrality in a distributed way. For example, Ref. [141] presented a reception-equal rate allocation strategy for cooperative streaming so that all nodes receive the stream with the minimal global use of resources by using a distributed version of the eigenvector centrality. Although the proposed centrality measure can be computed distributedly, every node still needs to be aware of the full network topology to calculate the centrality. In Ref. [1], the authors studied a distributed computation of the PageRank algorithm, a variant of the eigenvector centrality. In our work, we focus on a distributed version of the classic eigenvector centrality, which can be measured individually by each node of a directed loop-free wireless network consisted of resource constrained devices.

4.4 System Model

Due to scalability, low cost and ease of deployment, IoT networks are gaining increasing interests in the research community. Depending on the particular application, different network architecture may be of interest. We consider an IoT network, where both nodes and routers are autonomous and

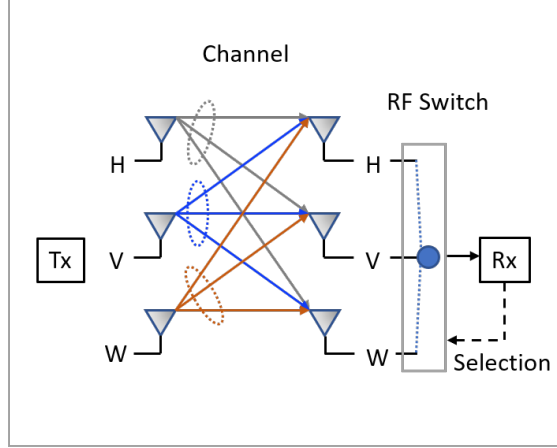


Figure 4.1: Block diagram of transmission and reception using tripolar antenna.

characterized as energy-constrained devices with limited memory and poor processing capabilities. Routers function as data aggregators and relay the received data to the base station, which has unlimited power supply and is far from the sensing area, in a directed multi-hop fashion through other routers. In addition, all the deployed devices are only aware of their next hop neighbors and have no global knowledge of network. An example of such network is a time-driven IoT network, used to collect spatio-temporal readings of various environmental parameters through densely deployed sensor nodes.

We assume that all devices are equipped with tripolar antenna consisting of three orthogonal mutual collocated antenna elements to create vertical (V) polarization, horizontal (H) polarization and a third polarization (W) which is perpendicular to the other two [1].

Figure 4.1 demonstrates available channel gains for such systems which can be described using a 3×3 complex channel matrix. During transmission, we assume that the signal gets affected by Rayleigh fading, which is independent and identically distributed on each antenna element. Both nodes and routers use selection diversity to determine the best polarization for transmission and reception. To reduce hardware complexity, a single RF chain is used by the tripolar antenna which changes antenna element using a RF switch. IoT devices receive pilot symbols using different polarization from their next hop router to estimate the channel gain of all three antenna elements by means of received signal strength. The receiver antenna then selects one of the polarizations based on its estimates. The base is assumed to be unaffected by multipath fading and uses vertical polarization only for transmission.

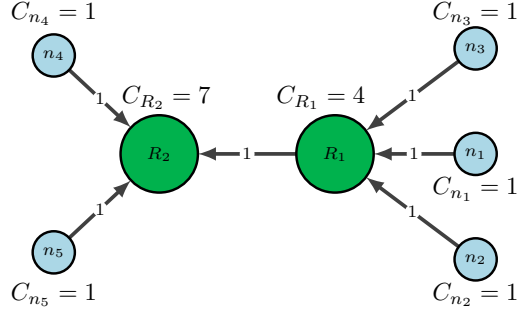


Figure 4.2: Sample network of two routers and five sensor nodes with routers depicted in green and sensors depicted in light blue color.

4.5 Distributed Eigenvector Centrality

Classic eigenvector centrality, which measures how well connected a node is to other well-connected nodes in the network, is computed globally. To facilitate faster computation and reduce memory usage of resource-constrained IoT devices, we use distributed eigenvector centrality (DEC), where each device (sensor or router) will calculate their own centrality. To model the IoT network, we let $G(V, E)$ be a directed graph with N sensor nodes and R router nodes, where V is a set of vertices representing all devices of the network and E is a set of edges representing links between the devices. To calculate the centrality of node k with neighbor set $\{1, 2, \dots, j\}$, we define an edge-weight matrix \mathbf{W} , which is a $j \times 1$ column matrix, and neighbor-centrality matrix $\bar{\mathbf{C}}_{v_k}$, which is a $1 \times j$ row matrix, as,

$$\mathbf{W} = \begin{bmatrix} w_{1,k} \\ w_{2,k} \\ \vdots \\ w_{j,k} \end{bmatrix}_{j \times 1} \quad \text{and} \quad \bar{\mathbf{C}}_{v_k} = [c_{v_1} \quad c_{v_2} \quad \dots \quad c_{v_j}]_{1 \times j} \quad (6)$$

here weight of each edge $w_{i,k}$ is either 1 or 0 and i is one hop neighbor of node k . In the context of our network, a directed edge from node i to node k indicates data packet flow direction from i to k .

If there is an edge from node i to node k , then $w_{i,k} = 1$, otherwise $w_{i,k} = 0$. Also, c_{v_i} denotes the centrality of the node i . The proposed centrality scheme is initialized by awarding one centrality point to each vertices. After that each node calculates its own centrality by summing the centrality of its neighbor nodes that have edges directed towards them. Thus, DEC for node k is defined as the weighted sum of the centralities of all its neighbor sensor nodes and routers and can be written

as

$$c_{v_k} = 1 + \mathbf{W}\bar{\mathbf{C}}_{v_k} = 1 + \sum_{i=1, i \neq k}^j w_{i,k} c_{v_i} \quad (7)$$

Fig. 4.2 illustrates an example of centrality calculation using two routers and five sensors. Sensor nodes n_1 , n_2 and n_3 do not have any directed edge towards them and hence each sensor has centrality 1. On the other hand, R_1 has a centrality of 4 since there are three directed links from three neighbor nodes each having a centrality of 1. Although R_2 is a neighbor of R_1 , it does not contribute to the centrality of R_1 as there is no directed edge from R_2 to R_1 . Similarly R_2 has a centrality of 7 since it has directed edges from neighbors with centrality 1, 1 and 4.

Under the assumption that each device knows their type and total number of devices present in the network, it can compute their centrality by only using local interactions with its neighbor. Our goal is to allow nodes to limit their antenna switching based on their centrality. We can then define the interval slot for node k as

$$\lfloor s_k \rfloor = \frac{1}{(N + R)} \alpha c_{v_k} \quad (8)$$

where, N and R are the total number of sensors and routers, respectively. Also, s_k is the number of transmissions during which a node will not use selection diversity unless the signal strength of the currently used antenna branch falls below the threshold and α is an integer that denotes the interval parameter. We note that the interval slot, i.e., the waiting period between two consecutive antenna switching is proportional to a node's centrality and it increases for large values of α .

Fig. 4.3 presents an illustration of transmission rates between nodes and a router for the example network presented in Fig. 4.2, where sensor nodes (denoted as n_1 , n_2 , and n_3) are transmitting data packets to the router R_1 at different rates. We note that, when R_1 uses conventional selection diversity (see Fig. 4.3 *Top*), it requires antenna switching before every transmission. On the other hand, when R_1 employs centrality based switching (see Fig. 4.3 *Bottom*), antenna checks for best polarization among the three elements only after some fixed (3 in this example) transmission slots. For high centrality routers, the interval between consecutive receptions and transmissions will be smaller and hence it's highly likely that the channel conditions will not change between consecutive transmissions. Thus, restricting the use of selection diversity for such routers before every transmission will reduce excessive switching and minimize energy consumption at the same time. With a time complexity scaling linearly with the number of vertices in the network, DEC offers fast computation and requires little memory usage. Moreover, with DEC, any changes in network topology can be dealt locally as only a part of nodes need to recalculate their centrality.

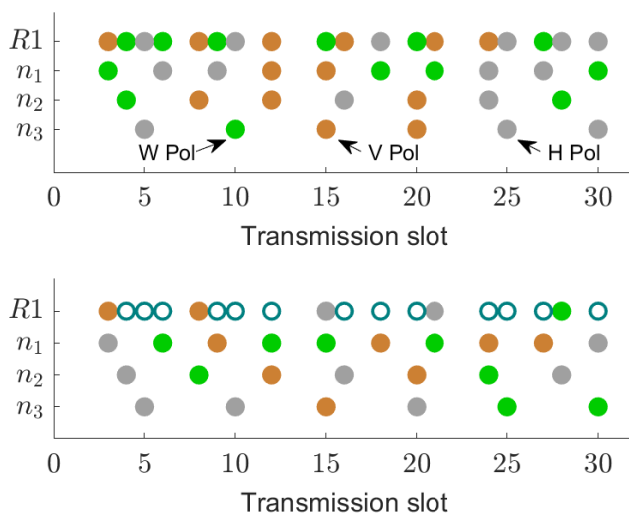


Figure 4.3: An illustration of data transmission by sensors and router. Solid circles indicate usage of selection diversity before transmission while empty circles indicate no antenna switching occurred and colors represent different polarizations. *Top*: Router $R1$ uses conventional selection diversity *Bottom*: $R1$ uses centrality based selection diversity.

4.5.1 Centrality based diversity scheme

We now describe the infrastructure of the IoT network that is used for simulation and also how experimental data is incorporated to assess the performance of the proposed scheme in a Rayleigh-fading environment. The network is initialized with random sensor node deployment and the base is located at one corner of the monitoring area. The routers are equidistant from one another and when a router joins the network, it sends a multicast packet to discover its adjacent sensors and routers and creates a routing table based on the received response. The time difference between two consecutive data packet transmission by sensor nodes is varied randomly between one to ten seconds. Centrality is calculated in a bottom-up approach, where each sensor and router use their own routing table to calculate their centrality and share the score to their next level router only. Once calculated, devices will keep using the centrality unless there are changes in their neighborhood. If a new sensor or router joins, then their neighboring devices update centrality. After computing centrality, devices determine their individual switching rate, which defines how often a device will use selection diversity to select the best antenna element. Once a device selects a polarization for transmission/reception, it may need to wait for a couple of transmission slots to use selection diversity again and, importantly, this waiting period is chosen proportionally to its centrality. During the interval, the antenna will keep monitoring the signal strength of the currently used antenna branch and if the branch falls below a predetermined threshold, it will use selection diversity to select the best branch among the

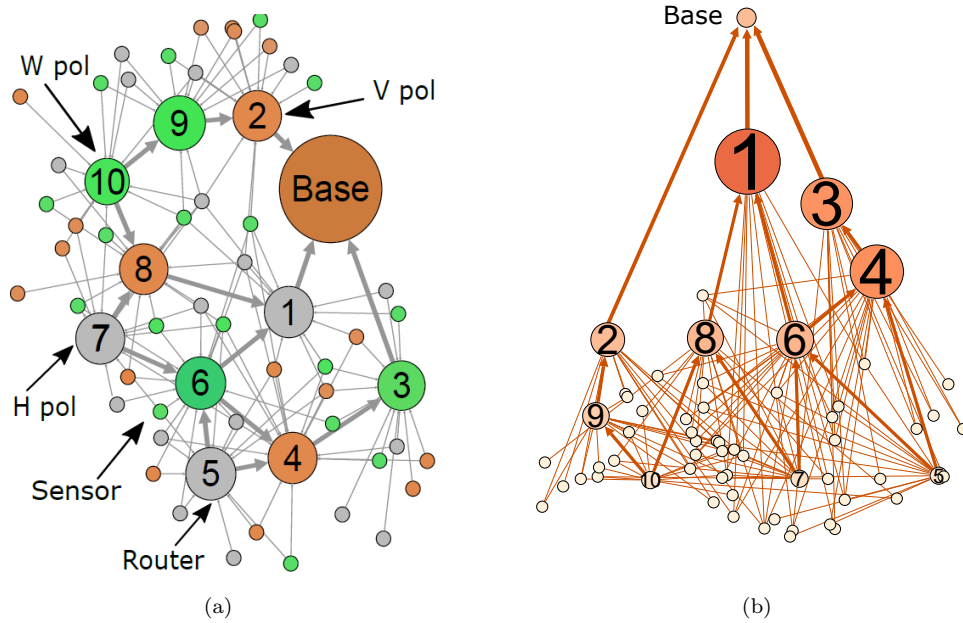


Figure 4.4: (a): Basic architecture of an IoT network consisting of 50 sensors and 10 routers. Colors represents different polarizations, sizes represents different type of IoT devices. (b): Representation of the network presented in Fig. (a) using DEC. Color coding and size indicates centrality of sensor and router nodes. Less central nodes have smaller size and lighter color compared to more central nodes which have larger size and darker colors.

three branches. To assess the performance under a setting similar to real world environment, we exploit the signal strength and energy consumption data obtained experimentally, as described in Ref. [1], using embedded devices equipped with tripolar antennas in a high multipath environment.

4.6 Performance Evaluation

In this section, we describe the simulation parameters used to evaluate the performance of the proposed diversity scheme. Furthermore, we also compare the results with existing selection diversity technique.

4.6.1 Simulation model

We present the results for a case with 50 sensors and 10 routers as depicted in Fig. 4.4a, where devices are using different antenna polarization at a certain time. We note that, routers that are closer to the base station see substantially more data traffic compared to the routers that are far away from the base or on the edge of the sensing area. Fig. 4.4b demonstrates the use of DEC, where high centrality is assigned to the routers that are closer to the base and tend to aggregate

Table 4.1: Simulation parameters

Parameter	Value
Area of deployment	$300 \times 300 \text{ m}^2$
Number of sensors	50
Number of routers	10
Energy: transmission	0.01 J
Energy: reception	0.008 J
Energy: switching	0.001 J
Energy: pilot packets (transmission/reception)	0.002 J
Data packet size	32 bytes
Data rate	250 kbit/s
Pilot packet size	16 bytes
Battery capacity	18.7 KJ
Frequency	2.4 GHz
MAC protocol	802.15.4
Number of repetitions	10

more data packets compared to routers that are far from the base.

In order to evaluate the performance of the proposed centrality based diversity scheme, we consider an IoT network that performs periodic data collection through sensor nodes based on IEEE 802.15.4 protocol. Sensor nodes are static and unable to relay data from other nodes. Routers receive data from other nodes and forward the data to the next hop routers in a tree-based routing fashion. We built a discrete event simulator based on Matlab where a rectangle region is used to deploy the nodes. The default parameters used in our simulation are presented in Table 4.1.

We then run a comparative analysis between our proposed scheme and selection diversity technique. Three performance metrics are used: switching frequency, packet delivery ratio and energy consumption. In the baseline scenario, we consider a network, where each device uses selection diversity to determine the best antenna element for transmission and reception. To analyse the performance of our proposed model, we experiment with different network sizes in terms of the number of sensors and routers.

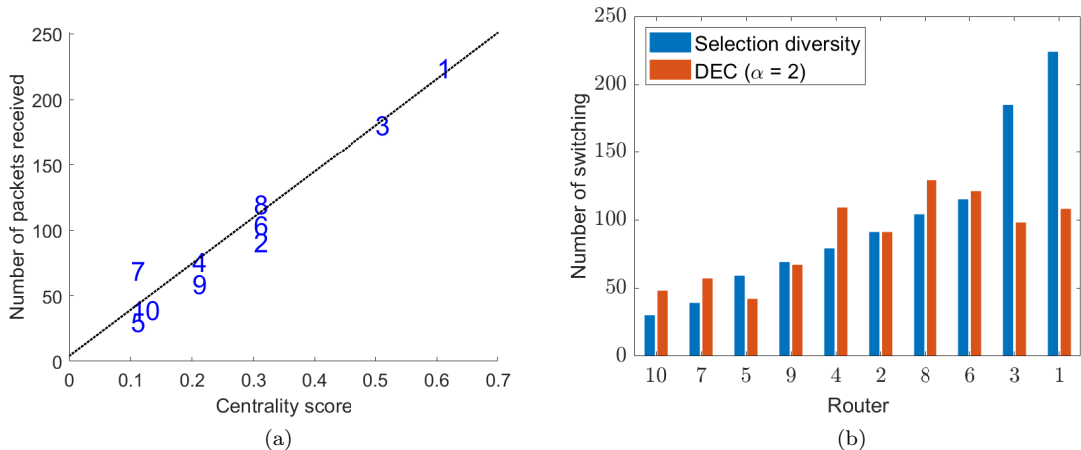


Figure 4.5: (a): The number of packets received by routers, plotted against their normalized centrality. We observe that routers which receive more data packets have higher centrality. (b): Comparison between selection diversity and the proposed technique in terms of switching frequency. Routers are plotted in ascending order based on the number of switching. Note that the number of switching is decreased for high scoring routers.

4.6.2 Simulation results

Figure 4.5 presents our results on the impact of the centrality metric in decreasing antenna switching rate. We focus on the routers only since sensor nodes are assumed to be unable to perform data forwarding. Figure 4.5a illustrates the centrality of routers calculated based on Eq. (7) and normalized by the total number of devices 60. We note that few routers stand out amongst other routers due to high centrality and thus, serve as central points of data aggregations. We also see that the high scoring routers receive and forward more data traffic, which deplete their energy rapidly, compared to other routers with low centrality values. The results also show the heterogeneity among routers in terms of data traffic through them and hence, reinforces the requirement of node-specific diversity scheme. Figure 4.5b shows the effect of using interval parameter α , where the antenna switching of routers with high centrality are restricted compared to other routers. Even though the number of switching varies for routers for different simulation runs, we observe that when α is set to 2, our proposed diversity scheme decreases antenna switching approximately by 17% compared to the conventional selection diversity.

Figure 4.6 demonstrates the use of interval parameter by comparing the centrality based diversity scheme with selection diversity technique in terms of packet delivery and energy consumption for different values of α . From Fig. 4.6a, we note that when $2 \leq \alpha \leq 3$, the proposed centrality based diversity scheme is on par with selection diversity technique in terms of packet delivery rate. However, as α increases, packet drop rate increases for our proposed scheme compared to the se-

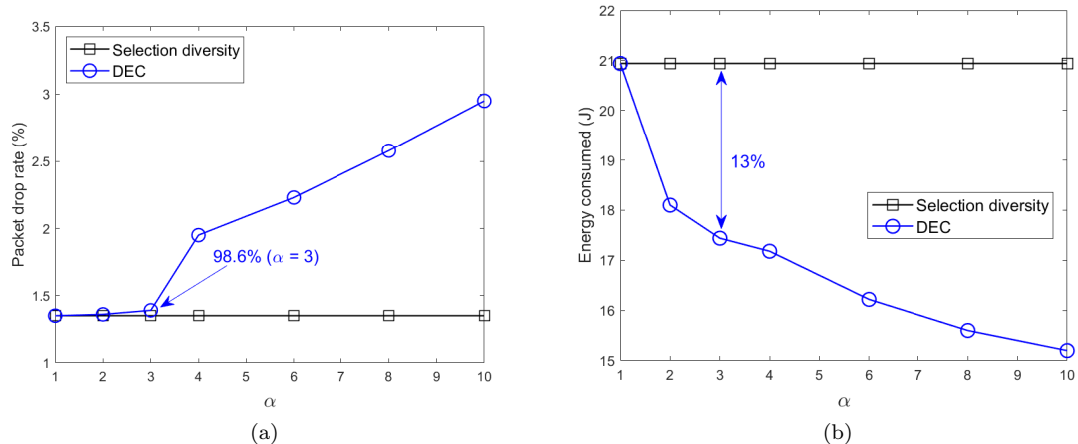


Figure 4.6: Comparison between selection diversity and the proposed technique for different values of α in terms of (a) packet drop rate and (b) energy consumption rate, for a network consisting of 50 sensor nodes and 10 routers. As can be seen in the figure, for $\alpha = 3$, our proposed scheme has approximately 99% successful packet delivery rate and reduces energy consumption by 13% compared to the selection diversity technique.

lection diversity. Since a large value of α increases the waiting time between consecutive antenna polarization selection, network reliability decreases. Fig. 4.6b demonstrates the influence of α on the energy consumption of routers, where energy consumption includes power consumed due to antenna switching, transmission and reception of both pilot packets and data packets. Since a large value of α implies that more routers have reduced switching rate, the energy consumption decreases considerably. However, restriction in updating antenna polarization for longer period results in greater packet loss compared to the selection diversity. Therefore, selecting an appropriate value of α is crucial for achieving satisfactory performance in terms of reliability and energy efficiency.

4.7 Conclusion

In this work, we present an energy-aware polarization diversity scheme based on node centrality metric for IoT networks. We consider a typical IoT network composed of sensor devices that periodically sense data and utilizes tripolar antenna to forward it to the base station through routers in a multi-hop fashion. The proposed diversity scheme leverages distributed eigenvector centrality metric, calculated by all IoT devices individually without requiring global information about the network topology, to measure a router's importance based on the importance of its connected neighbors. The identification of most influential router nodes allows us to employ a node-specific diversity scheme that lets low scoring routers to switch polarization more frequently compared to high scoring routers and hence decreases excessive switching over the whole network.

Our results suggest that methods to rank the influence of different nodes in complex networks can be applied in IoT networks to save energy consumption without compromising fidelity. Indeed, our simulation results demonstrate that the proposed centrality based approach reduces switching by at least 17% compared to the approach of utilizing selection diversity for all sensor and router nodes irrespective of their roles. The results show that the proposed scheme is able to lessen energy consumption by at least 13% compared to the conventional selection diversity while offering similar network reliability. In future work, we plan to implement the proposed scheme in real devices using various topologies and routing strategies.

Summary

In this work, we developed an adaptive switched diversity technique where antenna switching frequency of a particular node depends on the number of neighbors it is connected with. Using centrality metric we determined which nodes will see more data flow and limited their antenna switching frequency compared to the nodes with small number of child nodes. Results demonstrated that our node-specific antenna selection technique reduced the energy depletion rate of the routers significantly and satisfactory network reliability. Following the exploration of the connection between antenna diversity and network architecture, we continue investigating on possible improvement of the switched diversity technique. For multi-element antennas, when several branches have signal level below the threshold, the conventional switched diversity need to switch branches multiple times to determine the antenna that has acceptable signal strength. To prevent such unnecessary switching, we developed a diversity technique where antenna switching is based off of probabilistic relationship between observed signal strength values and antenna elements. The proposed technique, which leverages Hidden Markov Model (HMM) to model the antenna polarizations as hidden states and RSSI values as output observations, is described in the next chapter.

5 Coordinating Three-Branch Diversity Switching Using a Hidden Markov Model

Foreword

In this chapter, we evaluate the performance of a switched diversity technique for a tripolar antenna systems that uses probabilistic approach based on Hidden Markov model and measured data to determine antenna branch during data transmission. Section 5.1 presents the paper published at *2019 IEEE Internet of Things Journal* [142]. By leveraging experimental received signal strength data collected in a high multipath environment, the proposed technique models the antenna polarizations as hidden Markov states and calculates the transition probability between antenna branches for different thresholds. The work considered IoT applications where the time between consecutive transmissions by the transmitting node is large compared to the coherence time of the channel and thus, each transmission experiences independent fading. Compared to standard switched diversity where a device needs signal strength data from multiple branches during switching, the proposed technique monitors the currently active branch only and thus reduces excessive antenna switching. Experimental implementation of the proposed approach shows increased diversity gain, reduced energy consumption compared to standard switched diversity approach.

5.1 Abstract

Multi-element antenna systems have been shown to provide improved performance over single-element antennas in harsh, depolarizing propagation environments. However, how best to leverage these systems is still a challenge for low-cost implementations, e.g., for Internet of Things (IoT) devices. In this paper, we present a three-branch switched diversity scheme that models the transition between the elements of a tripolar antenna by means of a Hidden Markov Model (HMM), parameterized from measurement data. The proposed technique determines antenna polarization before each transmission using RSSI values, their probabilistic relationship with antenna elements, and transition probabilities among the diversity branches. Simulation and experimental results show that in high multipath environments, similar to those expected for many IoT networks, selection of the most likely antenna element before every transmission using the HMM approach leads to a median gain of 0.4 dB and -0.9 dB and a 1% diversity gain of 2.4 dB and -6.8 dB over conventional switched diversity and selection diversity, respectively, with no additional hardware costs. In addi-

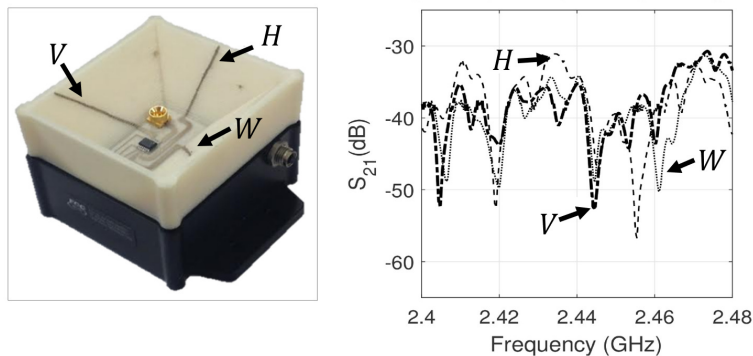


Figure 5.1: *Left*: A 3D tripolar antenna on top of a commercial sensor node. *Right*: Channel loss data (i.e., S_{21}) for each of the three mutually orthogonal elements of the tripolar antenna (i.e., V , H , and W) [3].

tion, a hardware implementation demonstrates that the proposed method can reduce power drain from the battery by at least 15% as compared to selection and switched diversity techniques, with no degradation in packet delivery rates [142].

5.2 Introduction

The Internet of Things (IoT) will enable physical objects to act as intelligent interconnected devices that can recognize events and changes in their surrounding environments and to gather, process, and share the collected data without any human intervention [143]. With the advent of small, low-power and low-cost embedded sensors and actuators, billions of physical objects around the world can be transformed into IoT devices to generate large amount of information of real-world physical processes in real time; thus effectively integrating the digital and physical world. There are numerous real-world applications of IoT such as smart grid [144], smart homes [145], industrial monitoring [146], object tracking [147], surveillance [148] and healthcare monitoring [149]. Depending on the application, IoT devices may be deployed in environments with less than ideal propagation environments due to the presence of significant multipath [150].

Cluttered conditions, as experienced by the industrial IoT networks deployed to monitor various industrial equipment [151] or environment inside of a factory [152], not only create multipath fading conditions, but have been shown to depolarize signals across all three spatial dimensions [7, 153, 154]. Antenna polarization diversity is an effective technique in such propagation environment as it leverages the depolarization phenomena to increase the capacity of wireless communication by using orthogonal polarizations (e.g., vertical vs. horizontal linear or right-hand vs. left-hand circular polarizations) [6].

Multipolarized antennas that exploit three-dimensional electric field vectors and realize different

polarizations by controlling the on/off states of PIN diodes or RF electromechanical switches have been investigated in recent years [155], [156]. For example, our recent works [3], [1] have shown that a compact three-element tripolar antenna performs better than dual-branch or monopole antenna system in multipath environments. As shown in Fig. 5.1, a tripolar antenna consists of three mutually orthogonal elements to create vertical (V) polarization, horizontal (H) polarization and a third polarization (W) which is perpendicular to the other two, experiences distinct fading conditions and illustrates the importance of using more than two antenna elements. To date, however, the implications of integrating multi-polarized antennas in IoT devices does not appear to have received much attention, which motivates the work presented herein.

One simple technique to leverage multi-polarized antennas is selection diversity, which continuously monitors each polarization branch in order to select the one with highest instantaneous power or received signal strength indication (RSSI) [6]. Although selection diversity ensures that the best diversity branch is always chosen, the hardware cost and energy associated with always monitoring each branch is not tenable for long-life, low-cost IoT devices, especially as the number of branches grows.

An alternative approach is switched diversity, where the receiver switches to alternative branches only when currently used branch has signal quality that is not acceptable, i.e., below a predetermined threshold [157]. A specific implementation of switched diversity is switch-and-examine combining, where if the RSSI goes below the threshold, the receiver keeps examining all available diversity branches until it finds a branch that satisfies the threshold. In case the receiver finds that none of the branches satisfy the RSSI requirement, it switches to the branch that has largest RSSI [158].

Although switched diversity offers an economical and cost-effective technique by reducing the number of receivers, the power gain is less than selection diversity as it keeps using currently selected antenna as long as the signal strength is above threshold and will not switch even though other antenna branches have better signal strength. Moreover, as the number of diversity branches grows more than two, the complexity of the scheme increases and the delay necessary to cycle through all the branches becomes problematic.

In this paper, we focus on implementing an energy efficient, reliable, and cost effective switch diversity technique for IoT networks. We introduce Hidden Markov Model (HMM) coordinated switching by modeling the antenna polarizations as hidden states and RSSI values as output observations. The proposed technique uses the received signal strength values from only the currently used branch and determines whether to stay at the current antenna element or switch to a different one before each transmission. In addition, the advantages of using the HMM approach over

conventional diversity schemes are quantified.

The original contributions of this paper are as follows:

- We propose a discrete-time, three-state HMM to implement switched diversity on a three-branch diversity antenna. The proposed technique requires monitoring only the currently used diversity branch and infers the most likely antenna element for transmission by analyzing the sequence of observed RSSI values, statistical properties of the observations, and derived transition probabilities of antenna elements.
- We conduct comprehensive experimental studies to analyze the performance of the proposed HMM approach and compare its performance with selection and switched diversity. We demonstrate that the proposed HMM approach, which is the most energy efficient compared to the other diversity schemes, yields a median gain of 0.4 dB and a 1% diversity gain of 2.4 dB over the conventional switched diversity, without additional hardware costs or compromising network reliability.

The subsequent parts of the paper are organized as follows. In Section 5.3, related works are discussed. We describe how an embedded device reaches the switching decision using a three-state, discrete-time HMM approach before every transmission in Section 5.4. The transition probabilities between the antenna elements are derived in Section 5.5. Section 5.6.1 describes experimental setup used for this work. The collected data are then used to determine the HMM model parameters (Section 5.6.2). In Section 5.6.3, both performance of the proposed approach is evaluated and compared to conventional diversity schemes using experimental and simulation results. Finally, Section 5.7 concludes this paper and discusses directions for future works.

5.3 Background

Related studies of note, both theoretical and experimental, have focused on switched diversity techniques and their performance in the presence of various fading conditions [1, 12, 91, 157–159].

The work of Blanco and Zdunek [12] analyzed the performance of ideal switched diversity, switch-and-stay diversity, and switch-and-examine diversity strategies theoretically for detecting frequency shift keying signals under Rayleigh fading environment and compared the performance to non-diversity and maximal ratio combining. Yang and Alouini [91] proposed a modified dual-branch diversity scheme by allowing the receiver to use the best branch when it cannot find any acceptable diversity branch after examining all available ones. Later, Nam and Alouini proposed a dual-branch switched diversity technique which used adaptive switching thresholds instead of a fixed thresh-

old [159]. Although the strategy of using a different threshold in every switching improves performance over conventional switched diversity, it also increases computation complexity. In [92], Tsouri *et al.* considered dual-branch switched diversity for compact wireless devices using a single RF combiner and analyzed the performance of implementing the the Karhunen-Loeve transform prior to down-conversion to baseband prior to the RF switch. Despite demonstrated performance improvements over conventional switched diversity, further studies are needed to explore the implementation complexity of the proposed techniques in low-cost, low-resourced IoT embedded devices.

Recent studies have shown an increased interest in diversity schemes with more than two branches [91, 92, 159–163]. For example, Lukama *et al.* [160] proposed a three-branch polarization diversity antenna system for indoor wireless communications and demonstrated that the antenna can achieve more than 2 dB diversity gain over dual-branch diversity antenna. In that work, diversity gain was defined as the difference between the equal-gain combined diversity signal and the antenna with the strongest signal. Similarly, [161–163] also proposed polarization reconfigurable diversity antenna systems with switchable radiation patterns realized through different combinations of PIN diodes and analyzed the RF characteristics in terms of sensitivity and overall gain of the antenna. In [164], Alexandropoulos, *et al.* studied the performance of switch-and-examine diversity over L arbitrarily correlated Nakagami- m fading channels which were not necessarily identically distributed. The work also presented analytical performance expressions for $L \leq 3$. In [165], Peppas *et al.* analyzed the compared the performance of triple-branch, generalized selection combining (GSC) receivers under Nakagami- m fading to other conventional diversity techniques. However, few related studies have addressed the issue of realizing diversity schemes in an energy efficient manner for resource-constrained IoT devices.

In the work presented herein, we investigate the performance of a HMM coordinated switched diversity technique in a relatively static and slowly varying Rayleigh-fading environment where minimal changes occur over longer periods of time and analyze the performance of our proposed scheme through simulation and experimental study to demonstrate that the proposed method can be an attractive alternative to the conventional selection and switched diversity scheme for constrained IoT devices.

To our knowledge, the closest match to the work herein is a second study conducted by Yang and Alouini [166], where the authors presented a Markov chain-based analytical framework for dual-branch switched diversity schemes under various fading environments. In the Markov approach, with a transition probability matrix that does not change over time, the next state (i.e., chosen antenna element) is determined only by the current state and RSSI is not considered. In contrast,

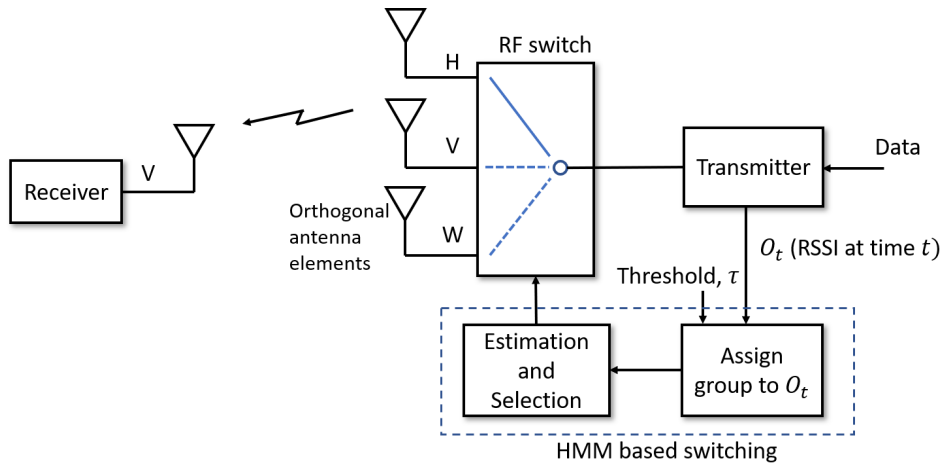


Figure 5.2: Block diagram of an HMM-based diversity system. H , V , and W correspond to the three mutually orthogonal antenna elements as well as the three hidden states in the HMM. O_t is the observable state (RSSI) at time t .

the switching decisions in HMM-based approach presented herein (Fig. 5.2) are also informed by the RSSI observations, O_t , and how close they are from a predetermined threshold, τ , thus enabling better branch selection results. When conventional switched diversity is employed, the antenna will not switch to a new branch until signal strength gets below a chosen threshold. Whereas, under our HMM approach, the antenna may switch even though the signal strength is above τ given the sequence of observations and the conditional distribution of the RSSI values governed by the antenna polarizations, i.e., unobserved states, and thus has higher probability to improve power gain. Additionally, in the case where multiple branches have signal strength below the threshold, the conventional switch diversity may have to switch branches several times to find the branch that has signal strength above the threshold. We show herein however that by choosing branches based on an HMM, ineffective switching can be avoided thereby reducing energy consumption.

5.4 HMM Coordinated Switching

In this section, we present our proposed HMM coordinated switched diversity scheme. A brief overview of the HMM is provided first. Next, we formulate switched diversity based on an HMM, including defining the probabilistic relationship between the observed RSSI values and antenna elements. Finally, we describe the steps of the algorithm employed by the proposed HMM approach to determine the most likely antenna element. The notation used in this work and respective descriptions are presented in Table 5.1.

Table 5.1: List of Notations

Symbol	Definition
X_t	state variable at time t
N	the number of hidden states
K	the number of distinct observation states
A	state transition probability matrix of size $N \times N$, where $a_{i,j}$ represents the probability of moving from state i to state j and $i, j \in \{H, V, W\}$
$\{H, V, W\}$	three polarizations of the tripolar antenna which correspond to the three hidden states of HMM
O_t	RSSI observation at time t
τ	received signal strength threshold, below which the signal is considered unacceptable
B	the emission probability matrix of size $N \times K$ and consists of emission probabilities $b^i(O_t)$
$b^i(O_t)$	probability that the antenna selects state i at time t , when the observation is O_t
π	the initial state probability vector of the hidden states of length N , where $\sum_{i=1}^N \pi_i = 1$
$\{Z_1, Z_2, Z_3\}$	set of possible observation states
$\delta^t(j, i)$	probability of HMM being in state j and transitioning to state i at based on observation O_t time t
μ_i^t	the highest probability that antenna selects state i at time t
$\{h_t, v_t, w_t\}$	the signal strength received on the horizontal, vertical and the third antenna elements, at time step t , respectively
$\{\alpha, \beta, \gamma\}$	mean received power at the horizontal, vertical and the third antenna elements, respectively

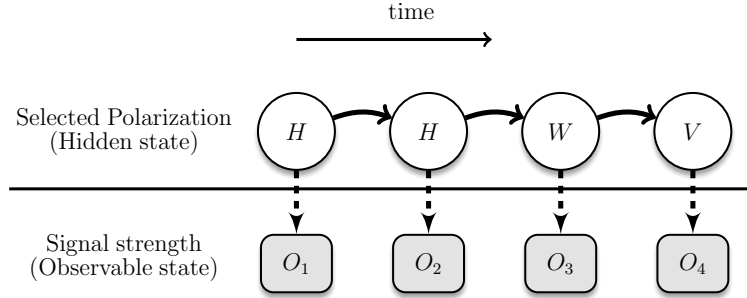


Figure 5.3: Block diagram of HMM states. Observations, O_t , i.e., RSSI values, which are explicit and antenna polarizations (H, V, W), which are hidden.

5.4.1 An overview of HMM

Characterizing the outputs of real-time processes, which can be discrete or continuous, is crucial in many research works. One way to do so is to model the output observations as a parametric random process using well-defined mathematical formalism while providing a theoretical framework for the underlying process which is hidden from the observer. The HMM is one such statistical tool that consists of a finite state Markov Chain with unobservable states and observable sequences that are associated with each state of the underlying Markov chain through probabilistic functions [167]. HMMs can be used to estimate model parameters, find most likely state sequences, and train models. Interested readers are referred to [168], [169], [170] for a comprehensive study of the topic. HMMs and their variants have been extensively used in a wide range of applications ranging from speech recognition [171] to biological sequence analysis [172]; in addition, HMMs have also been successfully used in time-series analysis [173], computational finance [174], pattern recognition [175], and transportation forecasting [176].

5.4.2 Proposed HMM approach

We model the switching between antenna polarizations as a discrete-time HMM, where at different time instances (i.e., transmission slots) the device is selecting one of the states (polarizations) in the finite state space for data transmission. The HMM modeling of the polarization diversity system is illustrated in Fig. 5.3, where the antenna elements (hidden states) are not directly observed. The observed states, i.e., RSSI values, which do not necessarily exhibit the Markov property and depend only on the currently used antenna polarization, are assumed statistically independent of the previous observations. Let X_1, X_2, \dots, X_t represent the state variables at different time steps denoted by the subscript with state space $S = \{H, V, W\}$, where H, V and W are the three hidden states of the HMM and represent the three mutually orthogonal antenna elements (Fig. 5.1). We now

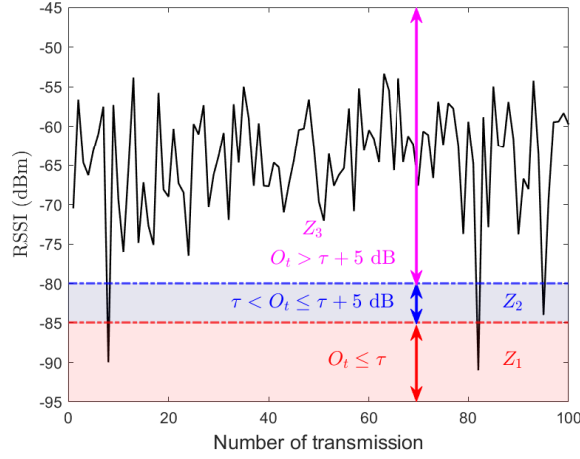


Figure 5.4: An example of partitioning RSSI values in three groups Z_1 , Z_2 and Z_3 , where τ is the predetermined threshold. The likelihood that the antenna selects one of the polarizations at each time step under a given observed state is provided in emission probability matrix B .

introduce the parameters used in our proposed HMM approach to determine the appropriate antenna polarization. For simplicity, mathematical notations are kept similar to prior work [171–173].

5.4.2.1 Transition probability matrix The matrix A of size $N \times N$, where N is the number of hidden states, is expressed as follows

$$A = \begin{bmatrix} a_{H,H} & a_{H,V} & a_{H,W} \\ a_{V,H} & a_{V,V} & a_{V,W} \\ a_{W,H} & a_{W,V} & a_{W,W} \end{bmatrix} \quad (9)$$

Here $a_{H,H}$ is the transition probability from hidden state H at time step $t - 1$ to hidden state H at time step t . Section 5.5 describes the derivation of these transition probabilities in detail.

5.4.2.2 Emission probability matrix As illustrated in Fig. 5.4, we classify the output RSSI observations (O_t) into three groups: Z_1 , Z_2 and Z_3 , where $O_t \leq \tau \in Z_1$, $\tau < O_t \leq \tau + 5 \text{ dB} \in Z_2$, and $O_t > \tau + 5 \text{ dB} \in Z_3$, where O_t is the RSSI observation at time t . Thus, the emission probability matrix, B of size $N \times K$, where K is the number of distinct observation states per hidden state, can

be expressed as:

$$B = \begin{bmatrix} b^H(Z_1) & b^H(Z_2) & b^H(Z_3) \\ b^V(Z_1) & b^V(Z_2) & b^V(Z_3) \\ b^W(Z_1) & b^W(Z_2) & b^W(Z_3) \end{bmatrix} \quad (10)$$

Here, $b^H(Z_1) = P(X_t = H | O_t \in Z_1)$ is the probability that the antenna selects state H at time t , when the observed RSSI being in Z_1 . The probability is calculated using our collected RSSI dataset by monitoring the frequency of selection of different antenna polarizations given the observation state.

5.4.2.3 Initial probability matrix The initial probability distribution vector, which has a length of N , can be written as

$$\pi = \{\pi_H, \pi_V, \pi_W\}, \quad \pi_i \in [0, 1] \quad (11)$$

where, π_H, π_V and π_W are the probabilities that the antenna will be in H, V or W state during the first transmission. The probabilities are initialized from uniformly distributed random numbers withing the interval $(0, 1)$ such that $\sum_{i=1}^3 \pi_i = 1$.

5.4.2.4 Algorithm The objective of the algorithms is to infer the best antenna polarization at different time instances based on just the RSSI observations of the currently used branch. The proposed approach consists of three steps as follows.

1. The first step is to initialize the polarization selection and we start with an uniform probability for all the polarizations of the antenna. Let, Z^0 be one of the observation groups depending on the initial RSSI observation O_0 at $t = 0$. Then, we can compute μ_i^o , where $i \in \{H, V, W\}$, by multiplying the initial probability of each states with $b^i(Z^0)$.
2. The next step is to determine the transition probabilities based on observed RSSI. Now, at time $t = 1$, let's say the observed signal strength of the currently used antenna element belongs in Z_1 . Having this observation will change our choice of antenna polarization. Now we will have higher probability of switching the antenna element as RSSI of the currently used antenna element is below the acceptable level, as shown in Fig. 5.4. If we are at time instance $t = 2$ and have signal strength in Z_3 , we expect to have the highest probability to remain in same hidden state. To determine the probability of being in sate j at time $t - 1$ and selecting state i at time t given

the observation being in Z^t , for each state i , we multiply μ_j^{t-1} with the transition probability $a_{j,i}$ and emission probability $b^i(Z^t)$. Since, we know the currently used antenna element from which the observation is generated, we don't have to iterate over j .

3. In the final step, we find the most likely state i and maximum probability μ_i^t , where the maximum is taken over the index i . Thus combining transition probabilities between antenna elements, emission probabilities and the information of the current RSSI readings, we can select the most likely antenna element before each transmission.

We describe the pseudocode that is used to implement the proposed HMM approach in the Arduino based embedded devices during the experiments below. Since we sort a $N \times 1$ array for N individual antenna polarizations, which has a time complexity of $\mathcal{O}(N)$, and then find the maximum value among the N antenna elements, the computational complexity of the proposed HMM approach becomes $\mathcal{O}(N^2)$, where N is the number of hidden states.

Algorithm 1: Algorithm for HMM approach

```

Input:  $O_t, A, B, \pi$ 
Output: Most probable antenna polarization
Init: - evaluate group for the first observation  $O_0$ 
        -  $\mu_i^0 \leftarrow \pi_i b^i(Z^0), i = 1, \dots, N$ 
foreach state  $i$  from 1 to  $N$  do
  |  $\delta^t(j, i) = \mu_j^{t-1} a_{j,i} b^i(Z^t)$ 
end
                                                    /* find most probable polarization */

for  $i = 1$  to  $N$  do
  |  $value \leftarrow \delta^t(j, i)$ 
  | if  $value > \mu_i^t$  then
  | |  $\mu_i^t \leftarrow value;$ 
  | |  $maxindex \leftarrow i;$ 
  | end
end
return  $maxindex$ 

```

5.5 Defining State Transition Probability

The transition probability matrix, denoted by A , describes the probability of transition from one antenna element to another and depends on the channel conditions where the devices are deployed. We consider three independent Rayleigh channels which may not necessarily be identically distributed for the operating environment, where the power of the signal is exponentially distributed the PDF is given by Eq. (7.56) of [53].

$$P(x_i) = \frac{1}{\bar{x}_i} \exp\left(-\frac{x_i}{\bar{x}_i}\right) \quad (12)$$

where \bar{x}_i and x_i is the mean and received power at the i^{th} branch and $i \in \{H, V, W\}$. We also assume perfect channel estimation and negligible time delay between channel estimation, diversity technique implementation, and packet transmission. Channel realization are drawn randomly at each time step and remains fixed during each time step. We start with deriving the probability that the antenna will not switch for two consecutive time steps. For example, $a_{H,H}$ represents the probability that the antenna will stay at the same state H at time $t - 1$ and t . Now, to determine $a_{H,H}$, we need to consider two events. One scenario is when the received signal strength at the horizontally polarized antenna element stays above the threshold τ at time steps $t - 1$ and t . Another when at time t the signal strength at the horizontal branch falls below τ but none of the other branches has better signal strength than the horizontal branch. Hence, $a_{H,H}$ can be expressed as

$$\begin{aligned} a_{H,H} &= \{X_t = H \mid X_{t-1} = H\} \\ &= P(h_{t-1} > \tau)P(h_t > \tau) \\ &\quad + P(h_t \leq \tau)P(h_t > v_t, w_t \mid \{h_t, v_t, w_t\} \leq \tau) \end{aligned} \quad (13)$$

where h_t, v_t and w_t represent the signal strength received on the horizontal, vertical and the third antenna element at time step t , respectively.

Next, we define the probability of transition from one state to another. For example, $a_{H,V}$ represents the probability that the antenna was in state H at time $t - 1$ and will switch to state V at time t as the signal strength at the horizontal branch falls below the threshold at time t . We can express this as

$$\begin{aligned} a_{H,V} &= \{X_t = V \mid X_{t-1} = H\} \\ &= P(h_t \leq \tau)P(v_t > \tau)P(v_t > w_t) \\ &\quad + P(h_t \leq \tau)P(v_t > h_t, w_t \mid \{h_t, v_t, w_t\} \leq \tau) \end{aligned} \quad (14)$$

$a_{H,W}$ is similar to $a_{H,V}$ if we replace V with W . Now we want to find $P(v_t > h_t, w_t \mid \{h_t, v_t, w_t\} \leq \tau)$.

Let, $\wedge \equiv \max$ and we note that

$$P(v_t > h_t \wedge w_t \mid \{h_t \wedge v_t \wedge w_t\} \leq \tau) = \frac{P((v_t > h_t \wedge w_t) \cap (\{h_t \wedge v_t \wedge w_t\} \leq \tau))}{P(\{h_t \wedge v_t \wedge w_t\} \leq \tau)} \quad (15)$$

Let h, v and w have exponential distributed densities with mean \bar{x}_h, \bar{x}_v and \bar{x}_w , respectively, where $\bar{x}_h = \alpha, \bar{x}_v = \beta$ and $\bar{x}_w = \gamma$ [[53] Eq. (7.56)].

$$\begin{aligned} P(\{h_t \wedge v_t \wedge w_t\} \leq \tau) &= P(h_t \leq \tau)P(v_t \leq \tau)P(w_t \leq \tau) \\ &= (1 - e^{-\frac{\tau}{\alpha}}) \left(1 - e^{-\frac{\tau}{\beta}}\right) \left(1 - e^{-\frac{\tau}{\gamma}}\right) \end{aligned} \quad (16)$$

The numerator of Eq. (15) can be determined as follows

$$P((v_t > h_t \wedge w_t) \cap (\{h_t \wedge v_t \wedge w_t\} \leq \tau)) = \int_0^\tau \int_0^\tau \int_{h \wedge w}^\tau f_v(v) f_h(h) f_w(w) dv dh dw \quad (17)$$

We can then rewrite Eq. (17) as

$$P((v_t > h_t \wedge w_t) \cap (h_t \wedge v_t \wedge w_t \leq \tau)) \equiv \int_0^\tau f_w(w) \overbrace{\int_0^\tau f_h(h) \underbrace{\int_{h \wedge w}^\tau f_v(v) dv}_{I_1(h,w)} dh}_{I_2(w)} dw \quad (18)$$

We can write the innermost integral of Eq. (18) as:

$$I_1(h, w) = \frac{1}{\beta} \int_{h \wedge w}^\tau e^{-v/\beta} dv = e^{-(h \wedge w)/\beta} - e^{-\tau/\beta} \quad (19)$$

and the middle integral of Eq. (18) as:

$$\begin{aligned} I_2(w) &= \int_0^\tau f_h(h) I_1(h, w) dh \\ &= \frac{1}{\alpha} \int_0^\tau e^{-\frac{h}{\alpha}} \left(e^{-\left(\frac{h \wedge w}{\beta}\right)} - e^{-\frac{\tau}{\beta}} \right) dh \\ &= \frac{1}{\alpha} \int_0^\tau e^{-\left(\frac{h}{\alpha} + \frac{(h \wedge w)}{\beta}\right)} - e^{-\left(\frac{h}{\alpha} + \frac{\tau}{\beta}\right)} dh \end{aligned} \quad (20)$$

Now, the easiest way to handle $h \wedge w$ in Eq. (20) is to split the integral up into “cases”, which can be written using the indicator function. In particular, since $w \geq 0$, then

$$\begin{aligned}
I_2(w) &= \frac{1}{\alpha} \int_0^\tau e^{-\left(\frac{h}{\alpha} + \frac{w}{\beta}\right)} \mathbf{1}_{(0,w)}(h) + e^{-\left(\frac{h}{\alpha} + \frac{h}{\beta}\right)} \mathbf{1}_{(w,\tau)}(h) dh \\
&\quad - \frac{1}{\alpha} \int_0^\tau e^{-\left(\frac{h}{\alpha} + \frac{\tau}{\beta}\right)} dh \\
&= \frac{1}{\alpha} \int_0^w e^{-\left(\frac{h}{\alpha} + \frac{w}{\beta}\right)} dh + \frac{1}{\alpha} \int_w^\tau e^{-\left(\frac{h}{\alpha} + \frac{h}{\beta}\right)} dh \\
&\quad - \frac{1}{\alpha} \int_0^\tau e^{-\left(\frac{h}{\alpha} + \frac{\tau}{\beta}\right)} dh \\
&= e^{-\frac{w}{\beta}} \left(-e^{-\frac{h}{\alpha}}\right) \Big|_0^w + \frac{\beta}{\alpha + \beta} \left(-e^{-h\left(\frac{1}{\alpha} + \frac{1}{\beta}\right)}\right) \Big|_w^\tau \\
&\quad + e^{-\frac{\tau}{\beta}} \left(e^{-\frac{h}{\alpha}}\right) \Big|_0^\tau \\
&= e^{-\frac{w}{\beta}} - e^{-w\left(\frac{1}{\alpha} + \frac{1}{\beta}\right)} + \frac{\beta}{\alpha + \beta} e^{-w\left(\frac{1}{\alpha} + \frac{1}{\beta}\right)} \\
&\quad - \frac{\beta}{\alpha + \beta} e^{-\tau\left(\frac{1}{\alpha} + \frac{1}{\beta}\right)} + e^{-\tau\left(\frac{1}{\alpha} + \frac{1}{\beta}\right)} - e^{\frac{\tau}{\beta}} \\
&= e^{-\frac{w}{\beta}} - \left(\frac{\alpha}{\alpha + \beta}\right) e^{-w\left(\frac{1}{\alpha} + \frac{1}{\beta}\right)} - e^{\frac{\tau}{\beta}} \\
&\quad + \left(\frac{\alpha}{\alpha + \beta}\right) e^{-\tau\left(\frac{1}{\alpha} + \frac{1}{\beta}\right)}
\end{aligned} \tag{21}$$

where $\mathbf{1}$ is the indicator function. The indicator function can be considered as a simple function that takes value “1” when an event happens and value “0” when the event does not happen. Lastly, plugging Eq. (19) and Eq. (21) in Eq. (18), we can write,

$$\begin{aligned}
P(v_t > h_t \wedge w_t, \{h_t \wedge v_t \wedge w_t\} \leq \tau) &= \frac{1}{\gamma} \int_0^\tau f_w(w) I_2(w) dw \\
&= \frac{1}{\gamma} \int_0^\tau e^{-w\left(\frac{1}{\gamma} + \frac{1}{\beta}\right)} dw - \frac{\alpha}{\gamma(\alpha + \beta)} \int_0^\tau e^{-w\left(\frac{1}{\alpha} + \frac{1}{\beta} + \frac{1}{\gamma}\right)} dw \\
&\quad + \frac{\alpha}{\gamma(\alpha + \beta)} e^{-\tau\left(\frac{1}{\alpha} + \frac{1}{\beta}\right)} \int_0^\tau e^{-\frac{w}{\gamma}} dw - \frac{1}{\gamma} \int_0^\tau e^{-\frac{w}{\gamma} - \frac{\tau}{\beta}} dw \\
&= \frac{\beta}{\beta + \gamma} \left(1 - e^{-\tau\left(\frac{1}{\beta} + \frac{1}{\gamma}\right)}\right) - \frac{\alpha^2 \beta}{(\alpha + \beta)(\alpha\beta + \beta\gamma + \alpha\gamma)} \\
&\quad \left(1 - e^{-\tau\left(\frac{1}{\alpha} + \frac{1}{\beta} + \frac{1}{\gamma}\right)}\right) + \frac{\alpha}{\alpha + \beta} e^{-\tau\left(\frac{1}{\alpha} + \frac{1}{\beta}\right)} \left(1 - e^{-\frac{\tau}{\gamma}}\right) \\
&\quad - e^{-\frac{\tau}{\beta}} \left(1 - e^{-\frac{\tau}{\gamma}}\right) \\
&= \frac{\beta}{\beta + \gamma} \left(1 - e^{-\tau\left(\frac{1}{\beta} + \frac{1}{\gamma}\right)}\right) - \frac{\alpha^2 \beta}{(\alpha + \beta)(\alpha\beta + \beta\gamma + \alpha\gamma)} \\
&\quad + \frac{\alpha}{\alpha + \beta} e^{-\tau\left(\frac{1}{\alpha} + \frac{1}{\beta}\right)} - \frac{\alpha\gamma}{(\alpha\beta + \beta\gamma + \alpha\gamma)} e^{-\tau\left(\frac{1}{\alpha} + \frac{1}{\beta} + \frac{1}{\gamma}\right)}
\end{aligned} \tag{22}$$

To define all the transition probabilities of the underlying Markov chain for our proposed HMM approach, we compute α , β and γ by exploiting the RSSI data obtained from embedded devices equipped with tripolar antenna (see Section 5.6.1). The collected data from multiple devices are used to validate our assumption of exponential densities, estimate the mean, and compute transition and emission matrices of HMM.

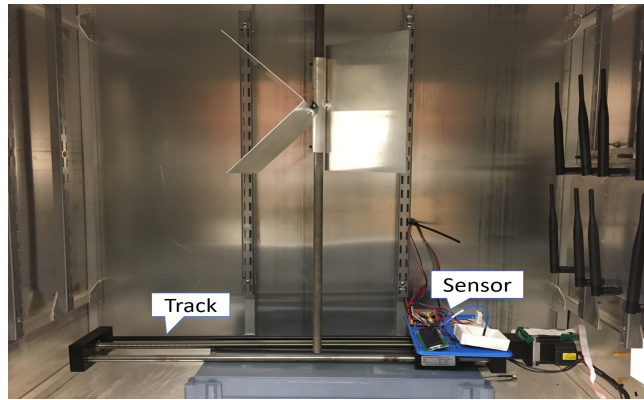
5.6 Implementation and Performance Evaluation

In this section, we describe how experiments were performed to collect channel measurements and how the obtained data were used to train and implement our proposed HMM approach. Furthermore, we compare the HMM approach with selection diversity and conventional switched diversity using real and simulated datasets.

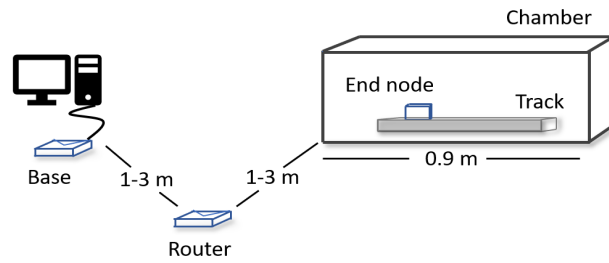
5.6.1 Data collection

IoT networks consist of power conserving, tiny embedded devices that use very little bandwidth. ZigBee is a protocol that offers secure and robust communications and that considers these constraints [177]. For our setup, we used an Arduino-based temperature sensor supported by XBee wireless modules to exchange data between the deployed devices. The Arduino, whose main component is a microcontroller, supports a number of analog and digital pins that can be used to manage hardware devices effectively while ensuring scalability and power efficiency.

To collect data from real-world environment, we deployed three prototype devices classified as end device, router and base station, respectively. The end device sensed temperature in every minute and forwarded temperature data to the router along with RSSI values obtained from all three elements of the tripolar antenna operating at 2.4 GHz. To emulate a high multipath environment, the end node was placed inside of a reverberation chamber (see Fig. 5.5), which can create highly reflective wireless propagation conditions. The router, which was deployed outside of the chamber, forwarded the data packets to the base station for further processing. The base station, connected to a desktop computer via USB cable, acted as a coordinator of the ZigBee network. The distance between the devices were varied from 1 meter to 3 meter by placing an end device on a LabVIEW [178] controlled linear actuator, which moved the device to 50 repeatable positions and retracted to the initial position once measurements were done. The tripolar antenna uses a low-cost non-reflective single pole triple throw RF switch (model HMC245AQS16) to control the switching between antenna polarizations [3]. The antenna, which is fabricated on 3D printed acrylonitrile butadiene styrene



(a)



(b)

Figure 5.5: (a) Utilizing a compact reverberation chamber along with the end node (i.e., IoT sensor) on top of a linear track to create harsh propagation environment (b) Block diagram of the experimental setup used to collect signal strength data from embedded devices enabled with tripolar antenna system.

filament, has three microstrip lines along with the RF switch manually placed in the bottom ground plane.

During the data collection phase, data observed at all three antenna branches are collected at the base station to create the database for HMM modeling. Since the XBee modules used in our experiment have receiver sensitivity of -100 dBm, which is the minimum signal power level for the receivers to be able to demodulate the transmitted data successfully [179], we set τ to 15 dB higher than the receiver sensitivity, i.e., $\tau = -85$ dB.

5.6.2 Learning HMM parameters:

The transition probability matrix for the proposed HMM approach was calculated using Eq. (5 - 14), which are derived based on the definition of switched diversity as described in Section 5.5. It is worth mentioning that for the tripolar antenna there could be multiple scenarios such as all three branches may have RSSI less or above the threshold and the state transition will vary according to that. We ran the experiment by deploying an end node sensor device equipped with tripolar antenna inside of the reverberation chamber and collected 3000 data points (RSSI value) for each of the antenna polarizations. Next, we determined the mean received signal strength values from the experimental data for each antenna polarization and entered them into the probability equations to calculate the transition probability matrix.

The emission probability matrix was calculated based on the observed frequencies of antenna branch switching for each of the defined observation states Z_1 , Z_2 and Z_3 . Using a Matlab script, we processed a single trace of RSSI data captured using one of the polarizations. First, we determined the group for each observation (RSSI value) based on the classifications defined in Section 5.4. We then determined the polarization selected by the antenna given the observation state at time t by leveraging the definition of switched diversity. When observation value is in group Z_3 , the antenna will continue using the same polarization and it will switch to other polarization if RSSI value is in Z_2 or Z_1 provided that either of the remaining polarizations has RSSI value that is in Z_3 . If all three branches have RSSI that belong in either Z_2 or Z_1 , it switches to the branch that has the largest RSSI among all the branches. We then repeated the same procedure for the rest of the data points captured using other antenna polarizations and determined the frequency of selection of each antenna polarization from different observation states. To analyze the effects of using different group intervals for observation states on the proposed HMM approach, we varied the width of Z_2 ranging from $\tau + 3$ dB to $\tau + 15$ dB and found that for large intervals performance degrade due to excessive switching. While we present the results when $\tau < O_t \leq \tau + 5$ dB is defined as the interval

Table 5.2: Calculated HMM Parameters

Matrix A			Matrix B			
	H	V	W	Z_1	Z_2	Z_3
H	$\begin{bmatrix} 0.6 & 0.2 & 0.2 \end{bmatrix}$			H	$\begin{bmatrix} 0.2 & 0.3 & 0.3 \end{bmatrix}$	
V	$\begin{bmatrix} 0.2 & 0.7 & 0.1 \end{bmatrix}$			V	$\begin{bmatrix} 0.7 & 0.5 & 0.4 \end{bmatrix}$	
W	$\begin{bmatrix} 0.2 & 0.3 & 0.5 \end{bmatrix}$			W	$\begin{bmatrix} 0.1 & 0.2 & 0.3 \end{bmatrix}$	

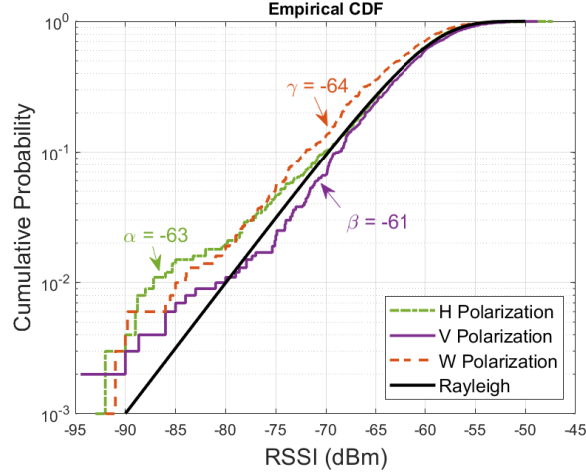


Figure 5.6: Empirical CDF of measurement data obtained from horizontal (H), vertical (V), and the third element (W) of the tripolar antenna, where mean values of the RSSI values obtained from three branches are $\alpha = -63$ dBm, $\beta = -61$ dBm and $\gamma = -64$ dBm, respectively

for Z_2 , similar performance were obtained when interval was varied ± 2 dB.

Table 5.2 presents the calculated transition probability matrix, A and the probabilities of emission matrix B . Fig. 5.6 shows three empirical CDF plots along with mean values for RSSI values observed at three elements of the tripolar antenna. We found that the link for vertical polarization exhibited approximately Rayleigh fading and other two polarizations had fading response worse than Rayleigh. To properly investigate the performance of the proposed HMM approach and validate our assumption of a static wireless propagation environment, we collected several datasets over time (each containing 9000 data points in total) and repeated the noted calculations. The probabilities for each cell in matrix A and B varied ± 0.1 across the datasets, which demonstrate that the conditions remain fairly constant and time variance can be neglected in the presented analysis. We also note that the matrices computed from the experimental data are asymmetric, which indicates that each branch has unique behavior which is captured by the HMM. Fig. 5.7 illustrates how the end device employs diversity using our proposed HMM approach. The HMM modeling on the right side of the Fig. 5.7 fits the experimental dataset to an appropriate exponential distribution. After determining the

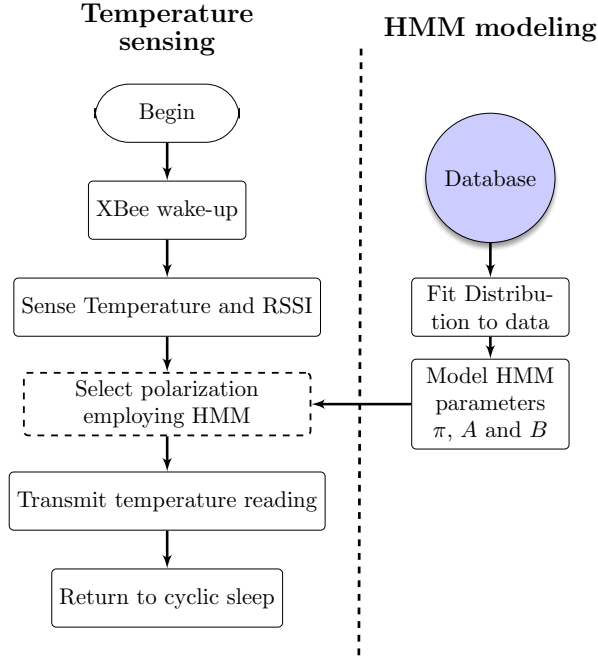


Figure 5.7: Flowchart of basic operation of the Arduino temperature sensor utilizing the proposed HMM approach

A and B matrices, to compare the performance between selection diversity, switched diversity and the proposed HMM approach, we let the end node to transmit 1000 packets to the base station using the three strategies separately. We repeated the procedure 10 times and for each subsequent experiment, the track was moved to a different place inside of the chamber and the position of the stirrers was changed. Next, we present and discuss the findings of the study based on simulation and experimental results.

5.6.3 Results

In this section, the performance of our proposed HMM approach is evaluated through simulation and empirical studies. We categorize the results in three parts and compare the effectiveness of our proposed technique with other related schemes in terms of power gain, reliability, and energy efficiency.

5.6.3.1 Power gain Fig. 5.8 shows the empirical CDF of different RSSI-driven diversity schemes when three diversity branches are used. We note that selection diversity has higher probability to obtain best RSSI values, but requires always observing all three antenna branches. For IoT systems, we assume only one receiver is available to keep costs low and the device will need to switch between all branches to monitor RSSI and then select the best branch. In case of switch

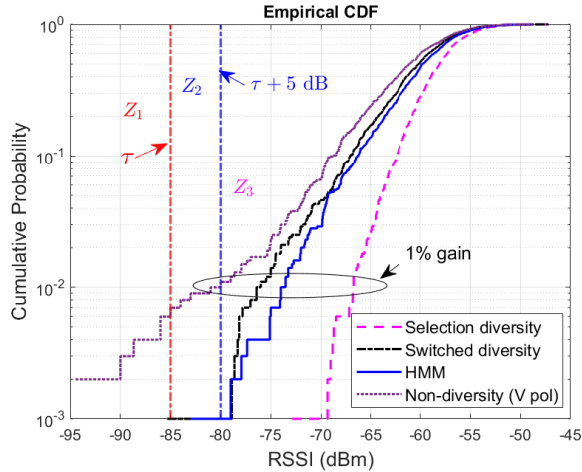


Figure 5.8: Comparison of empirical CDF among selection diversity, switched diversity, HMM approach and non-diversity techniques when tripolar antenna is used

and examine technique, the device only switches when signal strength of the currently used branch becomes lower than the threshold. In contrast, the proposed HMM approach allocates three distinct observation groups per branch, using observed signal strength of the currently selected antenna element, transition probability, and emission probability associated with each branch, the device might switch to another diversity branch even when the active branch is above τ . As illustrated in Fig. 5.8, the proposed HMM approach has high probability of obtaining better RSSI values than the switched diversity.

Table 5.3: Gain Comparison Among Various Schemes

Gain difference	Median (dB)	1% Gain (dB)
HMM vs Monopole	0.6	6.5
HMM vs Switched diversity	0.4	2.4
HMM vs Selection diversity	-0.9	-6.8

Table 5.3 summarizes the gain difference between the proposed HMM approach versus selection, switched diversity and monopole antenna system i.e., non-diversity system. Diversity gain is crucial since we prefer the received power to be greater than the receiver sensitivity so that the signal can be decoded successfully. We see that although selection diversity outperforms all other diversity schemes, our proposed scheme was able to perform better than switched diversity and non-diversity system. The results also show that the 1% link margin gain is 2.4 dB for our proposed technique relative to switched diversity with a median gain of 0.4 dB.

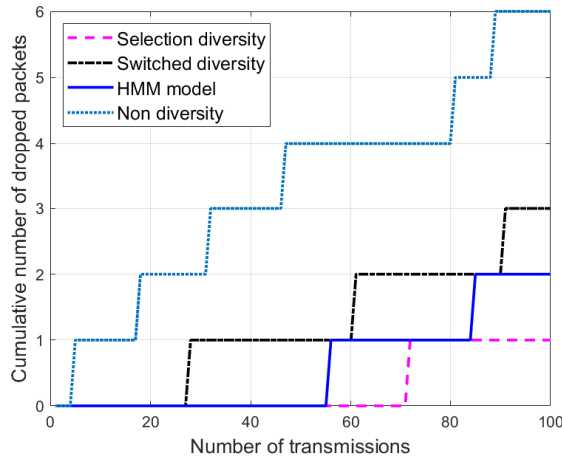


Figure 5.9: Comparison between selection diversity, switched diversity, HMM approach and non-diversity schemes in terms of data packet delivery

5.6.3.2 End-to-end packet delivery To assess the reliability of our proposed HMM coordinated diversity scheme, we compare the performance of packet delivery rate with selection and switched diversity. For this experiment, we configured an end device to transmit temperature data at an interval of 1 minute to its nearest router using each of the three diversity schemes. A packet is considered to be dropped if its RSSI is less than τ . Fig. 5.9 shows the simulation results, which were averaged over 10 runs. While selection diversity has the lowest packet drop rate (1%), our proposed HMM approach has slightly better packet delivery rate (98%) compared to the switched diversity (97%). Thus, the experimental results prove that the efficiency of the HMM coordinated switched diversity in terms of packet delivery reliability is on par with switched diversity, but again with non-insignificant received power gains.

5.6.3.3 Energy efficiency Finally, we evaluate the energy efficiency of the proposed HMM coordinated switched diversity scheme in terms of total energy consumed by the device during active period and compare to other existing diversity techniques. From Fig. 5.10, it can be seen that selection diversity requires the device to remain active for highest amount of time among the three schemes as the device has to switch between all three branches and compare the RSSI values to determine the best branch. When multiple receivers are available, wake time is not a concern for selection diversity as the device will be able to monitor all branches simultaneously (at a cost of more current draw). In case of the switched diversity, the device only switches when the RSSI of the currently used diversity branch drops below τ , and when the device is not switching both HMM approach and switched diversity consume the same amount of energy as the device

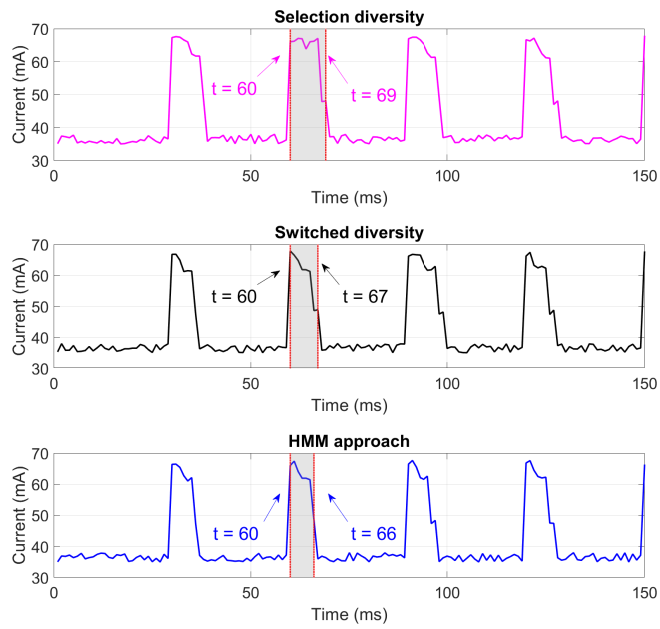


Figure 5.10: Current consumption vs time during packet transmission for different diversity techniques

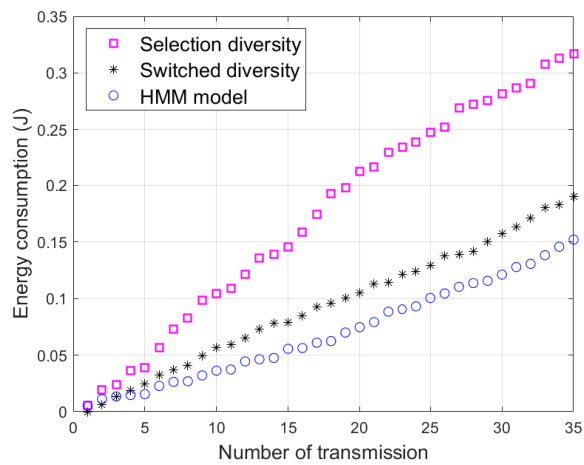


Figure 5.11: Comparison between selection diversity, switched diversity and the proposed HMM approach in terms of battery energy consumption

only monitors the active branch. However, under the switched diversity technique when the device switches between diversity branches, it can consume more energy than the HMM approach which selects the diversity branch based on probabilistic calculation. As illustrated in Fig. 5.11, energy consumption by the proposed HMM approach is 15% and 49% lower compared to the conventional switched diversity and selection diversity, respectively. We find from our results that power gain, data delivery and energy efficiency of IoT networks can be improved by using the proposed HMM coordinated switched diversity scheme compared to the conventional switched diversity technique. Although results presented here only show improvements for three-branch diversity antennas, the HMM approach, which has a quadratic time complexity, can easily be extended for antennas with more than three branches provided that the transition and emission matrices are derived properly from the RSSI data of the respective antenna.

5.7 Conclusion

In this paper, we have proposed a Hidden Markov Model based coordinated diversity technique that infers the best possible state, i.e., diversity branch, before every transmission by combining the underlying Markov chain structure of diversity branches along with the sequence of observations (RSSI values). The proposed approach eliminates ineffective or unnecessary switching between antenna elements that may result when conventional switched diversity is used.

We demonstrated the approach on a three-element, tripolar antenna integrated with a Zigbee-based system. We found that the HMM approach improved the median and 1% diversity gains by 0.4 and 2.4 dB, respectively, over a switch diversity implementation that utilized the same decision threshold. We also demonstrated that the developed approach, whose parameters were calculated using a large dataset of RSSI values collected in a highly cluttered environment, is on par with switched diversity in terms of packet delivery reliability. Finally, the efficacy of the proposed scheme was assessed in terms of energy use, where it reduced consumption by approximately 15% compared to the switched diversity. As the proposed approach does not require any additional hardware for this performance gain (as opposed to implementing selection diversity), we contend that it could be applicable for low-cost IoT devices.

In future work, the performance of online HMM coordinated diversity scheme that can determine and update model parameters dynamically by analyzing RSSI observation sequence over time rather than relying on previously-obtained datasets will be studied. In addition, determining appropriate number of observation states for experimental RSSI data and tuning the threshold to find optimal

group intervals will be examined. Finally, we would like to develop and illustrate the suitability of the HMM approach for diversity antennas with four or more branches.

5.8 Appendix

In this Appendix, we describe the pseudocode that is used to implement the proposed HMM approach in the Arduino based embedded devices during the experiments.

Algorithm 2: Algorithm for HMM approach

```

Input:  $O_t, A, B, \pi$ 
Output: Most probable antenna polarization
Init: - evaluate group for the first observation  $O_0$ 
         -  $\mu_i^0 \leftarrow \pi_i b^i(Z^0), i = 1, \dots, N$ 
foreach state  $i$  from 1 to  $N$  do
  |  $\delta^t(j, i) = \mu_j^{t-1} a_{j,i} b^i(Z^t)$ 
end

                                     /* find most probable polarization */

for  $i = 1$  to  $N$  do
  |  $value \leftarrow \delta^t(j, i)$ 
  | if  $value > \mu_i^t$  then
  | |  $\mu_i^t \leftarrow value;$ 
  | |  $maxindex \leftarrow i;$ 
  | end
end
return  $maxindex$ 

```

Since we sort a $N \times 1$ array for N individual antenna polarizations, which has a time complexity of $\mathcal{O}(N)$, and then find the maximum value among the N antenna elements, the computational complexity of the proposed HMM approach becomes $\mathcal{O}(N^2)$, where N is the number of hidden states.

Summary

In this work, a Hidden Markov Model based approach is developed to deduce the best diversity branch by modeling antenna transition probabilities as a Markov chain in addition to the signal strength values received at the currently active branch. Results demonstrated that by reducing unnecessary switching between diversity branches, our proposed approach achieved higher energy efficiency and better diversity gain compared to the conventional switched diversity scheme. Although the findings were promising, the results were based on point-to-point single link performance only and did not examine global network behaviour. We followed up the work by building an IoT network with three practical sensor devices equipped with tripolar antennas and explored the impact

of antenna selection of one node on its neighboring devices. The subsequent chapter described the work, where we focused on techniques to configure antenna element for tripolar antenna devices in a multi-hop network.

6 Switching-based Selection Techniques for Tripolar Antennas in Multi-hop IoT Networks

Foreword

Multi-hop based antenna selection techniques that consider lower and upper layer nodes' current antenna configuration status during antenna switching is presented in this chapter. The work presented here was accepted for publication in *IEEE Internet of Things Journal* on February, 2022. Multi-element antennas deployed in a high multipath environment experience different fading conditions between the lower link and upper link, which is used for reception and transmission, respectively. In contrast to standard diversity techniques, which considers single point to point link and determines antenna branch prioritizing transmission only, this work investigates the impact of antenna selection during reception and transmission. Two different multi-branch antenna selection approaches, namely Max-Sum and Max-Min, are proposed which maximizes joint SNR over different antenna branches and maximizes minimum SNR, respectively. Both analytical and experimental results are obtained and comparative analysis with standard diversity techniques are presented to emphasize the incorporation of dual-hop antenna configuration information during antenna selection of a node in a multi-hop based IoT network.

6.1 Abstract

Adaptive multi-element antennas can be leveraged to improve the reliability of wireless systems deployed in cluttered, depolarizing environments, such as those expected for Internet of Things (IoT) applications. While the performance improvement provided by such antennas has been well studied for individual links, multiple-hop networks have received little attention. In this work, we consider the problem of how devices in a multi-hop network should configure a three-element, tripolar antenna when deployed in a Rayleigh fading environment. We propose two switching-based antenna selection strategies, Max-Sum and Max-Min, each of which considers the channel conditions for communicating to nodes both higher and lower in the network hierarchy. We first derive the outage performance of the proposed schemes analytically and compare their performance with the well-known approaches of selection and switched diversity. Through simulations, which utilize empirical channel data from IoT devices equipped with a tripolar antenna, we show that the proposed Max-Sum and Max-Min scheme reduces antenna switching by over 80%, when compared to selection

diversity. In addition, these two approaches lead to a median gain of 1.8 dB and 0.3 dB and a 1% diversity gain of 3.6 dB and 1.4 dB, respectively, relative to switched diversity¹.

6.2 Introduction

The rapid development of wireless communications and sensor hardware technology over the past years have stimulated the widespread usage of low cost IoT devices and enabled a wide range of novel applications and services, e.g., industrial monitoring [180], intelligent vehicular networks [181], agricultural monitoring [182] and smart grids [183]. The pervasiveness of IoT applications implies systems being deployed in evermore complex environments with no line-of-sight and severe multipath conditions that reflect, refract, diffract and depolarizes the signal [184]. The loss of polarization orthogonality due to depolarization causes antenna imperfection at the transmitting end or receiving end or both which degrades the system's performance [185], [186]. Tripolar antennas, which achieve polarization diversity either by using three orthogonal ports [187] or a single port connected to three antenna elements placed orthogonally to each other [188], have recently garnered interest due to their robust performance in cluttered environments.

The compact size and low cost implementation of multi-polarized antennas have attracted researchers in designing and testing of polarization diversity antenna systems [189], [190]. However, the existing works have mainly focused on the performance analysis of antenna properties (e.g., return loss or patterns) [191], [192] either through simulations or theoretical analysis [193], which may be quite different from final location where the antennas will be deployed. The problem is further complicated by the fact that the test environment for the developed antennas considers point-to-point single link performance only and does not consider global network behaviour. In the latter case, antenna selection of one device impacts one or more neighboring networked devices. Furthermore, for actual representation of antenna performance the measurements should be taken on multipolarized antenna systems integrated with practical sensor devices in an IoT network consisting of multiple devices.

In this paper, we address the antenna selection problem for a single-port, tripolar antenna that uses the *same* element for transmission and reception - a scenario that would be expected for low-cost IoT deployments - and study the network-wide impact of this approach. Closest work to our approach is that by Delibasic *et al.* [194], which proposed maximal ratio combining based diversity scheme for multi-hop scenario and presented mathematical model of diversity gain, error rate performance and

¹S. Chowdhury, J. Frolik, and A. Benslimane, "Switching-based Selection Techniques for Tripolar Antennas in Multi-hop IoT Networks." in *IEEE Internet of Things Journal*. Early Access. Date of Publication: February 16, 2022.

total received SNR for a two-hop relay system with dual-polarized antennas. Our approach differs from [194] in both the usage of tripolar antenna, the switched-based antenna selection technique, and the incorporation of real data captured from IoT devices with multi-polarized antenna. More specifically, we present two switched based antenna selection techniques: (i) joint SNR maximization (Max-Sum) and (ii) minimum SNR maximization (Max-Min) and confine our focus on end-to-end network reliability and energy efficiency. The proposed switched-based schemes consider both upper and lower links at each node (as shown in Fig. 6.3) to select an antenna element for joint transmission and reception. The main contributions of this paper are shown as follows:

- We present two antenna selection schemes for tripolar antenna systems deployed in a multihop based IoT network. We derive closed-form expression for both schemes, showing relationship between outage probability and switched diversity based antenna selection over Rayleigh fading channels which are independent but not necessarily identically distributed.
- We provide comparative analysis of the proposed multi-hop based antenna selection schemes and single-hop based schemes through extensive simulations that leverages an experimental data set of channel losses. The proposed Max-Sum and Max-Min scheme achieve a median gain of 1.8 dB and 0.3 dB and a 1% diversity gain of 3.6 dB and 1.4 dB, respectively, over switched diversity that considers a point-to-point link only.
- We show that by considering multi-hop structure of the network, our proposed schemes can reduce antenna switching by more than three quarters and two fifths compared to selection and switched diversity, respectively. Furthermore, both schemes perform closely to the single hop based selection diversity approach in terms of reliability with packet drop probability of 1% only.

The manuscript is organized as follows. Section 6.3 highlights related work on antenna selection strategies in multi-hop networks. The two switched-based diversity schemes which we refer to as Max-Sum and Max-Min, respectively, are introduced and closed-form expression of the outage probability is derived in Section 6.4, followed by experimental setup and performance analysis of the schemes in Section 6.5 and 6.6, respectively. Finally, we present the concluding remarks and future work directions in Section 6.7.

6.3 Related Works

In many compact IoT devices proximity between antenna elements makes polarization diversity an useful form of improving overall system performance compared to other schemes [195]. In this

section, we describe existing state-of-the-art multi-element antenna based diversity techniques.

Many efforts have been devoted to improve the performance of diversity antenna selection for conventional wireless systems at both transmitter and receiver ends, e.g., [196], [197]. In [198], an analysis of link signal strength and correlation with respect to frequency and polarization of a dual-polarized antenna was presented for maximal-ratio combining and selection diversity scheme. Meanwhile, in [199], a multiple-input single-output mmWave system where transmitter utilizes joint transmit antenna selection and analog beamforming by low-resolution phase shifters to maximize the spectral efficiency is proposed. The authors in [200] numerically analyzed the performance of a multi-element antenna that has partial channel sensing information and uses a detection vector to improve outage performance. However, in these systems there exists a trade-off between performance and complexity, since, based on the implemented channel selection scheme and the number of active antennas, there is an increased need for channel information and/or circuit power consumption, which may not be an ideal choice for IoT devices.

Antenna selection techniques that exploit single RF chain and switchable antenna branches, which is an alternative to multiple RF chains, have been widely studied [201], [202]. As more antenna polarization or branches are added, antenna systems using selection diversity experience frequent switching and increased energy consumption [203]. Recently, many variations of switching strategies that offers low cost implementation and less energy consumption, have been proposed for multiple transmit and/or receive antenna systems [204], [205] and showed significant gains in capacity and reliability over single element antenna systems. In [206], the authors experimented with switch-and-stay and switch-and-examine diversity techniques for multi-element indoor off-body antenna. The work was followed by the performance analysis of a L-branch antenna ($L \geq 2$) that uses scan-and-wait combining scheme while operating over Nakagami- m fading channels [207]. However, these works either considered ideal channel conditions or focused on the performance of a single pair or nodes only while overlooking the network-wide impact of diversity schemes.

For large scale IoT networks, multihop relaying leads to reduced routing overhead, energy efficiency and better adaptability to frequent topology changes [38], [39], [208]. Furthermore, in cluttered environment with high multipath and path losses, multipath transmission with a short distance is more effective as error probability decreases when the number of hop increases [209]. However, very few studies have looked into exploiting the network topology or routing protocols to aid antenna selection of multiple antennas system. Fig. 6.1 demonstrates the correlation of Received Signal Strength Indicator (RSSI) values obtained from a tripolar antenna receiver's upper-level node and lower-level node, respectively during the indoor experiments described in Section

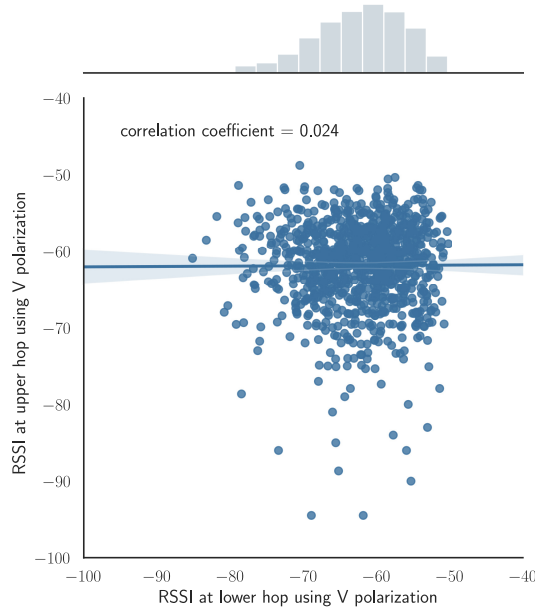


Figure 6.1: Correlation between RSSI values obtained at upper-level node and lower-level node when the intermediate node used vertical (V) polarization.

6.5. A low correlation coefficient implies that the channel condition of a single hop does not affect another hop, even though they share a common node. Thus, in a hierarchical IoT network, when a receiver selects a branch only based on next level node's channel condition (i.e., only single source and destination pair), the channel state information at the transmitter of the lower level nodes may become obsolete due to the possibility of fading variation at the other branch. For such reasons, therefore, it is necessary to consider the multi-hop based antenna selection scheme for hierarchical networks. In what follows, we present our proposed multi-hop polarization diversity schemes, derive analytical expressions for outage probability and verify their effectiveness by simulation results.

6.4 Proposed Multi-hop Based Switched Diversity for Tripolar Antennas

In this section, first we give a brief description about the hierarchical IoT network dealt with in our work. In addition, we also describe the wireless channel conditions and assumptions considered for this work. We then derive the closed form expressions of the proposed diversity schemes.

The wireless network considered in this work is a multi-hop IoT network comprised of stationary end devices, routers and a remote server as illustrated in Fig. 6.2. In order to evaluate end-to-end network performance of diversity schemes, we assume that no direct link is available between end devices to the remote server. Based on the application, the end devices either monitor environment

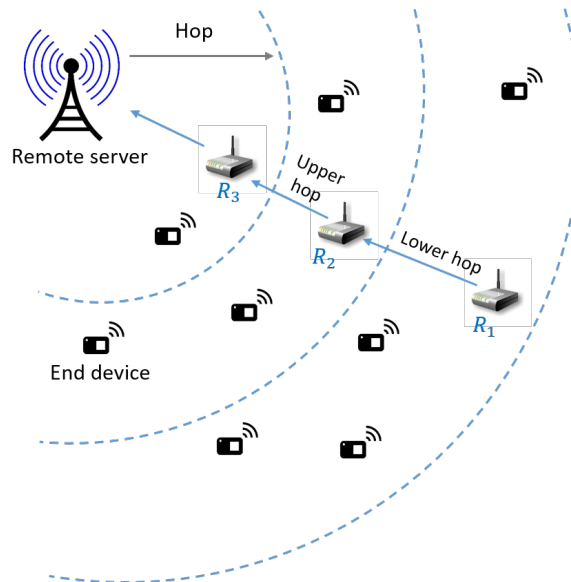


Figure 6.2: A block diagram of IoT network with end nodes and routers illustrating upper hop and lower hop node from router R_2 's perspective.

or detect events and send the sensing information to the nearest router. The routers, which have data relaying capability, forward the sensing data from individual sensors to the remote server for post-processing. In addition, we assume that all the devices in the network are equipped with tripolar antenna system. Each channel realization, which are drawn randomly at each time step is assumed to remain fixed during that step. Finally, we also assume the channel estimation by the receivers are perfect and the time delay between channel estimation, diversity technique implementation, and packet transmission is negligible [210], [211], [212].

Consider H , V and W are three independent Rayleigh fading channels available at the tripolar antenna system such that channel power gain changes independently with each channel use. We assume that both lower and upper hop nodes have already selected a branch for transmission and reception, which are W and H , respectively, as demonstrated in the sample case of Fig. 6.3. Specifically, we examined the scenario where the repeater node R_2 needs to select the appropriate element to communicate to the nodes both lower and higher in the network hierarchy, i.e., to receive data packets from R_1 and forward them to R_3 . Because of the multipath created by a cluttered environment, the channel conditions in the two links will differ and thus considering signal quality of both lower and upper hops may lead to better antenna selection. Thus the problem we address is how to choose the element (H , V or W) that provides the best network-wide performance.

Let L_H, L_V, L_W be the random variables representing instantaneous SNR for wireless links between the lower hop node and router at H , V and W branch of the router (as depicted in Fig. 6.3). The distribution of the SNR at any branch, for example L_H , is exponentially distributed and

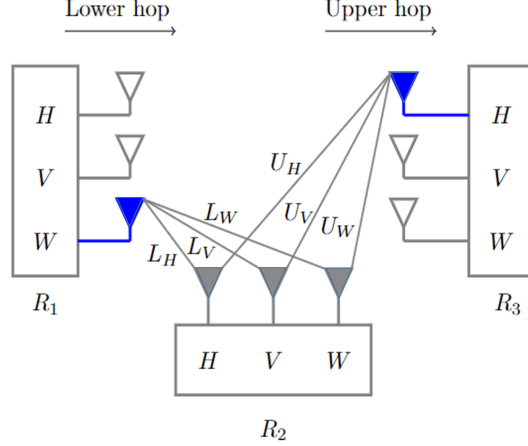


Figure 6.3: Illustration of an IoT network where router R_2 utilizes channel information from two hops for antenna selection. H , V and W represent the three branches of tripolar antenna and the highlighted elements represent the currently used branch of nodes R_1 and R_3 . Received signal strengths for the hop branches are represented by L_H, L_V, L_W, U_H, U_V , and U_W , where L and U depicts the lower and upper hops, respectively.

proportional to the instantaneously received signal power at any time, which can be described by the following equation [53]

$$P(L_H \leq l_h) = \alpha_h \exp^{-\alpha_h l_h} \quad (23)$$

Here $P(L_H \leq l_h)$ means the probability that the random variable L_H is less than or equal to the realization l_h . The lowercase l_h is the instantaneous SNR at the horizontal branch (H) of the receiver and defined as $l_h = r_h^2/N$, where r_h is Rayleigh fading received signal amplitude at the H branch and N is the noise power. Also, $\alpha_h = 1/\mathbf{E}[l_h]$, where $\mathbf{E}[l_h]$ represents the average SNR on the H branch [213]. Similarly, L_V and L_W have exponentially distributed density defined as, $\alpha_v \exp^{-\alpha_v l_v}$ and $\alpha_w \exp^{-\alpha_w l_w}$, where $\alpha_v = 1/\mathbf{E}[l_v]$, and $\alpha_w = 1/\mathbf{E}[l_w]$, $\mathbf{E}[l_v]$ and $\mathbf{E}[l_w]$ are the average SNR, l_v and l_w are the realizations of the random variables on the V and W branch of the lower hop, respectively. Also let U_H, U_V, U_W be the random variables representing instantaneous SNR for wireless links between the router and upper hop destination (which can be a router or base station) at H, V and W branch of the router (as depicted in Fig. 6.3) with average SNR values $\mathbf{E}[u_h]$, $\mathbf{E}[u_v]$ and $\mathbf{E}[u_w]$, respectively.

6.4.1 Joint SNR maximization (Max-Sum)

In Max-Sum scheme, router considers all the available transmit/receive links between its lower level and upper level nodes and selects a polarization that maximizes the joint signal strength of the transmission and reception links. Unlike selection diversity, where receiver monitors the signal

strength of all available branches, the switching event for the Max-Sum scheme depends on the received SNR of the current branch only.

First, we need to find the probability distribution of summation of L_i and U_i , where $i \in T$ and $T = \{H, V, W\}$. Now, for the ease of analytical derivation, we start by deriving the probability distribution for the horizontal branch (H) first. Let S_H has the distribution of the sum of the two random variables L_H and U_H . We want to find the probability $P(S_H > s_h | L_H > \tau \text{ and } U_H > \tau)$, where τ is the signal strength threshold and both L_H and U_H are conditioned to be greater than τ . The threshold τ , which is a pre-determined number and depends on the receiver's sensitivity, determines whether the received signal is acceptable or not. A packet will be dropped if the signal strength between two nodes falls below the threshold τ . Now since L_H and U_H are both exponentially distributed, using the memoryless property of these continuous random variables, we see that the conditional distribution of the event $L_H - \tau$ given that $L_H > \tau$ is $\alpha_h e^{-\alpha_h l_h} dl_h$ for $l_h > 0$, and the density function does not depend on l_h . If we condition on the event that both $L_H > \tau$ and $U_H > \tau$, the conditional distribution of $L_H - \tau$ is still the same, since U_H and L_H are independent. Similarly the conditional distribution of $U_H - \tau$ given that same event is $\beta_h e^{-\beta_h u_h} du_h$ for $u_h > 0$, where $\beta_h = 1/\mathbf{E}[u_h]$. Therefore, the probability that the sum of two independent (but not identical) exponentially distributed random variables is greater than a specified quantity

$$\begin{aligned}
P(S_H > s | L_H > \tau \text{ and } U_H > \tau) &= P((L_H - \tau) \\
&+ (U_H - \tau) > s - 2\tau | (L_H - \tau) > 0 \text{ and } (U_H - \tau) > 0)
\end{aligned} \tag{24}$$

We get

$$\iint_{\substack{l_h > 0 \\ u_h > 0 \\ l_h + u_h > s - 2\tau}} \alpha_h \beta_h e^{-\alpha_h l_h - \beta_h u_h} d(l_h, u_h) \tag{25}$$

This can be expressed as

$$\begin{aligned}
& \int_0^{s-2\tau} \left(\int_{s-2\tau-l_h}^{\infty} \alpha_h \beta_h e^{-\alpha_h l_h - \beta_h u_h} du_h \right) dl_h + \\
& \int_{s-2\tau}^{\infty} \left(\int_0^{\infty} \alpha_h \beta_h e^{-\alpha_h l_h - \beta_h u_h} du_h \right) dl_h \\
&= \int_0^{s-2\tau} \left(-\alpha_h \exp^{\alpha_h l_h} \int_{s-2\tau-l_h}^{\infty} \exp^{-\beta_h u_h} du_h \right) dl_h + \\
& \int_{s-2\tau}^{\infty} \left(\alpha_h \exp^{-\alpha_h l_h} \int_0^{\infty} \exp^{-\beta_h u_h} du_h \right) dl_h \\
&= \int_0^{s-2\tau} \alpha_h \exp^{-\alpha_h l_h} \exp^{-(s-2\tau-l_h)\beta_h} dl_h + \\
& \int_{s-2\tau}^{\infty} \alpha_h \exp^{-\alpha_h l_h} dl_h \\
&= \frac{\alpha_h}{(\alpha_h - \beta_h)} \left(\exp^{\beta_h(2\tau-s)} - \exp^{\alpha_h(2\tau-s)} \right) + \\
& \exp^{\alpha_h(2\tau-s)}
\end{aligned} \tag{26}$$

Thus, the density function of S_H is [[214] , Eq. (8)]

$$\begin{aligned}
& f_{S_H|L_H>\tau, U_H>\tau}(s) \\
&= \frac{d}{ds} (P(S_H \leq s | L_H > \tau, U_H > \tau)) \\
&= -\frac{\alpha_h}{\alpha_h - \beta_h} \left(\frac{d}{ds} (\exp^{2\beta_h\tau - \beta_h s}) \right. \\
& \quad \left. \frac{d}{ds} (-\exp^{2\alpha_h\tau - \alpha_h s}) \right) - \frac{d}{ds} (\exp^{\alpha_h(2\tau-s)}) \\
&= \frac{\alpha_h \left((-\beta_h + \frac{d}{ds}(2\beta_h\tau)) \exp^{2\beta_h\tau - \beta_h s} \right)}{\alpha_h - \beta_h} \\
& - \frac{\alpha_h \exp^{2\alpha_h\tau - \alpha_h s} \frac{d}{ds}(2\alpha_h\tau - \alpha_h s)}{\alpha_h - \beta_h} - \alpha_h \exp^{\alpha_h(2\tau-s)} \\
&= \frac{\alpha_h \beta_h \exp^{-(\beta_h + \alpha_h)s} (\exp^{\beta_h s + 2\alpha_h\tau} - \exp^{\alpha_h s + 2\beta_h\tau})}{\beta_h - \alpha_h}
\end{aligned} \tag{27}$$

Suppose $S_V = L_V + U_V$ and $S_W = L_W + U_W$, S_V having the distribution function $F_{S_V}(s_v)$ and S_W having the distribution function $F_{S_W}(s_w)$. Then, we can write the conditional CDF of S_V and S_W using Eq. (25) as

$$\begin{aligned}
P(S_V > s \mid L_V > \tau \text{ and } U_V > \tau) = \\
\frac{\alpha_v}{(\alpha_v - \beta_v)} \left(\exp^{\beta_v(2\tau-s)} - \exp^{\alpha_v(2\tau-s)} \right) + \exp^{\alpha_v(2\tau-s)}
\end{aligned} \tag{28}$$

and

$$\begin{aligned}
P(S_W > s \mid L_W > \tau \text{ and } U_W > \tau) = \\
\frac{\alpha_w}{(\alpha_w - \beta_w)} \left(\exp^{\beta_w(2\tau-s)} - \exp^{\alpha_w(2\tau-s)} \right) + \exp^{\alpha_w(2\tau-s)}
\end{aligned} \tag{29}$$

Now, let $\mathcal{Z}_A = \max(S_H, S_V, S_W)$, where \mathcal{Z}_A is the event when the tripolar antenna selects the branch with joint maximum signal strength over the two hops. Then for $s > 0$, using the independence of the conditional probability of S_H , S_V and S_W given that L_i and U_i are greater than the signal strength threshold τ for H , V and W branches, we obtain the distribution function of \mathcal{Z}_A

$$\begin{aligned}
P(\mathcal{Z}_A \leq s) &= P(S_H \leq s \mid L_H > \tau, U_H > \tau) P(S_V \leq s \mid \\
&\quad L_V > \tau, U_V > \tau) P(S_W \leq s \mid L_W > \tau, U_W > \tau) \\
&= (1 - P(S_H > s \mid L_H > \tau, U_H > \tau)) \\
&\quad (1 - P(S_V > s \mid L_V > \tau, U_V > \tau)) \\
&\quad (1 - P(S_W > s \mid L_W > \tau, U_W > \tau))
\end{aligned} \tag{30}$$

By substituting Eq. (26), (28) and (29) into Eq. (30), the latter becomes

$$P(\mathcal{Z}_A \leq s) = \prod_{i \in \mathcal{T}} (1 - \Omega_i (\exp^{\beta_i \phi} - \exp^{\alpha_i \phi}) - \exp^{\alpha_i \phi}) \tag{31}$$

where

$$\Omega_i = \frac{\alpha_i}{(\alpha_i - \beta_i)} \tag{31a}$$

$$\phi = 2\tau - s \tag{31b}$$

Equation (31) provides the probability that the instantaneous signal strength of the selected branch using three-branch Max-Sum switched based selection scheme will be above the specified threshold

value τ and by using [[215], Eq. (4)] the outage probability for Max-Sum scheme is written as

$$P_O^s = 1 - P(\mathcal{Z}_A \leq s) \quad (32)$$

Eq. (32) is evaluated numerically.

6.4.2 Maximization of the minimum SNR (Max-Min)

With Max-Min antenna selection approach, the goal of the receiver is to select a branch that maximizes the minimum received SNR of all links. The receiver obtains channel state information of all the transmission and reception links and exploits the advantage of diversity to determine an acceptable branch.

Similar to the previous derivation, we start with the horizontal branch. Let M_H be the minimum of the exponential random variables L_H and U_H given that L_H and U_H denote the received signal strength at the router receiver from the lower level node and upper level node, respectively. Furthermore, M_H is conditioned on the event that $L_H > \tau$ and $U_H > \tau$.

To determine the expression for $P(M_H > m)$, where $M_H = \min(L_H, U_H)$, for some $m > 0$, we write the distribution function of M_H as

$$F_{M_H}(m) = P(M_H \leq m) = P(\min(L_H, U_H) \leq m) \quad (33)$$

which is equivalent to

$$F_{M_H}(m) = 1 - P(\min(L_H, U_H) > m) \quad (34)$$

Using the fact that L_H and U_H are independent, we get

$$\begin{aligned} P(\min(L_H, U_H) > m) &= P(L_H > m, U_H > m) \\ &= P(L_H > m)P(U_H > m) \end{aligned} \quad (35)$$

This means that

$$P(L_H > m) = 1 - F_{L_H}(m) = \int_m^\infty f_{L_H}(l_h) dl_h \quad (36)$$

and

$$P(U_H > m) = 1 - F_{U_H}(m) = \int_m^\infty f_{U_H}(u_h) du_h \quad (37)$$

where $F_{L_H}(m)$ and $F_{U_H}(m)$ are the cumulative distribution function of L_H and U_H , respectively. Also, $f_{L_H}(l_h)$ and $f_{U_H}(u_h)$ are the probability density function of L_H and U_H . Therefore, we can write Eq. (34) as

$$\begin{aligned} F_{M_H}(m) &= 1 - \left(\int_m^\infty f_{L_H}(l_h) dl_h \right) \left(\int_m^\infty f_{U_H}(u_h) du_h \right) \\ &= 1 - \left(\int_m^\infty \alpha_h \exp^{-\alpha_h l_h} dl_h \right) \left(\int_m^\infty \beta_h \exp^{-\beta_h u_h} du_h \right) \\ &= 1 - \exp^{-\alpha_h m} \exp^{-\beta_h m} \end{aligned} \quad (38)$$

Thus, M_H is an exponential random variable with parameter $(\alpha_h + \beta_h)$. The density function of M_H is

$$\begin{aligned} f_{M_H}(m) &= \frac{d}{dm} F_{M_H}(m) \\ &= -\frac{d}{dm} (\exp^{-\alpha_h m - \beta_h m}) \end{aligned} \quad (39)$$

Using the chain rule,

$$\frac{d}{dm} (\exp^{-\alpha_h m - \beta_h m}) = \frac{d \exp^u}{du} \frac{du}{dm} \quad (40)$$

where, $u = -\alpha_h m - \beta_h m$ and $\frac{d}{du} (\exp^u) = \exp^u$. Then, differentiating the sum term by term and factor out constants, we get

$$\begin{aligned} f_{M_H}(m) &= -\exp^{-\alpha_h m - \beta_h m} \left(-\alpha_h \frac{d(m)}{dm} - \beta_h \frac{d(m)}{dm} \right) \\ &= (\alpha_h + \beta_h) \exp^{-(\alpha_h + \beta_h)m} \end{aligned} \quad (41)$$

Suppose that M_i is the minimum of L_i and U_i , where $i = \{H, V, W\}$, then when $M_i \leq m_i$, it means that the minimum of L_i and U_i is less than m_i , where $i = \{H, V, W\}$. In other words, when the minimum is greater than m_i , i.e., $(M_i > m_i)$, then both L_i and U_i must be greater than m_i .

Thus, the density function of M_H conditioned on $L_H, U_H > \tau$ is

$$\begin{aligned}
f_{M_H|M_H>\tau}(m) &= \frac{f_{M_H}(m)}{P(M_H > \tau)} \\
&= \frac{(\alpha_h + \beta_h) \exp^{-(\alpha_h + \beta_h)m}}{\exp^{-(\alpha_h + \beta_h)\tau}} \\
&= (\alpha_h + \beta_h) \exp^{(\alpha_h + \beta_h)(\tau - m)} \quad \text{when } m > \tau
\end{aligned} \tag{42}$$

It can be shown that $\int_{\tau}^{\infty} f_{M_H|M_H>\tau}(m) dm = 1$, which validates the density function. Then the distribution function can be obtained as

$$\begin{aligned}
P(M_H \leq m | M_H > \tau) &= \int_{\tau}^m f_{M_H|M_H>\tau}(m) dm \\
&= (\alpha_h + \beta_h) \exp^{(\alpha_h + \beta_h)\tau} \int_{\tau}^m \exp^{-(\alpha_h + \beta_h)m} dm \\
&= \exp^{(\alpha_h + \beta_h)\tau} \left(\exp^{-(\alpha_h + \beta_h)m} - \exp^{-(\alpha_h + \beta_h)\tau} \right) \\
&= 1 - \exp^{(\alpha_h + \beta_h)(\tau - m)}
\end{aligned} \tag{43}$$

Similarly, we can obtain the conditional distribution function of M_V and M_W . Now let $\mathcal{Z}_{\mathcal{B}}$ denotes an event where the receiver of the tripolar antenna selects a branch whose minimum signal strength over the two hops is greater than the minimum signal strength of the other two branches. Therefore, we can write $\mathcal{Z}_{\mathcal{B}} = \max(M_H, M_V, M_W)$. Since M_H, M_V and M_W are independent, we can write

$$\begin{aligned}
P(\mathcal{Z}_{\mathcal{B}} \leq m) &= P(M_H \leq m | M_H > \tau) \\
&= P(M_V \leq m | M_V > \tau) P(M_W \leq m | M_W > \tau)
\end{aligned} \tag{44}$$

Substituting Eq. (43) in the above equation yields the desired distribution function of $\mathcal{Z}_{\mathcal{B}}$

$$P(\mathcal{Z}_{\mathcal{B}} \leq m) = \prod_{i \in T} (1 - \exp^{\Gamma_i(\tau - m)}) \tag{45}$$

where

$$\Gamma_i = \alpha_i + \beta_i \tag{45a}$$

Thus, the outage probability becomes [[216] Eq. (12)]

$$P_O^m = 1 - P(\mathcal{Z}_{\mathcal{B}} \leq m) \tag{46}$$

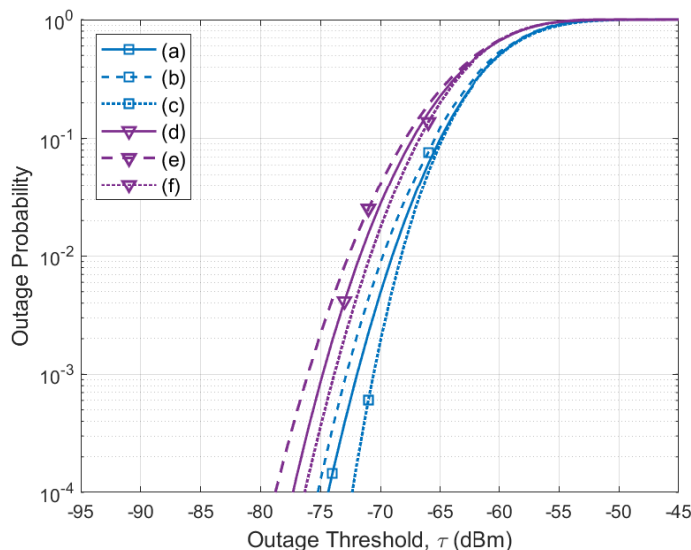


Figure 6.4: Outage probability of Max-Sum (Eq. (30)) and Max-Min (Eq. (44)) scheme for three independent but non-identical Rayleigh branches with mean values (in dBm) as follows: (a) Max-Sum with $\mathbf{E}[l_h] = -61$, $\mathbf{E}[l_v] = -63$, $\mathbf{E}[l_w] = -64$, $\mathbf{E}[u_h] = -62$, $\mathbf{E}[u_v] = -64$ and $\mathbf{E}[u_w] = -65$. (b) Max-Sum with mean - 3 dB (c) Max-Sum with mean + 3 dB, (d) Max-Min (e) Max-Min with mean - 3 dB (f) Max-Min with mean + 3 dB.

As an illustration of the analytical results, Fig. 6.4 shows the outage probability (or, equivalently, the CDF) of the RSSI for the proposed Max-Sum and Max-Min schemes and investigates the effect of different mean values. The mean values used in case (a) and (d) are obtained from experimental data at the H , V and W antenna branch of the end node and destination node, respectively (shown as continuous lines). Under Max-Sum scheme, assuming the horizontal branch is in operation, when $s > \tau$, outage condition can occur: if $l_h < \tau$ or $u_h < \tau$ even though $s_h > \tau$ as given in Eq. 24. In such case, the receiver will keep switching branches until signal strength at both lower and upper hop nodes satisfy the threshold $L_j > \tau$, $U_j > \tau$, $j \in \{H, V, W\}$. For Max-Min scheme, outage occurs if the currently selected branch of R_1 and/or R_3 are below τ . We observe that for a router with tripolar antenna receiver, maximizing the joint signal strength leads to higher diversity gain than maximize the minimum RSSI. While the impact of lower or higher mean signal power is quite similar on both techniques, the 1% diversity gain is higher (~ 0.3 dB) for Max-Sum compared to Max-Min scheme. This is expected since Max-Min tries to maximize the lowest signal power of the three branches of a tripolar antenna device, resulting in lower RSSI values.

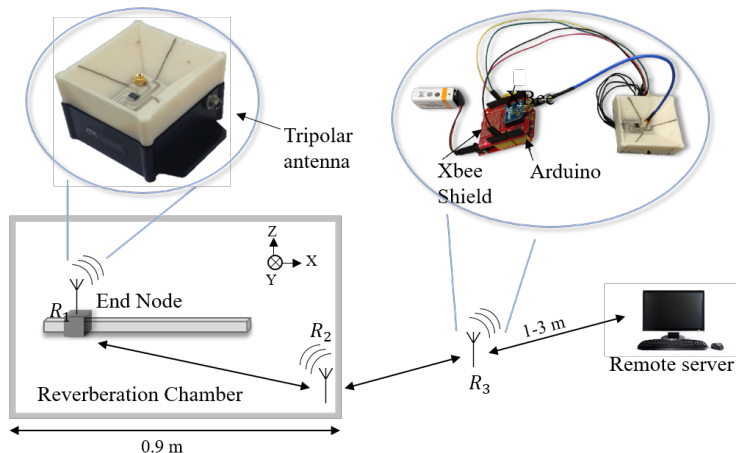


Figure 6.5: Block diagram of testbed setup that utilizes a reverberation chamber to create a severe multipath environment. The fabricated prototype tripolar antenna acts as a transmitter and receiver for the XBee module.

6.5 Experimental Setup

We conducted our experiments with prototype devices consisted of Arduino, Xbee and the tripolar antenna operating at 2.4 GHz. The tripolar antenna, which is fabricated on 3D printed acrylonitrile butadiene styrene filament, achieves three different polarization by using three microstrip lines in the bottom ground plane along with a non-reflective single pole triple throw RF switch (model HMC245AQS16). The Arduino controls the antenna and activates a desired polarization by controlling the RF switch. The overall structure of our experimental setup is depicted in Fig. 6.5. To emulate highly reflective wireless propagation environment, we deployed the end node and a router, denoted as R_1 and R_2 , respectively, inside of a reverberation chamber that can simulate high multipath conditions. The chamber and reflectors inside help to achieve rotation of polarization which eventually causes the decoupling of the transmitted polarization. The end node was placed on top of a LabVIEW [178] controlled linear actuator that moved the device to 50 different repeatable positions. Furthermore, to randomize channel fading, we also moved the track to different positions inside of the chamber during data collection. To measure energy consumption during various stages of operation of the device, a high precision digital multimeter in current mode with the probes of the multimeter inserted in series with the power supply to measure the current through the circuit.

During the data collection phase, the end node R_1 collected temperature data using a low-cost digital temperature and humidity sensor DHT22 with 10-second intervals and forwarded the sensed data using all three antenna polarization to R_2 , which is also placed inside of the chamber. Further, the router R_2 switches its polarization and receives and records the RSSI of the nine distinct links

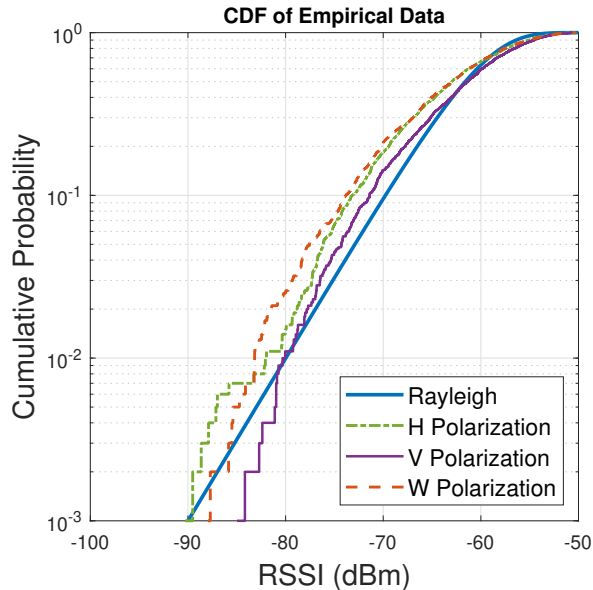


Figure 6.6: Cumulative distribution function (CDF) plots of RSSI data for three individual antenna elements of the end node (Fig. 6.5) when the router node is vertically polarized, where the mean RSSI values of H , V and W antenna branch are -63 dBm, -61 dBm and -64 dBm, respectively

between the two tripolar nodes (R_1 and R_2) and thereafter forwards the data to the next router (R_3) which is located outside of the chamber at a certain distance (varied between 1 to 3 meter). Finally, R_3 forwards the received data to the server where post-processing is done. The measured RSSI, which is measured in dBm, determines the signal strength, i.e., the amount the of power present in a radio signal and hence indicates the quality of a radio link for a particular antenna branch.

Fig. 6.6 illustrates the RSSI data measured during the data collection phase between a vertically polarized router and three mutually orthogonal antenna elements of the end node with mean values -61 dBm, -63 dBm, and -64 dBm for H , V and W branch, respectively. The variation among the CDF plots also confirms the depolarization of the transmitted wave caused by the highly reflective propagation environment inside of the reverberation chamber. Comparing curves for H , V and W polarization, we can conclude that for independent but non-identical branches with similar fading statistics, where no channel appears significantly better than others, the more available antenna elements, the better the performance of the switched-based diversity schemes, in particular, in multipath environments. Consequently, useful diversity gain can be obtained by using switched-diversity based three-branch receiver over dual-diversity based selection receivers [217], which further motivates us analyzing the performance of three-branch diversity systems in various scenario.

6.6 Performance Analysis

In this section, first we describe the simulation environment that leverages the empirical data to analyze the performance of various diversity schemes. Next, we present the results of our proposed Max-Sum and Max-Min diversity scheme and correlate their performance with popular one-hop based diversity schemes, namely, selection diversity and switched diversity. For comparison's sake, the performance of no diversity scheme, i.e., vertically polarized single input single output omnidirectional antenna system, is also compared. For performance metrics, we consider the output RSSI, packet delivery rate, antenna switching frequency, energy consumption and network size. We also compare the analytical and simulated performance of the proposed algorithms and present an analysis on algorithmic complexity of the proposed techniques.

6.6.1 Simulation model

For this work, the simulations are run in the MATLAB environment on an IoT network with fixed number of hops where source node (i.e., end device) is located at one end of the network and base station is at the other end (see Fig. 6.2). The routers receive the message from lower hop and forward it to the next hop router or to base station. For simplicity, we assume a single multihop path where each router can receive single message at any time and send it out to next destination which is pre-determined. During simulation, we leverage experimental signal strength data obtained from Arduino-based XBee wireless modules deployed inside of a reverberation chamber by assigning different RSSI traces for all three antenna branches that we measured to individual nodes. Nodes are selected randomly to emulate an inherently non-static environment between the transmitter and receiver. Nodes then use the RSSI values of all the diversity branches to determine an acceptable antenna branch depending on the predetermined threshold and other criteria required by the simulated diversity scheme. For assessing energy performance, transmit current and receive current for the nodes are set to 45 mA and 31 mA, respectively according to the specification of XBee S2C 802.15.4 models to simulate the actual performance. Furthermore, the receiver sensitivity of the nodes are set to -100 dBm and the DC bias current for ON operation of the non-reflective RF switch in the tripolar antenna is varied randomly between 10 to 15 mA.

To simulate selection diversity scheme deployed on a single receiver with three antennas, a node compares the RSSI traces of three branches received from the next level (i.e., upper layer) node neighbor only and selects the best branch for each transmission. Consider R_2 from Fig. 6.3 as an example, where U_H, U_V and U_W denote the signal power at the antenna branch H, V and W ,

respectively. Let, X_t represent the selected antenna branch of R_2 at different time steps. Then the selection diversity operation can be described mathematically by the following equation

$$X_t = \begin{cases} U_V, & \text{if } U_V \geq U_H, U_W \text{ at time } t \\ \text{or} \\ U_H, & \text{if } U_H \geq U_V, U_W \text{ at time } t \\ \text{or} \\ U_W, & \text{if } U_W \geq U_V, U_H \text{ at time } t \end{cases} \quad (47)$$

The selected branch is then used to transmit packets to the upper hop node R_3 and receive packets from lower hop node R_1 . A RSSI array index is incremented by 1 after each transmission to loop through the entire trace data assigned to that particular node.

For switched diversity, the receiver starts with either of the antennas connected and before every transmission it compares the quality of the currently active antenna with a fixed threshold and switches to another branch only if the signal quality falls below the threshold. The strategy can be mathematically described as follows

If $X_{t-1} = U_V$

$$X_t = \begin{cases} U_V, & \text{if } U_V \geq \tau \\ \text{or} \\ U_V, & \text{if } U_V, U_H, U_W < \tau \\ \text{or} \\ U_H, & \text{if } U_V < \tau \text{ and } U_H \geq \tau \text{ and } U_W \text{ unknown} \\ \text{or} \\ U_W, & \text{if } U_V, U_H < \tau \text{ and } U_W \geq \tau \end{cases} \quad (48)$$

where, X_{t-1} denotes the selected branch for R_2 at time $t - 1$ and τ is the switching threshold. For $X_{t-1} = U_H$ or $X_{t-1} = U_W$, switching strategy will be as above with interchanging V with H and W , respectively. Thus, compared to selection diversity, which needs to examine all three signals coming from the tripolar antenna, switched diversity examines the currently active branch only as long as the signal strength of the branch is above the threshold.

In the Max-Sum strategy, the receiver gets RSSI from multiple nodes and branch selection is

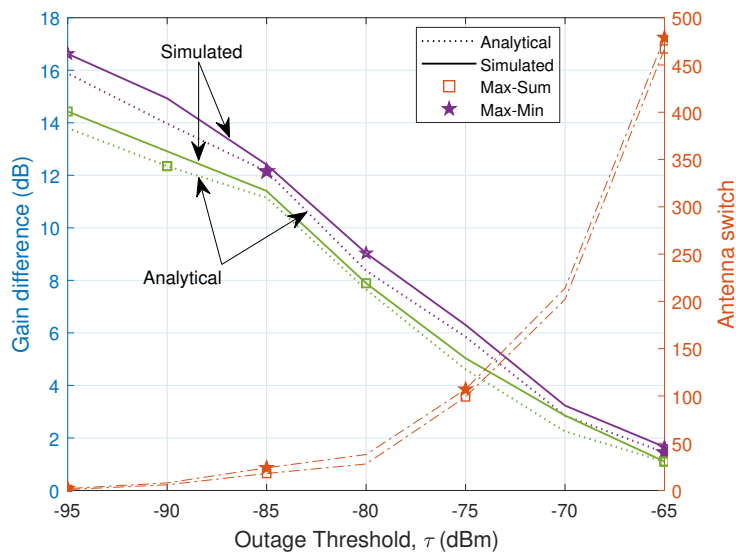


Figure 6.7: Diversity gain comparison of Max-Sum and Max-Min with selection diversity (simulated) for different switching thresholds with $\mathbf{E}[l_h] = -61$, $\mathbf{E}[l_v] = -63$, $\mathbf{E}[l_w] = -64$, $\mathbf{E}[u_h] = -62$, $\mathbf{E}[u_v] = -64$ and $\mathbf{E}[u_w] = -65$.

performed in the following manner: receiver adds the RSSI received from the lower and upper hop neighbor nodes for H , V , and W branches and selects the branch that maximizes the sum of the RSSI. Under the Max-Min approach, the receiver determines the minimum of the two RSSI values received from the lower and upper hop neighbors for each branch and selects the branch that maximizes the minimum signal quality. Similar to the conventional switched diversity approach, for both Max-Sum and Max-Min schemes, the receiver stays on the currently active branch as long as it is acceptable, i.e., $L_i, U_i > \tau$, where $i \in \{H, V, W\}$, L_i and U_i are the RSSI of the lower and upper hop for the currently used branch, respectively. Both schemes use a top-down approach to perform antenna selection. In this approach, all the nodes are initialized with vertical antenna selected as the currently active branch; subsequently, router nodes closest to the base station is configured. Hence, referring to Fig. 6.3, R_3 is configured first and afterward, R_2 selects its antenna. We assume that the base will use vertical polarization only and do not experience harsh propagation environment.

6.6.2 Performance of two-hop network

To confirm the correctness of our analytical expressions through simulations, first we consider a two-hop network having two routers and the number of end nodes assigned to each router is nine (9). Fig. 6.7 depicts comparison between the proposed diversity techniques and selection diversity for various switching threshold. Besides comparing the simulation results with theoretical data, the figure also highlights an inverse relationship between diversity gain (left y-axis) and antenna

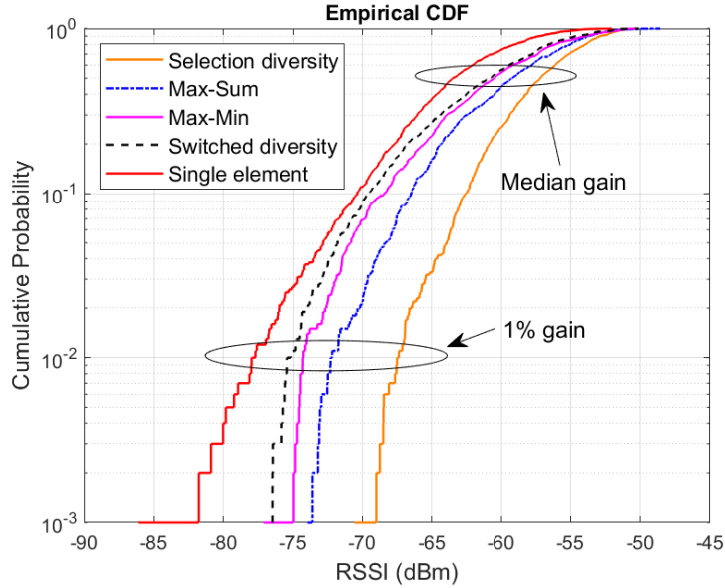


Figure 6.8: Comparison of CDF of signal strength values, which a router receives from the upper-hop router in a forty (40) node four-hop IoT network, for various antenna selection strategies in multipath environment with channel characteristics akin to those from our empirical data set (Fig. 6.6).

switching frequency (right y-axis). We note that the simulation results (continuous lines) were in very good agreement with the analytical results (dotted lines) for both Max-Sum and Max-Min techniques for varying switching thresholds. The delta between the two proposed schemes is smaller (~ 0.5 dB) when threshold is high and increases (~ 2.3 dB) as threshold is lowered. When threshold is high, the receiver using Max-Sum or Max-Min switches more frequently to find an antenna branch with acceptable signal level which causes considerable signal fluctuation. Moreover, when receiver switches from the currently active antenna branch, the signal level of the other branch can be even lower than the current branch which also contributes to increase switching rate. Such observation is also supported by the simulation result as Fig. 6.7 shows that switching frequency of the tripolar antenna receiver doubles when threshold was changed from -75 dBm to -70 dBm. On the other hand, selecting low threshold compared with the average received signal level, increases probability of a branch to be acceptable and decreases the antenna switching frequency. However, this also results in poor diversity gain and makes switch diversity ineffective. Thus, it is clear that the performance of any switched based diversity technique strongly depends on the switching threshold and choosing an optimal threshold can improve the achievable diversity gain significantly.

6.6.3 Performance of four-hop network

In this subsection, we present the simulation results obtained from simulations of a four-hop IoT network. Nodes are selected randomly to emulate the changes of diversity receiver in a dynamic environment with respect to time. While the object oriented network architecture allows to deploy large IoT network and simulate for substantial number of packets, here we present the case where simulation runs until each router receives and forwards 1000 data packets. The presented results are the average of 10 simulation runs and each run corresponds to one unique set of randomly assigned RSSI data for each of the nodes.

6.6.4 Diversity performance

Fig. 6.8 demonstrates the CDF of RSSI values obtained from a router node deployed at the second hop of a multi-hop network that is comparable to the network illustrated in Fig. 6.2. Although our proposed strategies uses RSSI from multiple hops, to compare the performance with single hop based diversity schemes, Fig. 6.8 only plots the RSSI between the diversity receiver that is selecting an antenna and it's next hop router. For example, consider R_2 in Fig. 6.3, which uses either a single hop or dual hop technique to select antenna branches during simulation of a particular scheme and forwards packets to R_3 . To make the comparison between various schemes, we compare the RSSI of link between R_2 and R_3 only, since single hop based techniques are not concerned with the signal strength values of links between R_1 and R_2 .

We observe that the use of selection diversity scheme for tripolar antenna systems provides the best power gain amongst all other schemes. The 1% link margin gain for selection diversity is higher than 5 dB and 7 dB approximately, compared to the Max-Sum and Max-Min scheme with a median gain of 1.9 dB and 3.4 dB, respectively. This is followed by Max-Sum, which is better than the Max-Min scheme and switched diversity (median gain of 1.5 dB and 1.8 dB and a 1% link margin gain is approximately 2 dB and 3.6 dB, respectively), whereas single element vertically polarized antenna has the lowest power gain among all strategies. We also note the the Max-Min scheme performs slightly better than the conventional switched diversity leading to a median gain of 0.3 dB and a 1% diversity gain of 1.4 dB. Although selection diversity achieves the highest SNR, it incurs excessive power consumption, which is prohibitive for low-powered IoT devices. On the other hand, our proposed strategies are able to achieve better SNR than conventional switched diversity by maximizing the SNR of both uplink and downlink which support our argument that the link quality of previous hop and next hop should be considered during antenna selection.

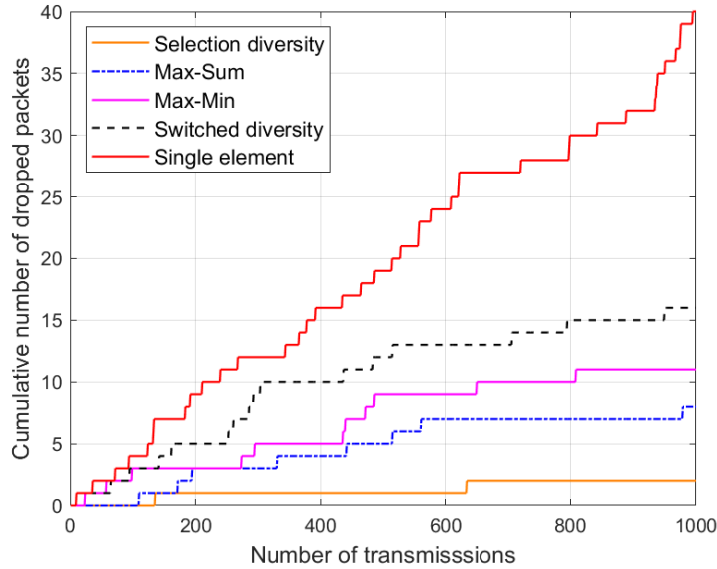


Figure 6.9: Average number of dropped packets for selection diversity, Max-Sum, Max-Min, switched diversity and single element antenna system.

6.6.5 End-to-end reliability

Fig. 6.9 presents the packet delivery performance of selection diversity, Max-Sum, Max-Min and switched diversity based on simulation. To analyze the reliability of the transmissions, we compared the amount of data packets sent with the amount of data packets received successfully by the nodes where any data packet received with RSSI value less than the predetermined threshold, is considered as a ‘lost’ packet. The threshold is set to -75 dBm, which is 25 dB higher than the receiver’s sensitivity that was used during channel measurement experiment. We can see that employing tripolar antenna minimizes packet loss across hops by at least 2% compared to a single element vertically polarized omnidirectional antenna system. Since the tripolar antenna has three available diversity paths, the receiver can switch away from the currently active branch if it becomes unacceptable, whereas the single element antenna has to wait until vertically polarized link becomes acceptable. In terms of network reliability, selection diversity offers the best packet delivery performance with a packet delivery rate of 99.8%. However, it comes with the cost of frequent switching and increased communication overhead. The results also indicate that although our proposed switching strategies with a approximate packet delivery rate of 99%, do not outperform the selection diversity scheme, they perform marginally better than the conventional switched diversity.

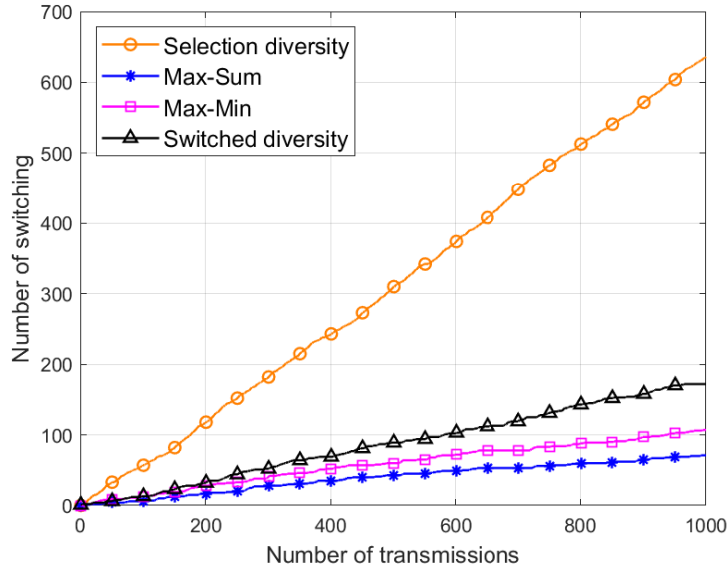


Figure 6.10: Comparison of antenna branch switching between selection diversity, Max-Sum, Max-Min and switched diversity scheme. Note: switching is not applicable to the single element approach.

6.6.6 Switching frequency

In diversity systems, switching frequency plays a key role in system’s reliability since each switching transient corrupts the receiver filters which may affect data reception. Fig. 6.10 shows a comparison between selection diversity, Max-Sum, Max-Min and switched diversity scheme for independent Rayleigh fading diversity branches. We observe that considering single hop and selecting the best branch results in significantly higher switching compared to the schemes that considers two hop switched-based scheme. Despite the transmission and reception of extra information required by the Max-Sum and Max-Min scheme due to their communication with upper and lower layer node, the overall antenna branch switching is reduced by the Max-Sum scheme is approximately 88% and 58% and by the Max-Min scheme is 83% and 37%, as compared to selection diversity and switched diversity approach, respectively, which eventually decrease system outage and contributes to the reduction of energy consumption in IoT devices. The results highlight the potential of dual-hop based antenna selection scheme over single hop based strategies and encourages more research on this area.

6.6.7 Energy efficiency

Fig. 6.11 compares the energy efficiency under different diversity methods. We observe a substantial increase in energy consumption when single element antenna is used, where the receiver consumed

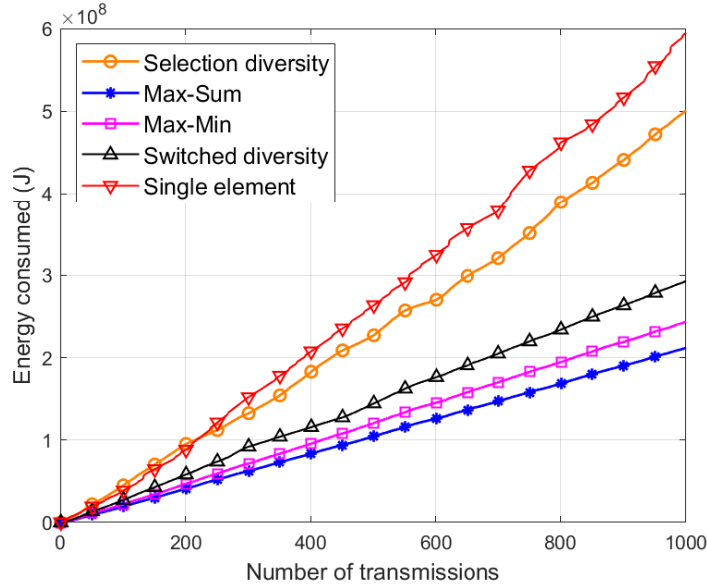


Figure 6.11: Energy consumption comparison of single element antenna and tripolar antenna system while using various diversity schemes.

more than 15% and 50% of the total energy of selection diversity and switched diversity, respectively. The higher packet drop rate for single element antenna systems contributes to a large number of retransmissions and results in decreased power efficiency. On the other hand, selection diversity requires the RSSI value of all three diversity branch to selection the best antenna for every transmission which makes it the second highest scheme with respect to energy consumption. Meanwhile, the switching-based schemes allow the receiver to use a branch as long as its signal strength is above the pre-determined threshold, which reduces the energy consumption significantly by over 40% compared to selection diversity. As shown in Fig. 6.11, after forwarding 1000 data packets, a router that employed either of the proposed techniques consumed at least 15% less energy than the conventional switched diversity. The use of feedback from the lower and upper hop in the proposed Max-sum and Max-min schemes allow the receiver to stay in the currently active branch longer and increases energy efficiency over time by reducing overall feedback messages and antenna switching compared to single hop based switched diversity scheme.

6.6.8 Impact of network size

Table 6.1 summarizes the simulated performance of the proposed and tradition diversity schemes for three different network sizes. During simulation, with each hop increase, the network size was increased by 5% and the results obtained are from routers only. As expected, 1% diversity gain of two-hop based diversity scheme is greater than the conventional switched based diversity scheme for

Table 6.1: Comparison of simulated performance between diversity schemes for various network sizes

Diversity Technique	Number of hops	Packet Loss (%)	Switching freq. increase (%)	Mean residual energy on routers (%)	Diversity gain (compared to switched diversity)
Max-sum	10	2	6	83	4.1
	15	4	12	77	4.4
	20	5	16	66	4.9
Max-min	10	3	7	81	1.9
	15	4	10	78	2.2
	20	6	15	69	2.7
Switched diversity	10	3	8	80	x
	15	5	14	74	x
	20	7	19	63	x
Selection diversity	10	2	13	76	9.5
	15	2	21	68	10.7
	20	3	35	47	11.8

all considered scenarios. We notice that as the number of hop is increased in a multihop network, switching frequency of the devices also increases irrespective of the diversity technique used. The nodes using selection diversity experience the worst switching rate (highlighted in shaded cells), which increases energy consumption of the nodes and reduces network lifetime. On the other hand, the proposed Max-min and Max-sum scheme achieved better energy efficiency, while providing reliability. Thus we can conclude that antenna selection by leveraging the channel knowledge of multiple nodes instead of a single transmitter leads to improved energy efficiency, without sacrificing reliability. We also note that as the network size increases Max-Min performs better than the Max-Sum in every metric except diversity gain. The reason behind this is most likely due to Max-Min aiming to maximize the lower bound ensures that the selected link for both transmission and reception satisfies the threshold and thus require less packet re-transmission and antenna switching. However, maximizing the sum may lead to selection of a link, which is good for transmission but not for reception or vice versa and will eventually require packet re-transmission. Based on the results, Max-Sum and Max-Min schemes should be considered for small scale and large scale networks, respectively.

6.6.9 Algorithmic complexity

For time complexity analysis of the proposed algorithms, we consider the worst-case time complexity to find the upper bound of the running time of the algorithms regardless of the network size. For Max-Sum scheme, the first step is to add signal strength values of each polarization obtained from

the upper level and lower level node, respectively and the second step is to sort the outputs of the first step. Assuming that searching for maximum or minimum in a data set will take a constant time, the required time complexity is $\mathcal{O}(n * o)$, where n is the number of inputs and o is the number of outputs. We also note that both n and o are “3”, since both nearest neighbour nodes are using tripolar antenna. Similarly, the Max-Min algorithm will also have same time complexity given that the diversity receiver will have same input size to process to make antenna selection. Although both algorithms offer low time complexity, the execution time of the algorithm will increase with the increment of the number of antenna branches since it is directly proportional to the input size.

The findings from the above results establishes that it is important to evaluate the impact of various diversity schemes from a global network perspective. We can also conclude that there is considerable benefit in practically implementing dual-hop based antenna selection techniques specially in energy constricted IoT networks, since it allows the receiver to dwell on the received signal for some time and decreases switching transients, which eventually ensures high reliability and minimize energy consumption.

6.7 Conclusion

In this work, we presented a performance analysis of three branch, switched diversity systems for resource-constrained IoT networks operating on independent but non-identical Rayleigh fading channels. The core feature of the proposed schemes is that the receiver switches antenna branch based on channel conditions of both preceding hop and the next hop, while satisfying a specific threshold and hence utilizes the inherent diversity of wireless links in a multi-user IoT network. First, we derived the closed-form expressions of outage probability for the proposed Max-Sum and Max-Min scheme. Through extensive simulations we then demonstrated the diversity gain obtained by Max-Sum and Max-Min are 3.6 dB and 1.4 dB, respectively compared to conventional switched diversity scheme. Results also showed that the proposed diversity schemes reduced antenna branch switching frequency by more than three quarters and two fifths compared to classic selection and switched diversity, respectively. In addition to achieving diversity gain over the conventional switched diversity system, the proposed schemes also provided satisfactory packet delivery ratio commensurate with selection diversity. Finally, comparison between the proposed techniques indicates that Max-Sum should be preferred for small-scale IoT networks while Max-Min should be preferred for large scale IoT networks.

Future works in this area includes the real-life implementation of multi-branch antenna systems

in hierarchical IoT networks under other channel fading conditions than the Rayleigh. Finally, an overall end-to-end network-wide energy efficiency analysis will be conducted to investigate the impact of antenna switching and communication overhead for various schemes on the lifetime of IoT devices.

Summary

In this work we highlighted the potential improvement in the received signal for IoT devices equipped with tripolar antennas using modified switched diversity techniques, which leveraged channel information from multiple neighbor nodes to make better antenna selection decisions. To verify the accuracy of the proposed analytical models, numerical results evaluated from the theoretical expressions have been obtained and compared against the simulation results. The goal of our research was to address the challenges faced by IoT devices in high multipath environment by leveraging 3D printed compact three-branch antenna system to achieve enhanced energy efficiency and better link reliability. The existing works in the literature considered dual-branch antenna systems and relied heavily on simulation to analyze the performance. Our work intended to bridge the gap in existing research by implementing IoT networks with prototype multi-branch antenna systems deployed in cluttered environment, likely to be experienced by many practical IoT applications. The next chapter concludes this work by reflecting upon our research as a whole and provides a incisive, yet insightful summary of our overall journey, findings and highlights other directions or approaches that could be further investigated.

7 Conclusion and Future Work

We aimed to investigate the efficacy of multi-branch antenna systems for IoT networks. The results demonstrate that both link reliability and energy efficiency can be improved by using multi-branch antenna systems with efficient diversity techniques developed for IoT devices. Sections of the chapter include summary of the findings, course of actions for future works and final remarks. The summary section condenses the central ideas in regards to the research goals and highlights the value and contribution thereof. In the future works sections, we make suggestions for further study to improve the performance of IoT networks by considering various indoor and outdoor wireless environments, utilizing testbeds and machine learning techniques. We conclude the chapter with some final thoughts on how IoT and emerging technologies will benefit by creating new experiences and opportunities.

7.1 Summary

Internet of Things (IoT) is a network of interconnected physical objects that are characterized by sensing, limited data processing and data sharing capabilities. Emerging applications of IoT devices, for example, industrial automation, power grid, smart automotive solutions, transportation, will use sensors, embedded devices that are expected to perform autonomously using standard wireless communication protocols with sparse human intervention. Due to the nature of the applications, IoT devices are expected to be deployed in particularly harsh radio propagation environment where the radio wave will be affected by severe multipath effects and signal depolarization. The use of polarization diversity antenna systems, which uses two or more orthogonally polarized signals at the diversity receiver, can improve the performance of IoT networks operating in high multipath fading environments. Since the different antennas can be co-located, polarized antenna systems offers added advantage for IoT devices with their compact size while providing antenna diversity. The idea behind this work is to investigate the performance of tripolar antenna systems in an IoT network consists of devices equipped with antenna containing three perpendicularly oriented antenna elements. The other aspect of this dissertation is to develop efficient antenna diversity techniques for the tripolar antenna that are specifically designed for low-cost, low-powered and small IoT devices.

We begin with proof-of-concept experiment to show that the tripolar systems can be effective in enhancing network reliability by mitigating multipath fading. Chapter 1 presents the work, where we compared the link reliability for two wireless mesh networks using hybrid wireless network simulator,

one network utilized wireless nodes with a single element antenna, in the second, nodes leveraged diversity enabled by a tripolar antenna system. Simulation results of measured channel loss data sets, show that the tripolar antenna can significantly improve the communication reliability in such networks. In the subsequent work we implement these approaches in hardware to demonstrate the benefits in practice. A prototype fabricated tripolar antenna mounted on Arduino based XBee devices is placed inside of a reverberation chamber which can emulate severe propagation environments, such as those expected for industrial IoT applications. Through experimental data obtained from point-to-point links, we showed that a tripolar antenna can provide better link reliability and end-to-end network throughput compared to single element antenna and thus prove the the necessity of employing tripolarized systems in multipath conditions.

Motivated by the efficacy of tripolar antenna systems over single point-to-point links, we focus on evaluating the impact of tripolar antenna systems on neighbouring nodes on a large-scale, mesh IoT network. Distinct fading scenarios seen by the IoT devices will led to different antenna branch selection for nodes that are far from each other resulting in polarization mismatch between two neighbour devices which either send or receiver data packets from each other. Chapter 3 analyzes the effect of choosing same and different antenna branches for the transmitting node and the receiving node on power loss of the received signal and link reliability. To address the issue, two polarization matching techniques are proposed that aims to minimize the power loss due to polarization mismatch and improve data delivery ratio for an IoT network. The proposed Neighbor Matching and Opportunistic Polarization Matching approaches consider IoT network that employs predetermined routing paths and dynamic routing paths, respectively. Neighbor Matching scheme enables nodes to determine the best antenna branch among the three polarizations using Binary Integer Optimization which requires the knowledge of neighbour nodes' antenna branch status. Under the Opportunistic Polarization Matching scheme, nodes select antenna branch based on the load on the next level router. A load balance factor for routers is defined based on which child nodes select the next level router from multiple available options and determine antenna branch according to the selected routers' antenna configuration status. Through extensive simulations, we demonstrate that by utilizing antenna polarization information from neighboring nodes, the proposed schemes can still achieve high successful data delivery ratio than the baseline networks which uses single antenna systems.

The observations from Chapter 3 prompted further investigation on relationship between IoT network structure and antenna selection techniques for tripolar antenna systems. Chapter 4 proposed energy-aware polarization diversity scheme that leverages complex network theory to identify the

most influential router nodes. The work considers a typical IoT network where sensed data are forwarded to a base station from the end nodes in a multi-hop manner. The proposed algorithm uses distributed eigenvector centrality metric to rank the routers where a router's score or importance is proportional to the number of child nodes that are connected to the router. The centrality score, which is calculated by IoT devices autonomously based on antenna configuration information from their neighbour connected nodes only, enables implementing a node-specific antenna diversity approach. Since a router with high centrality score will consume more energy than routers with low centrality score as it will see increased data flow from its child nodes, it is essential to consider a diversity technique that varies antenna switching frequency depending on the energy depletion rate of the routers. Results demonstrate that by using the adaptive antenna selection technique, which allows low scoring routers to switch polarization more frequently compared to high scoring routers, we successfully decrease the energy consumption by at least 13% compared to the conventional selection diversity while offering similar network reliability. Simulation results also show that the proposed centrality based approach reduces switching by at least 17% compared to the technique of employing selection diversity for all the nodes of an IoT network irrespective of their roles.

Chapter 3 and 4 encouraged our exploration for improved antenna selection techniques for tripolar antennas that can improve overall antenna switching and network performance. Considering that most of the conventional switching techniques are proposed for mobile devices that have more capabilities than the low-cost IoT devices and lack of research on suitability of these algorithms in the context of IoT networks, it is necessary to evaluate the performance of the existing algorithms on an IoT network as well as improving the conventional diversity techniques to address the resource-limitation of IoT devices. Chapter 5 proposed an antenna selection technique that utilizes Hidden Markov Model based approach to infer the best diversity branch, before every transmission by modeling the probabilistic relationship between antenna branches as an underlying Markov chain structure along with the sequence of observations (RSSI values) obtained from the currently active antenna branch. The parameters required by the HMM coordinated diversity technique were calculated using a measured dataset obtained from an Arduino based sensor devices equipped with tripolar antenna deployed in a highly clutter environment. Experimental results demonstrate that the HMM approach improved the median and 1% diversity gains by 0.4 and 2.4 dB, respectively, over a switch diversity implementation that utilized the same decision threshold. By eliminating ineffective or unnecessary switching between antenna elements that may result when conventional switched diversity is used, the developed approach reduced energy consumption by approximately 15% compared to the switched diversity.

Finally, in Chapter 6, we continue network-wide performance analysis of three branch switched diversity receivers while emphasizing on the importance of leveraging the diversity of wireless links in a multi-user IoT network and incorporating neighbor nodes antenna selection polarization status during antenna selection. The work proposed two antenna selection schemes where the receiver switches antenna branch based on channel conditions of both preceding hop and the next hop while maintaining signal quality above a predefined threshold. Closed-form expressions of outage probability for the proposed Max-Sum and Max-Min schemes are derived for radio propagation environment where antenna branches see independent but not identical Rayleigh fading. Both analytical and simulation results demonstrate the improvements provided by the proposed diversity schemes over classic selection diversity and switched diversity scheme in terms of decreased antenna switching and reduced energy consumption. Simulation results, which utilized measured data from over the air testing that included three distinct 3D printed tripolar antennas deployed in a high multipath environment and operating at ~ 2.4 GHz, demonstrated that the proposed dual-hop based diversity schemes can achieve better diversity gain while reducing antenna switching frequency compared to conventional switch diversity systems.

7.2 Future Work

There are a number of different ways that the work in this dissertation could be extended. These proposed paths for future research can be described as follows.

7.2.1 Real life implementation

The current works with the tripolar antenna conducted over the air measurements for a pair of devices using reverberation chamber to create multipath environment. While there are several existing research works related to hardware implementation of IoT devices, they either focus on specific wireless environment [218], [219] or focuses on data processing from the IoT devices [220]. Extending the number of devices that uses polarization diversity based multi-element antenna systems and the state-of-the-art diversity techniques is essential to evaluate the performance of such approaches in real life scenarios. Validating the performance of the tripolar antenna through hardware implementation of a large network in indoor and outdoor environment, for example, inside of a factory or in an agricultural field, is significant for analyzing the efficiency of the antenna in real-life scenarios. Moreover, a large scale experimental platform with tripolar antenna systems will allow to apply and optimize different diversity techniques, leading to the development of low complexity antenna

diversity techniques for low-cost IoT devices. Recent development of wireless cellular technology structure and design have enabled 5G communication systems to meet the diverse requirements of IoT networks [221], [222]. Current works in the literature studied suitable random access channel model [222], transceiver design [222] and channel conditions [222] and analyzed proposed solutions for 5G IoT applications based on simulations only. A framework that will deploy a low-cost testbed infrastructure, which can empirically validate and evaluate any proposed methodology or diversity technique through realistic emulation and analyze the obtained results, is necessary to assess these technologies. Investigating the framework of the IoT testbed, for example, the workflow of each single experiment, the process of nodes communicating with other, software artefacts and data collection etc. is the next step in the development of practical implementation of IoT.

7.2.2 Testing scalability and robustness

Selection of routing strategies is crucial in IoT networks for not only ensuring efficient delivery of the packets to their destination but to help preventing the resource-limited devices from exhausting significant energy during data packet routing. Various energy-efficient routing protocols have been designed and developed for IoT based sensor networks aiming to provide satisfactory data delivery performance in an energy-efficient manner. Due to the wide variety of IoT applications and services with vastly varying requirements, both network architecture and routing protocol may have specific characteristics suited to a particular application. Researchers have studied several IoT network architecture such as centralized [223], decentralized [224] and hierarchical [225]. Clustered network topology where cluster can be formed using top-down or a bottom-up approach based on pre-defined or dynamic requirements have also been studied extensively [226], [227]. Our works have shown that antenna diversity performance can be improved when network-structure is taken into account and nodes have local knowledge of neighbours' antenna configuration. However, the proposed works only considered a centralized multi-hop network. The lack of understanding of the network-wide impact of multi-branch antennas may result in many unresolved or unclear issues in performance analysis, since performance measurement based on single communication link only provides a partial view and may not be sufficient or accurate. Studies have shown that packet drop rate induced by fading and energy consumption grows linearly as network size increases [228]. As the scale of the network increases, the data packets are routed through more hops and the probability one of the links in the routing path will experience severe fading increases. Furthermore, the cascading effect due to the change of branch of a higher level node will propagate through the network and the subsequent frequent switching of lower level nodes may cause loss of sensed data due to issues

with synchronization or possible delays, corrupt receiver filters. [229]. Hence, the effectiveness of the tripolar antenna diversity needs to be evaluated for different network topologies and routing protocols that are likely to be implemented in various IoT applications.

7.2.3 Leveraging machine learning techniques

The current HMM coordinated diversity scheme require measured data from the environment where the IoT devices will be deployed to calculate the transition probabilities between antenna branches. However, for practical implementation of the technique, the algorithm needs to update its parameters dynamically according to the surrounding environment where the device is operating. Therefore, further study is needed on how the HMM coordinated approach can analyze the time series data obtained from the RSSI observation and model the parameters in real time. In addition, determining appropriate number of observation states and tuning the threshold to find optimal group intervals needs to be examined. Developing and illustrating the suitability of the HMM approach for diversity antennas with more than three branches can also be addressed. On the other hand, Machine Learning (ML) techniques can be used to optimize the diversity performance of multi-branch antenna systems. Data-driven ML techniques have the ability to utilize empirical data in order to learn and model behaviours of a system by classification and feature extraction from the dataset [230]. Therefore, ML can be used to infer knowledge from signal strength data and antenna switching decisions of IoT devices with multi-branch antenna systems under certain fading conditions and subsequently leverage the knowledge to adapt the antenna selection based on the acquired knowledge. While existing works studied the use of ML for managing massive data generated from IoT devices with minimized resources [231] and various aspects of security and privacy in IoT networks [232], no work has examined dynamic optimizing control of antenna systems using ML. In the wake of 5G communication systems, it is crucial to explore the power of ML techniques for embedded IoT devices with smart antenna systems deployed in sophisticated indoor and outdoor channel environments.

7.2.4 Different fading environments

The proposed approaches in this dissertation consider Rayleigh fading environment where random fading signals on each of the diversity branches of the tripolar antenna are independent, non-identical and hence uncorrelated. However, many factors, such as the distribution of scattering, correlation between fading channels may also cause signal degradation. Many theoretical analysis on the effect of correlated fading on the performance of antenna diversity techniques can be found in the literature. Al-Juboori *et al.* [233] and Yishvaksenan *et al.* [234] give the cumulative distribution function (CDF)

for a dual diversity scheme with Maximal Ratio Combining (MRC), Equal Gain Combining (EGC) over correlated Nakagami- m multipath fading and frequency-selective channels, respectively. Zhang *et al.* [235] give a general expression for the bit error rate performance under correlated fading for dual-polarized antennas. They introduces polarization dimension to transmit additional information and offer extra transmit diversity and analyzed the performance through simulations. An analytical expression for the outage probability expressions with dual diversity for MRC, EGC and SC and correlated fading conditions is derived by Zhu *et al.* [236]. However, most of the aforementioned work did not consider multi-branch antenna with three elements. In addition, the antenna selection techniques used for deriving analytical expressions for BER or outage probability such as MRC, EGC and selection diversity, may not be ideal for IoT devices due to requirement of extra hardware and implementation complexity. Thus, analyzing the performance of the proposed tripolar antenna selection techniques under correlated fading condition need to be studied further.

7.2.5 Hybrid approaches combining routing and antenna diversity

The idea of exploiting topology information and channel diversity for improving the performance of IoT networks has been studied in the literature in recent years [237–239]. By jointly coordinating transmission power of each IoT device, wireless channel selection and route selection for data packets based on network structure and exchange of information among multihop neighbor nodes The throughput of an IoT network can be improved by jointly coordinating transmission power of each IoT device, wireless channel assignment and route selection among multihop neighbor nodes in a distributed manner [240, 241]. In [240], the authors studied a hybrid ubiquitous sensor network and proposed a cross layer topology information based diversity scheme that integrates cooperative diversity between nodes and attributes of topology space. The authors in [238] studied an algorithm that determines the shortest route from all nodes to the base station (sink node) using real-time dynamic planning to mitigate the volatility of the network while striking a sound balance between energy consumption and delay in forwarding data packets. Later, in [242] the authors focused on maximizing the network lifetime and throughput simultaneously by grouping sensors into clusters and selecting wireless channel links among clusters using a weighted link function in a cooperative manner. Under the proposed strategy, nodes send broadcast message to their 1-hop neighbors along with their residual energy and the cluster head uses inter-cluster and intra-cluster messages to reduce collisions and interference between nodes. While hybrid approaches discussed above can improve outage probability and ensure efficient utilization of available channels, these ideas can be extended further given the wide range of IoT applications and their versatile requirements. The integration of

information from medium access control layer (for wireless channel information) and network layer (for routing information) by low-cost IoT devices can be challenging due to their low computational capability, which can be potential future works in this field.

7.3 Final Comments

The work presented in this thesis serves as an example of the importance of multi-branch antenna in compact embedded devices and seeks to bridge the gap between analytical and experimental performance of diversity techniques. By utilizing the fabricated tripolar antenna and wireless nodes for typical sensing application, the work demonstrated possible improvement in link performance while improving energy efficiency. We hope that the work will motivate researchers to develop communication protocols and routing schemes specifically targeted for IoT devices with multi-branch antenna systems to exploit the advantage of the polarized radio wave in a rich multipath environment.

The advent of semiconductor technology has led to declining costs of embedded devices which will enable deployment of new IoT applications that require not only high reliability, but also much faster data rates. Many studies including the proposed work in this dissertation considers IoT devices and protocols that are focused on low frequency around 2.4 GHz only. The extension of the current multi-branch antenna designs and diversity techniques for compact sensor devices that supports mmWave data transmission is crucial. Moreover, usage of software-defined radios, cognitive radios along with IoT devices will led to a hybrid network and diversity techniques will have to adapt based on the network architecture.

References

- [1] R. A. Ramirez, D. Lugo, T. M. Weller, M. Golmohamadi, and J. Frolik, "Additive manufactured tripolar antenna system for link improvement in high multipath environments," in *Antennas and Propagation & USNC/URSI National Radio Science Meeting, 2017 IEEE International Symposium on*. IEEE, 2017, pp. 2539–2540.
- [2] S. Chowdhury, M. Golmohamadi, and J. Frolik, "Improving reliability in hybrid mesh networks with tripolar antennas," *2018 IEEE International Symposium on Antennas and Propagation & USNC/URSI National Radio Science Meeting*, pp. 189–190, 2018.
- [3] R. A. Ramirez, M. Golmohamadi, J. Frolik, and T. M. Weller, "3D printed on-package tripolar antennas for mitigating harsh channel conditions," *2017 IEEE Radio and Wireless Symposium (RWS)*, pp. 62–64, 2017.
- [4] M. M. Rana, W. Xiang, E. Wang, and M. Jia, "IoT infrastructure and potential application to smart grid communications," in *GLOBECOM 2017 - 2017 IEEE Global Communications Conference*, Dec 2017, pp. 1–6.
- [5] S. Abraham, J. Beard, and R. Manijacob, "Remote environmental monitoring using internet of things (IoT)," in *2017 IEEE Global Humanitarian Technology Conference (GHTC)*, Oct 2017, pp. 1–6.
- [6] A. F. Molisch, *Wireless Communications*. John Wiley & Sons, 2012.
- [7] M. R. Andrews, P. P. Mitra *et al.*, "Tripling the capacity of wireless communications using electromagnetic polarization," *Nature*, vol. 409, no. 6818, p. 316, 2001.
- [8] A. S. Kurji, A. H. Al-Nakkash, and O. A. Hussein, "Lora in a campus: Reliability and stability testing," in *IOP Conference Series: Materials Science and Engineering*, vol. 1105, no. 1. IOP Publishing, 2021, p. 012034.
- [9] B. Jolly, *Solving the Critical Issues at End of Battery Life for IoT Devices*. Available: <https://www.powerelectronicsnews.com/solving-the-critical-issues-at-end-of-battery-life-for-iot-devices/>, 2019.
- [10] O. Jo, J. Kim, J. Yoon, D. Choi, and W. Hong, "Exploitation of dual-polarization diversity for 5G millimeter-wave MIMO beamforming systems," *IEEE Transactions on Antennas and Propagation*, vol. 65, no. 12, pp. 6646–6655, 2017.
- [11] C. Fang, E. Liu, and M. Ur Rehman, "Analysis of subchannel correlation in dual-polarised MIMO systems via a polarisation diversity scheme," *IEEE Transactions on Antennas and Propagation*, vol. 65, no. 5, pp. 2635–2644, 2017.
- [12] M. Blanco and K. Zdunek, "Performance and optimization of switched diversity systems for the detection of signals with Rayleigh fading," *IEEE Transactions on Communications*, vol. 27, no. 12, pp. 1887–1895, 1979.
- [13] S. Bemanali and M. Eslami, "Low complexity capacity maximizing transmit antenna selection schemes for massive MIMO wireless communications," *Wireless Personal Communications*, vol. 96, no. 3, pp. 3873–3887, May 2017. [Online]. Available: <https://doi.org/10.1007/s11277-017-4355-4>
- [14] H. Nam and M.-S. Alouini, "Multi-branch switched diversity with adaptive switching thresholds," *2008 International Symposium on Information Theory and Its Applications*, pp. 1–6, 2008.
- [15] M. Jana, L. Lampe, and J. Mitra, "Dual-polarized faster-than-Nyquist transmission using higher order modulation schemes," *IEEE Transactions on Communications*, vol. 66, no. 11, pp. 5332–5345, 2018.
- [16] A. Kalla, P. Prombage, and M. Liyanage, "Introduction to IoT," *IoT Security: Advances in Authentication*, pp. 1–25, 2020.

- [17] P. Wang, R. Valerdi, S. Zhou, and L. Li, "Introduction: Advances in IoT research and applications," *Information Systems Frontiers*, vol. 17, no. 2, pp. 239–241, 2015.
- [18] P. Gokhale, O. Bhat, and S. Bhat, "Introduction to IOT," *International Advanced Research Journal in Science, Engineering and Technology*, vol. 5, no. 1, pp. 41–44, 2018.
- [19] A. Deshpande, P. Pitale, and S. Sanap, "Industrial automation using Internet of Things (IOT)," *International Journal of Advanced Research in Computer Engineering & Technology (IJARCET)*, vol. 5, no. 2, pp. 266–269, 2016.
- [20] M. A. Rahim, M. A. Rahman, M. Rahman, A. T. Asyhari, M. Z. A. Bhuiyan, and D. Ramasamy, "Evolution of IoT-enabled connectivity and applications in automotive industry: A review," *Vehicular Communications*, p. 100285, 2020.
- [21] F. Al-Turjman and M. Abujubbeh, "IoT-enabled smart grid via SM: An overview," *Future Generation Computer Systems*, vol. 96, pp. 579–590, 2019.
- [22] M. Gautam, S. Raviteja, S. Sivanesh, and R. Mahalakshmi, "Data acquisition for residential energy management employing IoT using ThingSpeak," in *2019 IEEE Region 10 Symposium (TENSymp)*. IEEE, 2019, pp. 272–276.
- [23] D. A. Gandhi and M. Ghosal, "Intelligent healthcare using IoT: A extensive survey," in *2018 Second International Conference on Inventive Communication and Computational Technologies (ICICCT)*. IEEE, 2018, pp. 800–802.
- [24] N. Zou, S. Liang, and D. He, "Issues and challenges of user and data interaction in healthcare-related IoT," *Library Hi Tech*, 2020.
- [25] H.-C. Cheng and W.-W. Liao, "Establishing an lifelong learning environment using IOT and learning analytics," in *2012 14th International Conference on Advanced Communication Technology (ICACT)*. IEEE, 2012, pp. 1178–1183.
- [26] T. Wasson, T. Choudhury, S. Sharma, and P. Kumar, "Integration of RFID and sensor in agriculture using IOT," in *2017 International Conference On Smart Technologies For Smart Nation (SmartTechCon)*. IEEE, 2017, pp. 217–222.
- [27] A. Alshamsi, Y. Anwar, M. Almulla, M. Aldohoori, N. Hamad, and M. Awad, "Monitoring pollution: Applying IoT to create a smart environment," in *2017 International Conference on Electrical and Computing Technologies and Applications (ICECTA)*. IEEE, 2017, pp. 1–4.
- [28] H. Kaur and S. K. Sood, "Fog-assisted IoT-enabled scalable network infrastructure for wildfire surveillance," *Journal of Network and Computer Applications*, vol. 144, pp. 171–183, 2019.
- [29] V. V. Daigavane and M. Gaikwad, "Water quality monitoring system based on IoT," *Department Electronics & Telecommunication Engineering, Advances in Wireless and Mobile Communications*, vol. 10, no. 5, pp. 1107–1116, 2017.
- [30] V. S. Nagmode and S. Rajbhoj, "An intelligent framework for vehicle traffic monitoring system using IoT," in *2017 International Conference on Intelligent Computing and Control (I2C2)*. IEEE, 2017, pp. 1–4.
- [31] V. Adjiski, Z. Despodov, D. Mirakovski, and D. Serafimovski, "System architecture to bring smart personal protective equipment wearables and sensors to transform safety at work in the underground mining industry," *Rudarsko-geološko-naftni zbornik*, vol. 34, no. 1, 2019.
- [32] M. Muttillio, V. Stornelli, R. Alaggio, R. Paolucci, L. Di Battista, T. de Rubeis, and G. Ferri, "Structural health monitoring: An IoT sensor system for structural damage indicator evaluation," *Sensors*, vol. 20, no. 17, p. 4908, 2020.
- [33] H. Al-Hamadi, M. Saoud, I.-R. Chen, and J.-H. Cho, "Optimizing the lifetime of IoT-based star and mesh networks," *IEEE Access*, vol. 8, pp. 63 090–63 105, 2020.
- [34] M. N. Ochoa, A. Guizar, M. Maman, and A. Duda, "Evaluating LoRa energy efficiency for adaptive networks: From star to mesh topologies," in *2017 IEEE 13th International Conference*

- on *Wireless and Mobile Computing, Networking and Communications (WiMob)*, 2017, pp. 1–8.
- [35] H. Mamat, B. Ibrahim, and M. Sulong, “Network topology comparison for internet communication and IoT connectivity,” in *2019 IEEE Conference on Open Systems (ICOS)*, 2019, pp. 1–5.
- [36] X. Jiang, H. Zhang, E. A. Barsallo Yi, N. Raghunathan, C. Mousoulis, S. Chaterji, D. Peroulis, A. Shakouri, and S. Bagchi, “Hybrid low-power wide-area mesh network for IoT applications,” *IEEE Internet of Things Journal*, vol. 8, no. 2, pp. 901–915, 2021.
- [37] A. Bader and M.-S. Alouini, “Localized power control for multihop large-scale internet of things,” *IEEE Internet of Things Journal*, vol. 3, no. 4, pp. 503–510, 2015.
- [38] G. Chen, J. P. Coon, A. Mondal, B. Allen, and J. A. Chambers, “Performance analysis for multihop full-duplex IoT networks subject to poisson distributed interferers,” *IEEE Internet of Things Journal*, vol. 6, no. 2, pp. 3467–3479, 2018.
- [39] X. Liu, Z. Li, N. Zhao, W. Meng, G. Gui, Y. Chen, and F. Adachi, “Transceiver design and multihop D2D for UAV IoT coverage in disasters,” *IEEE Internet of Things Journal*, vol. 6, no. 2, pp. 1803–1815, 2018.
- [40] D. Airehrour, J. Gutierrez, and S. K. Ray, “Secure routing for Internet of Things: A survey,” *Journal of Network and Computer Applications*, vol. 66, pp. 198–213, 2016.
- [41] A. Dhumane, R. Prasad, and J. Prasad, “Routing issues in Internet of Things: a survey,” in *Proceedings of the international multiconference of engineers and computer scientists*, vol. 1, 2016, pp. 16–18.
- [42] I. F. Akyildiz and M. C. Vuran, *Wireless sensor networks*. John Wiley & Sons, 2010, vol. 4.
- [43] L. EL-Garoui, S. Pierre, and S. Chamberland, “A new SDN-based routing protocol for improving delay in smart city environments,” *Smart Cities*, vol. 3, no. 3, pp. 1004–1021, 2020.
- [44] T.-F. Shih and H.-C. Yen, “Location-aware routing protocol with dynamic adaptation of request zone for mobile ad hoc networks,” *Wireless Networks*, vol. 14, no. 3, pp. 321–333, 2008.
- [45] T. M. Behera, U. C. Samal, and S. K. Mohapatra, “Energy-efficient modified LEACH protocol for IoT application,” *IET Wireless Sensor Systems*, vol. 8, no. 5, pp. 223–228, 2018.
- [46] T. Samant, P. Mukherjee, A. Mukherjee, and A. Datta, “TEEN—V: A solution for intra-cluster cooperative communication in wireless sensor network,” in *2017 International Conference on I-SMAC (IoT in Social, Mobile, Analytics and Cloud)(I-SMAC)*. IEEE, 2017, pp. 209–213.
- [47] W. Yu, L. Bin, and Z. Zhou, “Secure direct diffusion protocol for WSN,” *Communications Technology*, vol. 12, 2007.
- [48] J. Grover, M. Sharma *et al.*, “Reliable spin in wireless sensor network,” in *Proceedings of 3rd International Conference on Reliability, Infocom Technologies and Optimization*. IEEE, 2014, pp. 1–6.
- [49] W. Sun, J. P. Wang, J. L. Wang, Q. Y. Li, and D. M. Mu, “QoS routing algorithm of WSN for smart distribution grid,” in *Advanced Materials Research*, vol. 1079. Trans Tech Publ, 2015, pp. 724–729.
- [50] G.-C. Deng and K. Wang, “An application-aware QoS routing algorithm for SDN-based IoT networking,” in *2018 IEEE Symposium on Computers and Communications (ISCC)*. IEEE, 2018, pp. 00 186–00 191.
- [51] H.-C. Lee and K.-H. Ke, “Monitoring of large-area IoT sensors using a LoRa wireless mesh network system: Design and evaluation,” *IEEE Transactions on Instrumentation and Measurement*, vol. 67, no. 9, pp. 2177–2187, 2018.
- [52] A. Goldsmith, *Wireless communications*. Cambridge university press, 2005.
- [53] T. S. Rappaport, *Wireless Communications: Principles and Practice*. Prentice Hall PTR New Jersey, 1996.

- [54] G. L. Stüber and G. L. Stèuber, *Principles of mobile communication*. Springer, 1996, vol. 2.
- [55] N. Blaunstein and C. G. Christodoulou, *Radio propagation and adaptive antennas for wireless communication links: terrestrial, atmospheric and ionospheric*. John Wiley & Sons, 2007, vol. 193.
- [56] M. Golmohamadi and J. Frolik, “Depolarization in three dimensions: theoretical formulations and empirical results,” in *2016 IEEE 17th Annual Wireless and Microwave Technology Conference (WAMICON)*. IEEE, 2016, pp. 1–6.
- [57] M. Mohammadkarimi, E. Karami, O. A. Dobre, and M. Z. Win, “Number of transmit antennas detection using time-diversity of the fading channel,” *IEEE Transactions on Signal Processing*, vol. 65, no. 15, pp. 4031–4046, 2017.
- [58] J. J. van Zyl and Y. Kim, “Synthetic aperture radar,” in *Encyclopedia of Physical Science and Technology (Third Edition)*, third edition ed., R. A. Meyers, Ed. New York: Academic Press, 2003, pp. 451–465. [Online]. Available: <https://www.sciencedirect.com/science/article/pii/B0122274105009017>
- [59] W. Liu, M. Sellathurai, C. Tang, and J. Wei, “Achieving space and time diversity by using lattice constellation based joint Alamouti coding,” *IEEE Communications Letters*, vol. 14, no. 1, pp. 33–35, 2010.
- [60] D. Arndt, A. Ihlow, A. Heuberger, and E. Eberlein, “Measurement-based evaluation of antenna and time diversity for mobile satellite systems,” in *Proceedings of the 11th International Conference on Telecommunications*, 2011, pp. 457–464.
- [61] W. Belaoura, K. Ghanem, and M. Nedil, “Performance of IDMA system with space time diversity over mmWave underground channel,” in *2020 IEEE International Symposium on Antennas and Propagation and North American Radio Science Meeting*, 2020, pp. 1149–1150.
- [62] F. Sun, F.-S. Zhang, H. Zhang, H. Zhang, C. Li, and C. Feng, “A frequency diversity printed-Yagi antenna element for apertures selectivity wideband array application,” *IEEE Transactions on Antennas and Propagation*, vol. 66, no. 10, pp. 5634–5638, 2018.
- [63] S. Y. Nusenu, S. Huaizong, Y. Pan, and A. Basit, “Directional modulation with precise legitimate location using time-modulation retrodirective frequency diversity array for secure IoT communications,” *IEEE Systems Journal*, vol. 15, no. 1, pp. 1109–1119, 2021.
- [64] P. Fan, X. Cui, and M. Lu, “Space and frequency diversity characterization of mobile GNSS receivers in multipath fading channels,” *Tsinghua Science and Technology*, vol. 25, no. 2, pp. 294–301, 2020.
- [65] E. Dinc and O. B. Akan, “Fading correlation analysis in MIMO-OFDM troposcatter communications: Space, frequency, angle and space-frequency diversity,” *IEEE Transactions on Communications*, vol. 63, no. 2, pp. 476–486, 2015.
- [66] L. Ye and A. Burr, “Frequency diversity comparison of coded SC-FDE amp; OFDM on different channels,” in *2007 IEEE 18th International Symposium on Personal, Indoor and Mobile Radio Communications*, 2007, pp. 1–5.
- [67] J. Geng, R. W. Ziolkowski, K. Wang, X. Zhao, H. Zhou, G. Chenhu, X. Liang, and R. Jin, “Dual CP polarization diversity and space diversity antennas enabled by a compact T-shaped feed structure,” *IEEE Access*, vol. 7, pp. 96 284–96 296, 2019.
- [68] H. M. Carvajal, N. G. Orozco, and C. de Almeida, “Signal space diversity in single and multiuser scenarios employing sphere decoder detector,” *IEEE Communications Letters*, vol. 22, no. 4, pp. 868–871, 2018.
- [69] S. Althunibat and R. Mesleh, “Enhancing spatial modulation system performance through signal space diversity,” *IEEE Communications Letters*, vol. 22, no. 6, pp. 1136–1139, 2018.
- [70] Y. Sharma, D. Sarkar, K. Saurav, and K. V. Srivastava, “Three-element MIMO antenna system with pattern and polarization diversity for WLAN applications,” *IEEE Antennas and Wireless Propagation Letters*, vol. 16, pp. 1163–1166, 2017.

- [71] H. Huang, S. Gao, S. Lin, and L. Ge, "A wideband water patch antenna with polarization diversity," *IEEE Antennas and Wireless Propagation Letters*, vol. 19, no. 7, pp. 1113–1117, 2020.
- [72] A. Sarkar, S. Mukherjee, A. Sharma, A. Biswas, and M. Jaleel Akhtar, "SIW-based quad-beam leaky-wave antenna with polarization diversity for four-quadrant scanning applications," *IEEE Transactions on Antennas and Propagation*, vol. 66, no. 8, pp. 3918–3925, 2018.
- [73] M. Paranthaman, "T-shape polarization reconfigurable patch antenna for cognitive radio," in *2017 Third International Conference on Science Technology Engineering Management (ICONSTEM)*, March 2017, pp. 927–929.
- [74] Y. Li, Y.-X. Guo, and S. Xiao, "Orientation insensitive antenna with polarization diversity for wireless capsule endoscope system," *IEEE Transactions on Antennas and Propagation*, vol. 65, no. 7, pp. 3738–3743, 2017.
- [75] J. P. González and B. Rodríguez, "Improving the indoor WLAN service by using polarization diversity and MRC," *Wireless Personal Communications*, vol. 95, no. 4, pp. 4917–4929, 2017.
- [76] H. Zhang and A. Abdi, "On the average crossing rates in selection diversity," *IEEE Transactions on Wireless Communications*, vol. 6, no. 2, pp. 448–451, 2007.
- [77] J. K. Cavers and P. Ho, "Switching rate and dwell time in M-of-N selection diversity," *IEEE Transactions on Wireless Communications*, vol. 6, no. 4, pp. 1218–1223, 2007.
- [78] S. Haghani and N. C. Beaulieu, "Performance of S + N selection diversity receivers in correlated Rician and Rayleigh fading," *IEEE Transactions on Wireless Communications*, vol. 7, no. 1, pp. 146–154, 2008.
- [79] G. Karagiannidis, D. Zogas, and S. Kotsopoulos, "Performance analysis of triple selection diversity over exponentially correlated Nakagami- m fading channels," *IEEE Transactions on Communications*, vol. 51, no. 8, pp. 1245–1248, 2003.
- [80] D. Wang, Y. Cao, and J. Xing, "A note on "a hybrid selection/equal-gain combining over correlated Nakagami- m fading channels"," *IEEE Communications Letters*, vol. 15, no. 9, pp. 925–925, 2011.
- [81] C. Tellambura, A. Annamalai, and V. Bhargava, "Unified analysis of switched diversity systems in independent and correlated fading channels," *IEEE Transactions on Communications*, vol. 49, no. 11, pp. 1955–1965, 2001.
- [82] A. S. Panajotović, M. Stefanović, D. L. Drača, and I. M. Petrović, "Effects of Rayleigh cochannel interference on switch and stay diversity system over correlated Rician fading channels," in *2009 International Conference on Ultra Modern Telecommunications Workshops*, 2009, pp. 1–6.
- [83] G. R. Tsouri, D. Wulich, and L. Goldfeld, "Enabling dual branch switched diversity in compact wireless devices," *IEEE Transactions on Consumer Electronics*, vol. 54, no. 4, pp. 1545–1549, 2008.
- [84] M. Blanco and K. Zdunek, "Performance and optimization of switched diversity systems for the detection of signals with Rayleigh fading," *IEEE Transactions on Communications*, vol. 27, no. 12, pp. 1887–1895, 1979.
- [85] A. Abu-Dayya and N. Beaulieu, "Analysis of switched diversity systems on generalized-fading channels," *IEEE Transactions on Communications*, vol. 42, no. 11, pp. 2959–2966, 1994.
- [86] —, "Switched diversity on microcellular Ricean channels," *IEEE Transactions on Vehicular Technology*, vol. 43, no. 4, pp. 970–976, 1994.
- [87] L. Yang and M.-S. Alouini, "Average level crossing rate and average outage duration of switched diversity systems," in *Global Telecommunications Conference, 2002. GLOBECOM '02. IEEE*, vol. 2, 2002, pp. 1420–1424 vol.2.

- [88] S. K. Yoo, S. L. Cotton, and W. G. Scanlon, “Switched diversity techniques for indoor off-body communication channels: An experimental analysis and modeling,” *IEEE Transactions on Antennas and Propagation*, vol. 64, no. 7, pp. 3201–3206, 2016.
- [89] H. Nam and M.-S. Alouini, “Optimization of multi-branch switched diversity systems,” *IEEE Transactions on Communications*, vol. 57, no. 10, pp. 2960–2970, 2009.
- [90] —, “Multi-branch switched diversity with adaptive switching thresholds,” in *2008 International Symposium on Information Theory and Its Applications*, 2008, pp. 1–6.
- [91] H.-C. Yang and M.-S. Alouini, “Improving the performance of switched diversity with post-examining selection,” *IEEE Transactions on wireless communications*, vol. 5, no. 1, pp. 67–71, 2006.
- [92] G. R. Tsouri, D. Wulich, and L. Goldfeld, “Enabling dual branch switched diversity in compact wireless devices,” *IEEE Transactions on Consumer Electronics*, vol. 54, no. 4, pp. 1545–1549, 2008.
- [93] X. Dong and N. Beaulieu, “Optimal maximal ratio combining with correlated diversity branches,” *IEEE Communications Letters*, vol. 6, no. 1, pp. 22–24, 2002.
- [94] W. Li, Y. Chen, and N. C. Beaulieu, “BER optimization of pilot symbol assisted MRC PSK for slow fading channels,” *IEEE Communications Letters*, vol. 13, no. 12, pp. 929–931, 2009.
- [95] J.-B. Kim and D. Kim, “Performance of dual-hop amplify-and-forward beamforming and its equivalent systems in Rayleigh fading channels,” *IEEE Transactions on Communications*, vol. 58, no. 3, pp. 729–732, 2010.
- [96] K. A. Hamdi, “Capacity of MRC on correlated Rician fading channels,” *IEEE Transactions on Communications*, vol. 56, no. 5, pp. 708–711, 2008.
- [97] K. Yan, J. Jiang, Y. G. Wang, and H. T. Liu, “Outage probability of selection cooperation with mrc in Nakagami- m fading channels,” *IEEE Signal Processing Letters*, vol. 16, no. 12, pp. 1031–1034, 2009.
- [98] X. Zhang and N. C. Beaulieu, “A closed-form ber expression for BPSK using MRC in correlated CCI and Rayleigh fading,” *IEEE Transactions on Communications*, vol. 55, no. 12, pp. 2249–2252, 2007.
- [99] M.-S. Alouini and M. Simon, “Performance analysis of coherent equal gain combining over Nakagami- m fading channels,” *IEEE Transactions on Vehicular Technology*, vol. 50, no. 6, pp. 1449–1463, 2001.
- [100] M.-S. Kim, M. Yoon, and C. Lee, “Performance analysis of a frequency-domain equal-gain-combining time-reversal scheme for distributed antenna systems,” *IEEE Communications Letters*, vol. 16, no. 9, pp. 1454–1457, 2012.
- [101] F. Yang, W. Xiong, and J. Song, “Equal gain combining-based maximum likelihood detector for FFH/MFSK systems,” *IEEE Communications Letters*, vol. 22, no. 7, pp. 1334–1337, 2018.
- [102] Q. T. Zhang, “Error rates for 4-branch equal-gain combining in independent Rayleigh fading: A simple explicit solution,” *IEEE Communications Letters*, vol. 26, no. 2, pp. 269–272, 2022.
- [103] B. Chun, “A hybrid selection/equal-gain combining over correlated nakagami- m fading channels,” *IEEE Communications Letters*, vol. 11, no. 2, pp. 161–163, 2007.
- [104] R. Ziemer and T. Welch, “Equal-gain combining of multichannel DPSK in doppler-spread Ricean fading,” *IEEE Transactions on Vehicular Technology*, vol. 49, no. 5, pp. 1846–1855, 2000.
- [105] J. Frolik, “Mitigating severe channel effects using tripolar antenna diversity,” in *Antennas and Propagation (EuCAP), 2015 9th European Conference on*. IEEE, 2015, pp. 1–4.
- [106] M. Golmohamadi, R. Ramirez, B. Hewgill, J. Jamison, J. Frolik, and T. Weller, “Characterization of a geometrically constrained tripolar antenna under M2M channel conditions,” in

- 2017 11th European Conference on Antennas and Propagation (EUCAP). IEEE, 2017, pp. 2998–3002.
- [107] I. Lee and K. Lee, “The Internet of Things (IoT): Applications, investments, and challenges for enterprises,” *Business Horizons*, vol. 58, no. 4, pp. 431–440, 2015.
- [108] H.-C. Lee and H.-H. Lin, “Design and evaluation of an open-source wireless mesh networking module for environmental monitoring,” *IEEE sensors journal*, vol. 16, no. 7, pp. 2162–2171, 2016.
- [109] L.-C. Lin, M. Guo, and K. T. Wong, “Two-branch selection in wireless space-diversity reception: An upper bound for its output power,” *IEEE transactions on communications*, vol. 60, no. 2, pp. 537–546, 2012.
- [110] S. Chowdhury, J. Jamison, and J. Frolik, “Leveraging tripolar antenna diversity to improve link reliability in severe multipath environments,” in *2018 IEEE 19th Wireless and Microwave Technology Conference (WAMICON)*. IEEE, 2018.
- [111] M. A. Rahman, E. Nishiyama, and I. Toyoda, “A frequency diversity reconfigurable antenna with circular polarization switching capability,” in *Antennas and Propagation & USNC/URSI National Radio Science Meeting, 2017 IEEE International Symposium on*. IEEE, 2017, pp. 1367–1368.
- [112] A. Ourir, K. Rachedi, D.-T. Phan-Huy, C. Leray, and J. de Rosny, “Compact reconfigurable antenna with radiation pattern diversity for spatial modulation,” in *Antennas and Propagation (EUCAP), 2017 11th European Conference on*. IEEE, 2017, pp. 3038–3043.
- [113] G. N. Alsath, H. Arun, Y. P. Selvam, M. Kanagasabai, S. Kingsly, S. Subbaraj, R. Sivasamy, S. K. Palaniswamy, and R. Natarajan, “An integrated tri-band/UWB polarization diversity antenna for vehicular networks,” *IEEE Transactions on Vehicular Technology*, vol. PP, no. 99, pp. 1–1, 2018.
- [114] R. Yahya, A. Nakamura, M. Itami, and T. A. Denidni, “A novel UWB FSS-based polarization diversity antenna,” *IEEE Antennas and Wireless Propagation Letters*, vol. 16, pp. 2525–2528, 2017.
- [115] Y. Sharma, D. Sarkar, K. Saurav, and K. V. Srivastava, “Three-element MIMO antenna system with pattern and polarization diversity for WLAN applications,” *IEEE Antennas and Wireless Propagation Letters*, vol. 16, pp. 1163–1166, 2017.
- [116] M. Kooijman, *Building Wireless Sensor Networks Using Arduino*. Packt Publishing Ltd, 2015.
- [117] S. Chowdhury, J. Frolik, and A. Benslimane, “Polarization matching for networks utilizing tripolar antenna systems,” in *2018 IEEE Global Communications Conference (GLOBECOM)*. IEEE, 2018, pp. 206–212.
- [118] J. Lin, W. Yu, N. Zhang, X. Yang, H. Zhang, and W. Zhao, “A survey on Internet of Things: Architecture, enabling technologies, security and privacy, and applications,” *IEEE Internet of Things Journal*, vol. 4, no. 5, pp. 1125–1142, 2017.
- [119] S. Ishikawa and T. Ninomiya, “Polarization diversity antenna with L-shaped slit for wireless sensor network,” in *2012 Asia Pacific Microwave Conference Proceedings*, Dec 2012, pp. 1181–1183.
- [120] Y. F. C. X. Ding, W. Shao, T. L. Liang, B. Z. Wang, and D. E. Anagnostou, “A polarization reconfigurable RFID reader antenna,” in *2017 IEEE International Symposium on Antennas and Propagation USNC/URSI National Radio Science Meeting*, July 2017, pp. 2213–2214.
- [121] H. Wong, W. Lin, L. Huitema, and E. Arnaud, “Multi-polarization reconfigurable antenna for wireless biomedical system,” *IEEE Transactions on Biomedical Circuits and Systems*, vol. 11, no. 3, pp. 652–660, June 2017.
- [122] K. Y. Yazdandoost and K. Hamaguchi, “Antenna polarization mismatch in body area network communications,” in *Antennas and Propagation (EuCAP), 2010 Proceedings of the Fourth European Conference on*. IEEE, 2010, pp. 1–4.

- [123] J. Zhang, Y. Huang, and Z. Li, "Analysis of polarization matching and transmitting/receiving pattern reciprocity of antenna," in *Antennas and Propagation (APCAP), 2014 3rd Asia-Pacific Conference on*. IEEE, 2014, pp. 248–251.
- [124] N. Yang, H. Zhu, P. Zheng, G. Zhao, H. Sun, and X. Lv, "Research on the impact of polarization basis mismatch on polarization error measurement of dual-polarization antenna," in *Microwave and Millimeter Wave Technology (ICMMT), 2012 International Conference on*, vol. 4. IEEE, 2012, pp. 1–4.
- [125] J.-K. Hong, H.-S. Jo, C. Mun, and J.-G. Yook, "Opportunistic polarization-matching for multiuser polarized MISO downlink," *IEEE Communications Letters*, vol. 21, no. 4, pp. 909–912, 2017.
- [126] C. Zhu, S. Wu, G. Han, L. Shu, and H. Wu, "A tree-cluster-based data-gathering algorithm for industrial WSNs with a mobile sink," *IEEE Access*, vol. 3, pp. 381–396, 2015.
- [127] S. Chowdhury, L. Hébert-Dufresne, and J. Frolik, "Effective implementation of energy aware polarization diversity for IoT networks using eigenvector centrality," in *International Conference on Network Science*. Springer, 2020, pp. 245–257.
- [128] M. I. Hussain, "Internet of Things: challenges and research opportunities," *CSI Transactions on ICT*, vol. 5, no. 1, pp. 87–95, Dec. 2016. [Online]. Available: <https://doi.org/10.1007/s40012-016-0136-6>
- [129] S. Hammoudi, Z. Aliouat, and S. Harous, "Challenges and research directions for Internet of Things," *Telecommunication Systems*, vol. 67, no. 2, pp. 367–385, Jul. 2017. [Online]. Available: <https://doi.org/10.1007/s11235-017-0343-y>
- [130] F. Wortmann and K. Flüchter, "Internet of Things," *Business & Information Systems Engineering*, vol. 57, no. 3, pp. 221–224, Mar. 2015. [Online]. Available: <https://doi.org/10.1007/s12599-015-0383-3>
- [131] W. Qin, S. Chen, and M. Peng, "Recent advances in industrial internet: insights and challenges," *Digital Communications and Networks*, vol. 6, no. 1, pp. 1–13, Feb. 2020. [Online]. Available: <https://doi.org/10.1016/j.dcan.2019.07.001>
- [132] S.-C. Kwon and G. L. Stuber, "Geometrical theory of channel depolarization," *IEEE Transactions on Vehicular Technology*, vol. 60, no. 8, pp. 3542–3556, Oct. 2011. [Online]. Available: <https://doi.org/10.1109/tvt.2011.2163094>
- [133] M. Gkizeli and G. N. Karystinos, "Maximum-SNR antenna selection among a large number of transmit antennas," *IEEE Journal of Selected Topics in Signal Processing*, vol. 8, no. 5, pp. 891–901, Oct. 2014. [Online]. Available: <https://doi.org/10.1109/jstsp.2014.2328329>
- [134] X. Wang, N. Yang, H. Zhang, T. M. Hoang, and T. A. Gulliver, "Generalised selection at multi-antenna sources in two-way relay networks," *IET Communications*, vol. 10, no. 7, pp. 824–831, May 2016. [Online]. Available: <https://doi.org/10.1049/iet-com.2015.0110>
- [135] A. Molina-Pico, D. Cuesta-Frau, A. Araujo, J. Alejandro, and A. Rozas, "Forest monitoring and wildland early fire detection by a hierarchical wireless sensor network," *Journal of Sensors*, vol. 2016, pp. 1–8, 2016. [Online]. Available: <https://doi.org/10.1155/2016/8325845>
- [136] M. F. Othman and K. Shazali, "Wireless sensor network applications: A study in environment monitoring system," *Procedia Engineering*, vol. 41, pp. 1204–1210, 2012. [Online]. Available: <https://doi.org/10.1016/j.proeng.2012.07.302>
- [137] V. Latora, V. Nicosia, and G. Russo, *Complex Networks*. Cambridge University Press, Sep. 2017. [Online]. Available: <https://doi.org/10.1017/9781316216002>
- [138] M. Newman, *Networks*. Oxford University Press, Oct. 2018. [Online]. Available: <https://doi.org/10.1093/oso/9780198805090.001.0001>
- [139] J. M. Bloodgood, J. S. Hornsby, M. Rutherford, and R. G. McFarland, "The role of network density and betweenness centrality in diffusing new venture legitimacy: an epidemiological approach," *International Entrepreneurship and Management Journal*, vol. 13, no. 2, pp. 525–552, Sep. 2016. [Online]. Available: <https://doi.org/10.1007/s11365-016-0412-9>

- [140] V. Aytaç and T. Turaci, “Closeness centrality in some splitting networks,” *Computer Science Journal of Moldova*, vol. 78, no. 3, pp. 251–269, 2018.
- [141] L. Baldesi, L. Maccari, and R. L. Cigno, “On the use of eigenvector centrality for cooperative streaming,” *IEEE Communications Letters*, vol. 21, no. 9, pp. 1953–1956, Sep. 2017. [Online]. Available: <https://doi.org/10.1109/lcomm.2017.2713361>
- [142] S. Chowdhury, J. Frolik, and A. Benslimane, “Coordinating three-branch diversity switching using a hidden Markov model,” *IEEE Internet of Things Journal*, vol. 7, no. 1, pp. 258–268, 2019.
- [143] M. A. Razzaque, M. Milojevic-Jevric, A. Palade, and S. Clarke, “Middleware for Internet of Things: a survey,” *IEEE Internet of things journal*, vol. 3, no. 1, pp. 70–95, 2016.
- [144] Y. Li, X. Cheng, Y. Cao, D. Wang, and L. Yang, “Smart choice for the smart grid: Narrowband Internet of Things (NB-IoT),” *IEEE Internet of Things Journal*, vol. 5, no. 3, pp. 1505–1515, 2018.
- [145] Y. Meng, W. Zhang, H. Zhu, and X. S. Shen, “Securing consumer IoT in the smart home: Architecture, challenges, and countermeasures,” *IEEE Wireless Communications*, vol. 25, no. 6, pp. 53–59, 2018.
- [146] T. Watteryne, P. Tuset-Peiro, X. Vilajosana, S. Pollin, and B. Krishnamachari, “Teaching communication technologies and standards for the industrial IoT? use 6TiSCH!” *IEEE Communications Magazine*, vol. 55, no. 5, pp. 132–137, 2017.
- [147] R. Niu and P. K. Varshney, “Performance analysis of distributed detection in a random sensor field,” *IEEE Transactions on Signal Processing*, vol. 56, no. 1, pp. 339–349, 2007.
- [148] D. Ciunzo and P. S. Rossi, “Quantizer design for generalized locally optimum detectors in wireless sensor networks,” *IEEE Wireless Communications Letters*, vol. 7, no. 2, pp. 162–165, 2017.
- [149] S. R. Islam, D. Kwak, M. H. Kabir, M. Hossain, and K.-S. Kwak, “The Internet of Things for health care: a comprehensive survey,” *IEEE Access*, vol. 3, pp. 678–708, 2015.
- [150] E. Tanghe, D. P. Gaillot, M. Liénard, L. Martens, and W. Joseph, “Experimental analysis of dense multipath components in an industrial environment,” *IEEE Transactions on Antennas and Propagation*, vol. 62, no. 7, pp. 3797–3805, 2014.
- [151] W. Zhang, W. Guo, X. Liu, Y. Liu, J. Zhou, B. Li, Q. Lu, and S. Yang, “LSTM-based analysis of industrial IoT equipment,” *IEEE Access*, vol. 6, pp. 23 551–23 560, 2018.
- [152] P. Aqueveque, A. S. Morales, R. L. Valenzuela, F. S. Rodríguez, E. J. Pino, and E. P. Wiechmann, “Temperature monitoring and flow estimation in electrolytic cells using wireless harsh environment sensors,” *IEEE Transactions on Industry Applications*, vol. 54, no. 4, pp. 3982–3990, 2018.
- [153] K. Raof and N. Prayongpun, “Impact of depolarization effects on MIMO polarized wireless configuration,” *2007 International Conference on Wireless Communications, Networking and Mobile Computing*, sep 2007.
- [154] J. Frolik and M. Golmohamadi, “On random and multidimensional channel effects in cluttered environments,” *IEEE Antennas and Wireless Propagation Letters*, vol. 16, pp. 1863–1866, 2017.
- [155] K. M. Mak, H. W. Lai, K. M. Luk, and K. L. Ho, “Polarization reconfigurable circular patch antenna with a C-shaped,” *IEEE Transactions on Antennas and Propagation*, vol. 65, no. 3, pp. 1388–1392, 2017.
- [156] P.-L. Chi and E. Deng, “Switchable quadri-polarization slot antenna using a single feed port,” *Antennas and Propagation & USNC/URSI National Radio Science Meeting, 2017 IEEE International Symposium on*, pp. 2211–2212, 2017.

- [157] S. K. Yoo, S. L. Cotton, and W. G. Scanlon, “Switched diversity techniques for indoor off-body communication channels: An experimental analysis and modeling,” *IEEE Transactions on Antennas and Propagation*, vol. 64, no. 7, pp. 3201–3206, 2016.
- [158] R. Agarwal, N. Srivastava, and H. Katiyar, “Analysis of switch and examine combining with post-examining selection in cognitive radio,” *International Journal of Electronics*, vol. 105, no. 6, pp. 941–950, 2018.
- [159] H. Nam and M.-S. Alouini, “Multi-branch switched diversity with adaptive switching thresholds,” *2008 International Symposium on Information Theory and Its Applications*, pp. 1–6, 2008.
- [160] L. Lukama, D. Edwards, and A. Wain, “Application of three-branch polarisation diversity in the indoor environment,” *IEEE Proceedings-Communications*, vol. 150, no. 5, pp. 399–403, 2003.
- [161] B. Wu, M. Okoniewski, and C. Hayden, “A pneumatically controlled reconfigurable antenna with three states of polarization,” *IEEE Transactions on Antennas and Propagation*, vol. 62, no. 11, pp. 5474–5484, 2014.
- [162] C. Gu, S. Gao, H. Liu, Q. Luo, T.-H. Loh, M. Sobhy, J. Li, G. Wei, J. Xu, F. Qin *et al.*, “Compact smart antenna with electronic beam-switching and reconfigurable polarizations,” *IEEE Transactions on Antennas and Propagation*, vol. 63, no. 12, pp. 5325–5333, 2015.
- [163] R. K. Singh, A. Basu, and S. K. Koul, “Novel high gain polarization switchable rectangular slot antenna for L-band applications,” *2017 11th European Conference on Antennas and Propagation (EUCAP)*, pp. 3820–3824, 2017.
- [164] G. C. Alexandropoulos, P. T. Mathiopoulos, and N. C. Sagias, “Switch-and-examine diversity over arbitrarily correlated Nakagami- m fading channels,” *IEEE Transactions on Vehicular Technology*, vol. 59, no. 4, pp. 2080–2087, 2010.
- [165] K. Peppas, N. C. Sagias, F. I. Lazarakis, A. A. Alexandridis, and K. P. Dangakis, “Error performance of triple-branch generalized selection diversity over Nakagami fading channels,” *2008 3rd International Symposium on Wireless Pervasive Computing*, pp. 722–726, 2008.
- [166] H.-C. Yang and M.-S. Alouini, “Markov chains and performance comparison of switched diversity systems,” *IEEE Transactions on Communications*, vol. 52, no. 7, pp. 1113–1125, 2004.
- [167] A. M. Fraser, *Hidden Markov Models and Dynamical Systems*. Siam, 2008, vol. 107.
- [168] A. Ankan and A. Panda, *Hands-On Markov Models with Python: Implement probabilistic models for learning complex data sequences using the Python ecosystem*. Packt Publishing Ltd, 2018.
- [169] M. Stamp, “A revealing introduction to hidden Markov models,” *Department of Computer Science San Jose State University*, pp. 26–56, 2004.
- [170] L. R. Rabiner, “A tutorial on hidden Markov models and selected applications in speech recognition,” *Proceedings of the IEEE*, vol. 77, no. 2, pp. 257–286, 1989.
- [171] Q. Huo, C. Chan, and C. H. Lee, “Bayesian adaptive learning of the parameters of hidden Markov model for speech recognition,” *IEEE Transactions on Speech and Audio Processing*, vol. 3, no. 5, pp. 334–345, 1995.
- [172] C. Ferles, G. Siolas, and A. Stafylopatis, “Scaled self-organizing map–hidden Markov model architecture for biological sequence clustering,” *Applied Artificial Intelligence*, vol. 27, no. 6, pp. 461–495, 2013.
- [173] M. Kozdoba and S. Mannor, “Source estimation in time series and the surprising resilience of HMMs,” *IEEE Transactions on Information Theory*, vol. 64, no. 8, pp. 5555–5569, 2018.
- [174] N. Nguyen and D. Nguyen, “Hidden Markov model for stock selection,” *Risks*, vol. 3, no. 4, pp. 455–473, 2015.

- [175] P. S. Rossi, D. Ciunozzo, and T. Ekman, "HMM-based decision fusion in wireless sensor networks with noncoherent multiple access," *IEEE Communications Letters*, vol. 19, no. 5, pp. 871–874, 2015.
- [176] Y. Qi and S. Ishak, "A hidden Markov model for short term prediction of traffic conditions on freeways," *Transportation Research Part C: Emerging Technologies*, vol. 43, pp. 95–111, 2014.
- [177] O. Hersent, D. Boswarthick, and O. Elloumi, *The Internet of Things: Key applications and protocols*. John Wiley & Sons, 2011.
- [178] R. H. Bishop, *LabVIEW 8*. Pearson, 2007.
- [179] XBee/XBee-PRO S2C Zigbee RF Module. [Online]. Available: <https://www.digi.com/resources/documentation/digidocs/pdfs/90002002.pdf>
- [180] F. Fraile, T. Tagawa, R. Poler, and A. Ortiz, "Trustworthy industrial IoT gateways for interoperability platforms and ecosystems," *IEEE Internet of Things Journal*, vol. 5, no. 6, pp. 4506–4514, 2018.
- [181] M. Liwang, S. Dai, Z. Gao, Y. Tang, and H. Dai, "A truthful reverse-auction mechanism for computation offloading in cloud-enabled vehicular network," *IEEE Internet of Things Journal*, vol. 6, no. 3, pp. 4214–4227, 2019.
- [182] N. Ahmed, D. De, and I. Hussain, "Internet of things (IoT) for smart precision agriculture and farming in rural areas," *IEEE Internet of Things Journal*, vol. 5, no. 6, pp. 4890–4899, 2018.
- [183] Z. Guan, J. Li, L. Wu, Y. Zhang, J. Wu, and X. Du, "Achieving efficient and secure data acquisition for cloud-supported Internet of Things in smart grid," *IEEE Internet of Things Journal*, vol. 4, no. 6, pp. 1934–1944, 2017.
- [184] M. Z. Hasan and F. Al-Turjman, "Optimizing multipath routing with guaranteed fault tolerance in Internet of Things," *IEEE Sensors Journal*, vol. 17, no. 19, pp. 6463–6473, 2017.
- [185] Y. Deng, A. Burr, and G. White, "Performance of MIMO systems with combined polarization multiplexing and transmit diversity," in *2005 IEEE 61st Vehicular Technology Conference*, vol. 2. IEEE, 2005, pp. 869–873.
- [186] P. Nagaradjane and T. Muthu, "Performance of feedback multiple-input–multiple-output system aided by polarisation multiplexing and pre-processing," *IET Communications*, vol. 9, no. 16, pp. 1988–1998, 2015.
- [187] Y. Sharma, D. Sarkar, K. Saurav, and K. V. Srivastava, "Three-element MIMO antenna system with pattern and polarization diversity for WLAN applications," *IEEE antennas and wireless propagation letters*, vol. 16, pp. 1163–1166, 2016.
- [188] K. Saurav, N. K. Mallat, and Y. M. Antar, "A three-port polarization and pattern diversity ring antenna," *IEEE Antennas and Wireless Propagation Letters*, vol. 17, no. 7, pp. 1324–1328, 2018.
- [189] Y. Sung, "Dual-band reconfigurable antenna for polarization diversity," *International Journal of Antennas and Propagation*, vol. 2018, 2018.
- [190] J.-S. Row and Y.-H. Wei, "Wideband reconfigurable crossed-dipole antenna with quad-polarization diversity," *IEEE Transactions on Antennas and Propagation*, vol. 66, no. 4, pp. 2090–2094, 2018.
- [191] I. T. McMichael, "A mechanically reconfigurable patch antenna with polarization diversity," *IEEE Antennas and Wireless Propagation Letters*, vol. 17, no. 7, pp. 1186–1189, 2018.
- [192] U. Ullah, M. Al-Hasan, S. Koziel, and I. B. Mabrouk, "Circular polarization diversity implementation for correlation reduction in wideband low-cost multiple-input-multiple-output antenna," *IEEE Access*, vol. 8, pp. 95 585–95 593, 2020.
- [193] B. Wang and S. Yan, "Design of smartwatch integrated antenna with polarization diversity," *IEEE Access*, vol. 8, pp. 123 440–123 448, 2020.

- [194] M. Delibasic and M. Pejanovic-Djurisic, "Performance improvement of relay system in Rayleigh/Rice fading using polarization diversity," *2017 40th International Conference on Telecommunications and Signal Processing (TSP)*, pp. 233–236, 2017.
- [195] P. Qin, Y. J. Guo, and C. Liang, "Effect of antenna polarization diversity on MIMO system capacity," *IEEE Antennas and Wireless Propagation Letters*, vol. 9, pp. 1092–1095, 2010.
- [196] S. Sandhu, R. U. Nabar, D. A. Gore, and A. Paulraj, "Near-optimal selection of transmit antennas for a MIMO channel based on Shannon capacity," *Conference Record of the Thirty-Fourth Asilomar Conference on Signals, Systems and Computers (Cat. No. 00CH37154)*, vol. 1, pp. 567–571, 2000.
- [197] D. A. Gore, R. W. Heath, and A. J. Paulraj, "Transmit selection in spatial multiplexing systems," *IEEE Communications Letters*, vol. 6, no. 11, pp. 491–493, 2002.
- [198] C. Fang, E. Liu, and M. Ur Rehman, "Analysis of subchannel correlation in dual-polarised MIMO systems via a polarisation diversity scheme," *IEEE Transactions on Antennas and Propagation*, vol. 65, no. 5, pp. 2635–2644, 2017.
- [199] H. Li, Q. Liu, Z. Wang, and M. Li, "Transmit antenna selection and analog beamforming with low-resolution phase shifters in mmWave MISO systems," *IEEE Communications Letters*, vol. 22, no. 9, pp. 1878–1881, 2018.
- [200] M. Gong, Z. Yang, and B. Lyu, "Antenna diversity for downlink MIMO-NOMA systems with partial channel state information," *IEEE Communications Letters*, vol. 22, no. 10, pp. 2172–2175, 2018.
- [201] X. Zhao, A. M. A. Abdo, Y. Zhang, S. Geng, and J. Zhang, "Single RF-chain beam training for MU-MIMO energy efficiency and information-centric IoT millimeter wave communications," *IEEE Access*, vol. 7, pp. 6597–6610, 2019.
- [202] I. A. Alimi, R. K. Patel, N. J. Muga, and P. P. Monteiro, "Performance analysis of 5G fixed wireless access networks with antenna diversity techniques," *WIRELESS PERSONAL COMMUNICATIONS*, 2020.
- [203] N. C. Beaulieu, "Switching rates of dual selection diversity and dual switch-and-stay diversity," *IEEE transactions on communications*, vol. 56, no. 9, pp. 1409–1413, 2008.
- [204] N. Kapucu, "On the performance of dual-branch selection diversity combining in α - κ - μ fading environments," *Transactions on Emerging Telecommunications Technologies*, vol. 30, no. 12, p. e3719, 2019.
- [205] L. Chen, X. Chen, W. Wang, and C. Zhang, "Performance analysis of multi-antennas combining and selection schemes for wireless-powered communication," *Journal of Communications and Networks*, vol. 19, no. 2, pp. 124–133, 2017.
- [206] S. K. Yoo, S. L. Cotton, and W. G. Scanlon, "Switched diversity techniques for indoor off-body communication channels: An experimental analysis and modeling," *IEEE Transactions on Antennas and Propagation*, vol. 64, no. 7, pp. 3201–3206, 2016.
- [207] G. C. Alexandropoulos, P. T. Mathiopoulos, and P. Fan, "Performance analysis of L -branch scan-and-wait combining (SWC) over arbitrarily correlated Nakagami- m fading channels," *IEEE Transactions on Vehicular Technology*, vol. 66, no. 3, pp. 2868–2874, 2017.
- [208] P. L. R. Chze and K. S. Leong, "A secure multi-hop routing for IoT communication," in *2014 IEEE World forum on Internet of Things (WF-IoT)*. IEEE, 2014, pp. 428–432.
- [209] G. Chen, J. P. Coon, A. Mondal, B. Allen, and J. A. Chambers, "Performance analysis for multihop full-duplex IoT networks subject to poisson distributed interferers," *IEEE Internet of Things Journal*, vol. 6, no. 2, pp. 3467–3479, 2018.
- [210] B. Holter and G. E. Oien, "Performance analysis of a rate-adaptive dual-branch switched diversity system," in *IEEE Vehicular Technology Conference*. IEEE, 2006, pp. 1–5.

- [211] E. L. Bengtsson, F. Rusek, P. C. Karlsson, F. Tufvesson, and O. Edfors, "Analysis of transmission schemes for dual-antenna terminals in massive MIMO systems," in *2018 25th International Conference on Telecommunications (ICT)*. IEEE, 2018, pp. 76–82.
- [212] G. A. Al-Suhail, "Performance of video quality in dual-branch diversity based SR-ARQ over Rayleigh fading channel," in *Proceedings of the 7th International Conference on Advances in Mobile Computing and Multimedia*, 2009, pp. 60–67.
- [213] A. Goldsmith, *Wireless communications*. Cambridge university press, 2005.
- [214] M.-S. Alouini and H.-C. Yang, "Minimum estimation and combining generalized selection combining (MEC-GSC)," in *Proceedings. International Symposium on Information Theory, 2005. ISIT 2005.*, 2005, pp. 578–582.
- [215] K. Sivanesan and N. C. Beaulieu, "Precise outage analysis of selection diversity and switched diversity in bandlimited microcellular systems with cochannel interference," *IEEE Transactions on Communications*, vol. 55, no. 10, pp. 2002–2011, 2007.
- [216] A. Abu-Dayya and N. Beaulieu, "Outage probabilities of diversity cellular systems with cochannel interference in Nakagami fading," *IEEE Transactions on Vehicular Technology*, vol. 41, no. 4, pp. 343–355, 1992.
- [217] H.-C. Yang and M.-S. Alouini, "Performance analysis of multibranch switched diversity systems," *IEEE Transactions on Communications*, vol. 51, no. 5, pp. 782–794, 2003.
- [218] C. Adjih, E. Baccelli, E. Fleury, G. Harter, N. Mitton, T. Noel, R. Pissard-Gibollet, F. Saint-Marcel, G. Schreiner, J. Vandaele *et al.*, "FIT IoT-lab: A large scale open experimental IoT testbed," in *2015 IEEE 2nd World Forum on Internet of Things (WF-IoT)*. IEEE, 2015, pp. 459–464.
- [219] G. Gardasevic, P. Plavsic, and D. Vasilievic, "Experimental IoT testbed for testing the 6TiSCH and RPL coexistence," in *IEEE INFOCOM 2019-IEEE Conference on Computer Communications Workshops (INFOCOM WKSHPS)*. IEEE, 2019, pp. 917–918.
- [220] M. G. Samaila, J. B. F. Sequeiros, T. Simões, M. M. Freire, and P. R. M. Inácio, "IoT-HarPsecA: A framework and roadmap for secure design and development of devices and applications in the IoT space," *IEEE Access*, vol. 8, pp. 16 462–16 494, 2020.
- [221] L. Chettri and R. Bera, "A comprehensive survey on Internet of Things (IoT) toward 5G wireless systems," *IEEE Internet of Things Journal*, vol. 7, no. 1, pp. 16–32, 2020.
- [222] A. Ijaz, L. Zhang, M. Grau, A. Mohamed, S. Vural, A. U. Quddus, M. A. Imran, C. H. Foh, and R. Tafazolli, "Enabling massive IoT in 5G and beyond systems: Phy radio frame design considerations," *IEEE Access*, vol. 4, pp. 3322–3339, 2016.
- [223] N. Dhieb, H. Ghazzai, H. Besbes, and Y. Massoud, "Scalable and secure architecture for distributed IoT systems," in *2020 IEEE Technology & Engineering Management Conference (TEMSCON)*. IEEE, 2020, pp. 1–6.
- [224] P. Angin, M. B. Mert, O. Mete, A. Ramazanli, K. Sarica, and B. Gungoren, "A blockchain-based decentralized security architecture for IoT," in *International Conference on Internet of Things*. Springer, 2018, pp. 3–18.
- [225] G. H. Raghunandan, A. S. Rani, A. Varma, M. S. Reddy, P. R. Dennis, and R. V. Kumar, "Centroid and gateway based hierarchical routing protocol for wireless sensor network," in *2018 4th International Conference for Convergence in Technology (I2CT)*, 2018, pp. 1–4.
- [226] M. Mathankumar, U. Rajkanna, and C. Mohanraj, "Implementation of optimised wireless sensor network using cluster architecture," in *2019 Innovations in Power and Advanced Computing Technologies (i-PACT)*, vol. 1, 2019, pp. 1–4.
- [227] A. Mohan and B. Bhaskara, "Multi-dimensional trust aware routing for clustered IOT framework," *International Journal of Engineering & Technology*, vol. 7, no. 4.20, pp. 15–21, 2018.
- [228] C. Liu, F. Song, H. Yan, and S. Zhang, "Modeling of multipath transport," *arXiv preprint arXiv:1306.4090*, 2013.

- [229] A. S. Lioumpas and A. Alexiou, "On the switching rate of ST-MIMO systems with energy-based antenna selection," *Proceedings of the 5th European Conference on Antennas and Propagation (EUCAP)*, pp. 2432–2435, 2011.
- [230] F. Hussain, R. Hussain, S. A. Hassan, and E. Hossain, "Machine learning in IoT security: Current solutions and future challenges," *IEEE Communications Surveys Tutorials*, vol. 22, no. 3, pp. 1686–1721, 2020.
- [231] M. I. AlHajri, N. T. Ali, and R. M. Shubair, "Classification of indoor environments for IoT applications: A machine learning approach," *IEEE Antennas and Wireless Propagation Letters*, vol. 17, no. 12, pp. 2164–2168, 2018.
- [232] S. K. Sharma and X. Wang, "Toward massive machine type communications in ultra-dense cellular IoT networks: Current issues and machine learning-assisted solutions," *IEEE Communications Surveys Tutorials*, vol. 22, no. 1, pp. 426–471, 2020.
- [233] S. Al-Juboori and X. N. Fernando, "Multiantenna spectrum sensing over correlated Nakagami-m channels with MRC and EGC diversity receptions," *IEEE Transactions on Vehicular Technology*, vol. 67, no. 3, pp. 2155–2164, 2017.
- [234] K. Vishvakshenan, S. Ramyaramalakshmi, and S. Sathiarani, "Performance of DSTTD-IDMA system using polarization diversity over correlated frequency-selective channel," in *2014 International Conference on Communication and Signal Processing*. IEEE, 2014, pp. 1126–1130.
- [235] K. Zhang, X.-Q. Jiang, M. Wen, R. Qiu, and H. Ge, "Precoding-aided spatial modulation with dual-polarized antennas over correlated channels," *IEEE Communications Letters*, vol. 24, no. 3, pp. 676–680, 2020.
- [236] B. Zhu and J. Cheng, "Asymptotic outage analysis on dual-branch diversity receptions over non-identically distributed correlated lognormal channels," *IEEE Transactions on Communications*, vol. 67, no. 10, pp. 7126–7138, 2019.
- [237] T.-K. Dao, J. Yu, T.-T. Nguyen, and T.-G. Ngo, "A hybrid improved mvo and fnn for identifying collected data failure in cluster heads in wsn," *IEEE Access*, vol. 8, pp. 124 311–124 322, 2020.
- [238] H. Wang, K. Li, and W. Pedrycz, "An elite hybrid metaheuristic optimization algorithm for maximizing wireless sensor networks lifetime with a sink node," *IEEE Sensors Journal*, vol. 20, no. 10, pp. 5634–5649, 2020.
- [239] L. Xu, Z. Li, and X. Li, "A hybrid approach using multistage collaborative calibration for wireless sensor network localization in 3d environments," *IEEE Access*, vol. 8, pp. 130 205–130 223, 2020.
- [240] Y. Zhong and K. S. Kwak, "Fault-tolerant cognitive diversity scheme for topology information-based hybrid ubiquitous sensor networks," in *2008 Third International Conference on Convergence and Hybrid Information Technology*, vol. 1. IEEE, 2008, pp. 102–110.
- [241] A. Bhawe and S. Jajoo, "Secure communication in wireless sensor networks using hybrid encryption scheme and cooperative diversity technique," in *2015 IEEE 9th International Conference on Intelligent Systems and Control (ISCO)*. IEEE, 2015, pp. 1–6.
- [242] A. Chaibrassou and A. Mouhsen, "A multi-channel cooperative mimo routing protocol for clustered wsns," in *2016 International Conference on Electrical and Information Technologies (ICEIT)*. IEEE, 2016, pp. 231–236.